AFRRI Reports

Fourth Quarter
1995

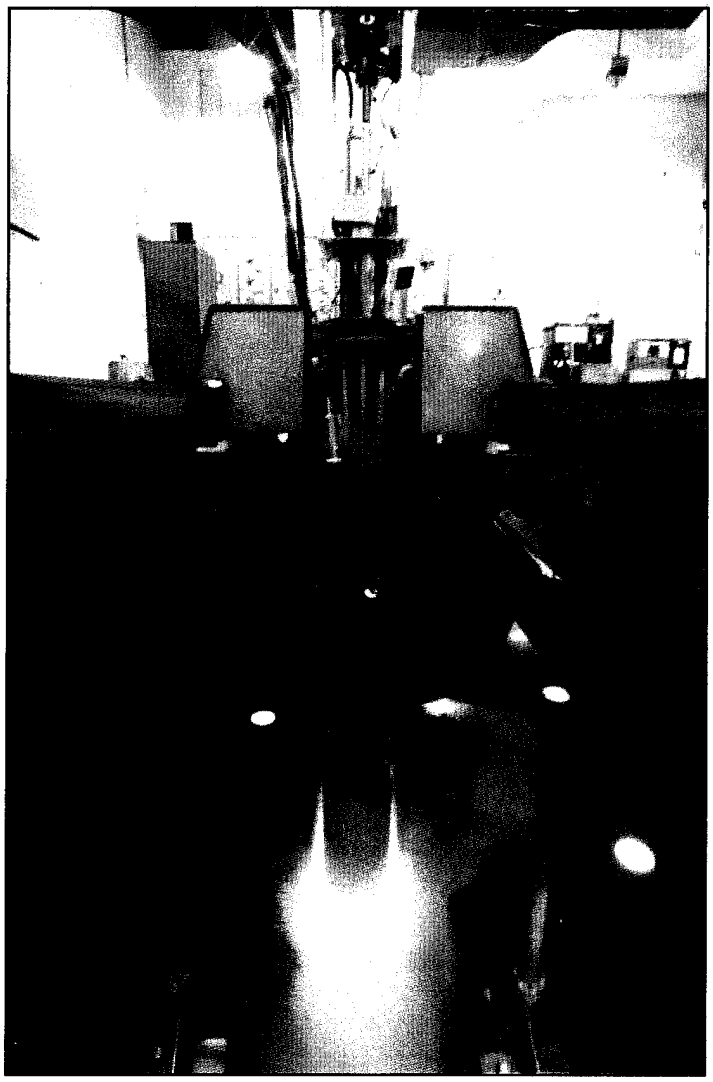

Armed Forces Radiobiology Research Institute
8901 Wisconsin Avenue
Bethesda, Maryland 20889-5603

On the cover: The glow in the pool of water shielding the core of AFRRI's Mark-F TRIGA nuclear reactor is known as Cherenkov radiation and is caused by electrons from the reactor traveling at speeds greater than the speed of light in water. The effect is named for Pavel Alekseyevich Cherenkov, a Soviet scientist who, along with his co-investigators, won the 1958 Nobel Prize for Physics for their observations.
AFRRI photo by David H. Morse.

REPORT DOCUMENTATION PAGE

Form Approved
OMB No. 0704-0188

1. AGENCY USE ONLY *(Leave blank)*	2. REPORT DATE	3. REPORT TYPE AND DATES COVERED
	February 1996	Reprints

4. TITLE AND SUBTITLE

AFRRI Reports, Fourth Quarter 1995

5. FUNDING NUMBERS

PE: NWED QAXM

6. AUTHOR(S)

7. PERFORMING ORGANIZATION NAME(S) AND ADDRESS(ES)

Armed Forces Radiobiology Research Institute
8901 Wisconsin Avenue
Bethesda, MD 20889-5603

8. PERFORMING ORGANIZATION REPORT NUMBER

SR95-22 - SR95-28

9. SPONSORING/MONITORING AGENCY NAME(S) AND ADDRESS(ES)

Uniformed Services University of the Health Sciences
4301 Jones Bridge Road
Bethesda, MD 20814-4799

10. SPONSORING/MONITORING AGENCY REPORT NUMBER

11. SUPPLEMENTARY NOTES

12a. DISTRIBUTION/AVAILABILITY STATEMENT

Approved for public release; distribution unlimited.

12b. DISTRIBUTION CODE

13. ABSTRACT *(Maximum 200 words)*

This volume contains AFRRI Scientific Reports SR95-22 through SR95-28 for October-December 1995.

14. SUBJECT TERMS

15. NUMBER OF PAGES
71

16. PRICE CODE

17. SECURITY CLASSIFICATION OF REPORT	18. SECURITY CLASSIFICATION OF THIS PAGE	19. SECURITY CLASSIFICATION OF ABSTRACT	20. LIMITATION OF ABSTRACT
UNCLASSIFIED	UNCLASSIFIED	UNCLASSIFIED	UL

CLASSIFIED BY:

DECLASSIFY ON:

CONTENTS

Scientific Reports

RADIATION RESEARCH 143, 320–326 (1995)

Comparison of Interleukin-1α Gene Expression and Protein Levels in the Murine Spleen after Lethal and Sublethal Total-Body Irradiation

William H. Baker,*,[1] Alex Limanni,* Cheng-min Chang,* William E. Jackson,† Ruth Seemann* and Myra L. Patchen*

*Departments of *Experimental Hematology and †Computer and Electronics, Armed Forces Radiobiology Research Institute, Bethesda, Maryland 20889-5603*

Baker, W. H., Limanni, A., Chang, C., Jackson, W. E., Seemann, R. and Patchen, M. L. Comparison of Interleukin-1α Gene Expression and Protein Levels in the Murine Spleen after Lethal and Sublethal Total-Body Irradiation. *Radiat. Res.* 143, 320–326 (1995).

To understand the effects of ionizing radiation on the production of IL-1α *in vivo* within a hematopoietic organ, we evaluated acute changes in splenic IL-1α mRNA and IL-1α protein after exposing B6D2F$_1$ mice to lethal and sublethal ^{60}Co radiation. Results suggest that *in vivo*, ionizing radiation induces a time- and dose-dependent accumulation of IL-1α mRNA in the mouse spleen after exposure to γ radiation. Time-dependent increases in the level of IL-1α protein were also observed, although the magnitude of increased protein expression did not complement the magnitude of the accumulation of the message. Selective concentration of cells producing IL-1α does not appear to account completely for the increase in splenic IL-1α mRNA observed in this *in vivo* system.

INTRODUCTION

The polypeptide cytokine interleukin 1 (IL-1) is capable of a wide range of activities involved in hematopoietic, inflammatory, immunological, metabolic, physiological, endocrine and neurological functions. An additional intriguing function of IL-1 is its protection of the bone marrow when administered before lethal irradiation. Furthermore, within the radiation dose range which results in the hematopoietic syndrome, IL-1 appears to be an endogenous mediator of radioprotection (*1*), as demonstrated by the fact that irradiated mice treated with anti-IL-1 receptor antibodies before such irradiation manifest increased radiosensitivity (*2*). It was concluded in the studies of Neta *et al.* that the presence of endogenous IL-1 both before and after irradiation appears to be required to achieve maximum radioprotection. *In vitro* studies have demonstrated mRNA specific for IL-1 as well as for other genes to be induced by γ- and X-ray exposures (*3*, *4*). Early-response gene activation appears to account for this induction (*5*, *6*). To understand better the effects of radiation on production of IL-1 *in vivo*, we evaluated changes in IL-1α mRNA and IL-1α protein after exposing mice to lethal and sublethal ionizing radiation. The levels of IL-1α were evaluated in the spleen because it is a hematopoietically active organ in mice and can be readily removed, allowing rapid isolation of total cellular RNA and the harvesting of relatively large amounts of RNA. Within the limits of these studies, results suggest that ionizing radiation may induce a time- and dose-dependent increase in IL-1α mRNA and protein within 24 h postirradiation after lethal and sublethal exposures.

MATERIALS AND METHODS

Experimental Design

Initial studies were performed in which IL-1α mRNA expression was evaluated in spleens from either sublethally or lethally irradiated mice at 5 min and 2, 4, 6, 8, 10 and 24 h after radiation exposure. Subsequent experiments focused on evaluating accumulation of IL-1α mRNA and production of IL-1α protein in spleens from sublethally and lethally irradiated mice at 5 min and 8 h after exposure. In each experiment, total cellular RNA was isolated, characterized by ethidium bromide staining of agarose gels to ensure use of only intact RNA, pooled (splenic RNA from three mice for each treatment group), quantified, reverse-transcribed and amplified by polymerase chain reaction (PCR).[2] The amplified product was separated by electrophoresis, Southern-blotted, hybridized with a ^{32}P-nick-translated probe and autoradiographed. The radiographic films were then scanned, and images were quantified using an image scanner. In additional experiments, splenic cellularities, total splenic RNA contents and differential counts were done on splenic cell suspensions at 5 min and 8 and 24 h after lethal or sublethal irradiation.

[1]Reprint requests to: William H. Baker, Walter Reed Army Institute of Research, Department of Comparative Pathology, Washington, DC 20307-5100.

[2]Abbreviations used: GAPDH, glyceraldehyde-3-phosphate dehydrogenase; LPS, lipopolysaccharide; PCR, polymerase chain reaction; RT-PCR, reverse transcriptase-polymerase chain reaction; *Taq*, *Thermus aquaticus*.

0033-7587/95 $5.00

Mice

B6D2F$_1$ female mice (approximately 20 g) were purchased from The Jackson Laboratory (Bar Harbor, ME). Mice were maintained in an accredited AAALAC (American Association for Accreditation of Laboratory Animal Care) facility in Micro-Isolator cages on hardwood-chip contact bedding and were provided commercial rodent chow and acidified water (pH 2.5) *ad libitum*. Animal rooms were maintained on a 12-h light/dark cycle at 70 ± 2°F, with 50 ± 10% relative humidity, and at least 10 air changes per hour of 100% conditioned fresh air. Upon arrival, all mice were tested for *Pseudomonas* and quarantined until test results were obtained. Only healthy mice were used for the experiments. All animal experiments were approved by the Institute Animal Care and Use Committee before performance.

Irradiation

The AFRRI ^{60}Co source was used for all irradiations. Mice were exposed bilaterally in ventilated plastic containers to total-body γ-ray doses ranging from 4 to 13 Gy at a dose rate of 0.4 Gy per min. Dosimetry was determined using ionization chambers (*7*) with standards traceable to the National Institute of Standards and Technology. The tissue-to-air ratio was determined to be 0.96, and the dose variation within the exposure field was <3%.

RNA Processing

Spleens were removed from mice euthanized by cervical dislocation. Total cellular RNA was immediately processed from intact spleens using the RNAzol™ (TEL-TEST, Inc., Friendswood, TX) method. Briefly, each spleen was placed in 4 ml of RNAzol, homogenized in a tissue homogenizer and distributed into 1-ml aliquots; 100 μl of chloroform was then added to each aliquot. Mixtures were vortexed, incubated on ice for 5 min and centrifuged at 12,000*g* (4°C) for 15 min. Supernatants were transferred to new tubes and an equal volume of isopropanol was added; they were then vortexed and incubated on ice for 30 min. The RNA was pelleted by centrifuging at 12,000*g* for 15 min. Supernatants were discarded, and the pellets were washed in 1 ml of 75% ethanol and re-pelleted by centrifuging at 12,000*g* for 10 min. The ethanol was then discarded, and the pellets were dried. Once dried, pellets were resuspended in TE buffer (10 m*M* Tris and 1 m*M* EDTA), and the sample was quantified spectrophotometrically. RNA samples from each spleen were qualified on a denaturing gel before samples were pooled.

Reverse Transcriptase-Polymerase Chain Reaction (RT-PCR)

RNA from pooled samples was reverse-transcribed in a mixture containing 0.5 μg total cellular RNA, 0.125 μg oligo dT primer, 50 m*M* Tris-HCl, 75 m*M* KCl, 3 m*M* $MgCl_2$, 1 m*M* dNTP mix and 50 U of Moloney murine leukemia virus reverse transcriptase (GIBCO-BRL, Gaithersburg, MD). The mixture was incubated at 37°C for 1 h and at 90°C for 10 min and then chilled on ice for 10 min. The PCR reagents were added to the reverse transcription products to final concentrations of 50 m*M* KCl, 10 m*M* Tris-HCl (pH 8.3), 1.5 m*M* $MgCl_2$, 1 μ*M* 5′-primer, 1 μ*M* 3′-primer (murine IL-1α specific primers, Clonetech, Palo Alto, CA, and murine GAPDH primers, Synthetic Genetics, San Diego, CA), 1.6 m*M* dNTP's and 1.25 U of *Taq* DNA polymerase (Perkin-Elmer, Norwalk, CT). Primer sequences were as follows:

IL-1α 5′ primer	5′-ATG GCC AAA GTT CCT GAC TTG TTT3′
IL-1α 3′ primer	5′-CCT TCA GCA ACA CGG GCT GGT C-3′
GAPDH 5′ primer	5′-CCA TGG AGA AGG CTG GGG-3′
GAPDH 3′ primer	5′-CCA GTA GGT ACT GTT GAA AC-3′

Samples were amplified for 20 cycles with denaturation at 94°C for 1 min, annealing at 60°C for 2 min, extension at 72°C for 3 min and a final extension at 72°C for 7 min in a thermocycler (Perkin-Elmer, Norwalk, CT). Negative controls consisted of samples in which reverse transcriptase was deleted.

Southern Blot Preparation, Hybridization and Autoradiography

Ten microliters of each PCR product from each time was electrophoresed in a 1% agarose gel with 1× TBE buffer (0.089 *M* Tris base, 0.089 *M* boric acid and 0.002 *M* EDTA) and transferred onto nylon membranes. Blots were prehybridized overnight at 37°C in 6× SSC (1× SSC = 150 m*M* NaCl, 15 m*M* sodium citrate dihydrate, pH 7.0), 5× Denhardt's solution (Sigma, St. Louis, MO), 0.1 mg/ml salmon sperm DNA, 48% formamide, 1% SDS and 0.05 *M* Tris. Blots were hybridized overnight with an IL-1α cDNA probe (*8*) containing a 1.9-kb insert, which was subcloned into the *Bam*HI site in pGEM-4 (Promega, Madison, WI). The probe was labeled by nick-translation with ^{32}P (Amersham, Arlington Heights, IL) using a commercial kit (GIBCO-BRL, Gaithersburg, MD) and added at a concentration of 1 to 2 × 10^6 counts per minute per milliliter of prehybridization fluid. Hybridized blots were then washed three times in 2× SSC/0.5% SDS for 15 min each at 42°C and then in 0.1× SSC/0.1% SDS for 1 h at 62°C. Excess fluid was removed from blots before wrapping them in plastic wrap and placing them in cassettes for autoradiography. Quantification by RT-PCR was relative and was based on the amount of expression per 0.5 μg of pooled total cellular RNA per time. Resulting autoradiographs were scanned and densitometric volumes for each band determined using a laser scanning densitometer (Molecular Dynamics, Sunnyvale, CA).

Spleen Cell Suspensions

Spleen cell suspensions for determination of the cell number, differential cell counts and protein levels were prepared by pressing whole spleens through a stainless-steel mesh screen and washing cells from the screen with medium. Cells were dispersed by gently aspirating suspensions through an 18-gauge needle. Cell counts were made using a Coulter counter.

Protein Assay

ELISA kits for murine IL-1α were used to measure IL-1α protein (Genzyme® Intertest IL-1α, Cambridge, MA). Briefly, splenic cell suspensions were prepared as described above and diluted to 4 × 10^7 cells/ml in PBS and 1% BSA. Preparations were frozen and thawed twice at –70°C/room temperature and centrifuged; supernatants were harvested and frozen for future analysis. Whole spleens were placed in a similar diluent, homogenized and centrifuged, and the supernatant was frozen at –70°C for future analysis.

Quantification and Analysis

Comparisons of all means were made using the Behring-Fischer *t* test or the Mann-Whitney *U* test. The mRNA responses of the initial experiments at sublethal and lethal doses at multiple times within the first 24 h postirradiation were compared using Friedmann's test.

RESULTS

Radiation Survival Responses

Preliminary studies were performed to determine sublethal and lethal ^{60}Co radiation doses for B6D2F$_1$ female mice. Results (Fig. 1) indicated that 100% of the mice survived after 7.75 Gy and 0% survived after at doses greater than 10 Gy. The $LD_{50/30}$ was 8.7 Gy. Based on these results, a sublethal 7.75-Gy radiation dose (<$LD_{1/30}$) on the shoulder of the survival curve and a lethal 9.75-Gy radiation dose (>$LD_{99/30}$) on the tail of the survival curve were used in subsequent studies.

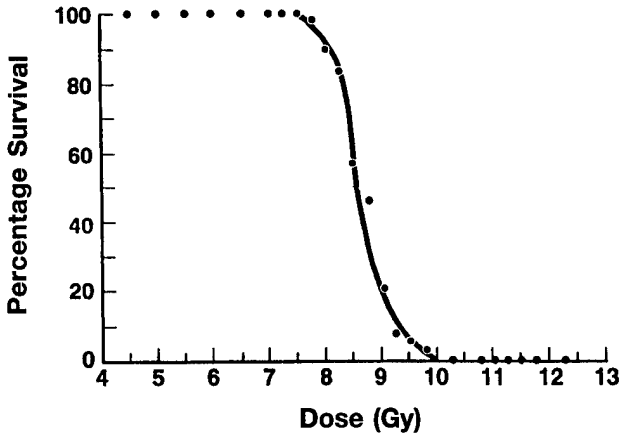

FIG. 1. Radiation dose–response survival curve for B6D2F$_1$ female mice exposed to total-body ^{60}Co radiation. At least 10 mice were exposed to each radiation dose.

Gene Expression

In initial experiments IL-1α gene expression was evaluated within the first 24 h after sublethal and lethal total-body irradiation. Figure 2 represents the responses of mice from two sublethal and two lethal radiation studies. In these studies, processing of total RNA was completed and samples stored frozen; then RT-PCR, electrophoresis, blotting, hybridization and scanning were done simultaneously for samples obtained from each radiation study. The IL-1α and GAPDH RT-PCR signals derived from identical 0.5-μg starting concentrations of total cellular RNA (Fig. 2A) and a graphic presentation of GAPDH-corrected IL-1α densitometric volumes at each time (Fig. 2B) are illustrated. Both sublethal and lethal radiation exposures produced similar early time-dependent effects: at 5 min after exposure, levels of IL-1α mRNA were not detectable; at 2 h after exposure normal levels of IL-1α mRNA were evident. Isolates obtained from later times demonstrated increased levels of IL-1α mRNA, ranging from 2.6 to 22.0 times the normal control levels. Based on the increased density of the bands obtained from the samples of the lethally irradiated mice compared to the sublethally irradiated mice, visual examination of these results appeared to suggest that IL-1α expression was dependent on the radiation dose. However, such a conclusion was approached with caution since these data represented separate experiments in which animals from different lot numbers were used for studies with sublethal and lethal doses.

To determine definitively if IL-1α expression was dependent on the radiation dose, additional experiments were performed to compare mRNA accumulations in sublethally and lethally irradiated mice from the same lot number simultaneously. The evaluations were performed at 5 min and 8 h after exposure (Fig. 3). In both groups, levels of IL-1α mRNA were comparable to normal responses at 5 min after exposure and at 8 h were significantly increased 9.1- and 11.4-fold above normal for sublethally ($P = 0.002$) and lethally ($P < 0.001$) irradiated mice, respectively. The 8-h responses for sublethal and lethal exposures also differed significantly ($P = 0.015$).

Protein Levels

Regardless of whether the protein source was whole spleen or spleen cell suspension, IL-1α protein levels in sublethally and lethally irradiated mice were comparable to normal levels at 5 min postirradiation but were significantly above normal levels at 8 h postirradiation (Fig. 4). In whole spleens (Fig. 4A), basal IL-1α protein levels were detectable in normal mice. In whole spleens the IL-1α protein levels were comparable to normal mice 5 min after exposure to sublethal and lethal irradiation. In contrast, 8 h after either radiation exposure, whole spleen IL-1α protein levels were significantly elevated above normal levels (sublethal $P = 0.001$; lethal $P = 0.007$). The levels of IL-1α protein in sublethally and lethally irradiated mice were comparable, indicating no radiation dose-dependent effect. Samples of spleen cell suspensions (Fig. 4B) from control mice exhibited IL-1α protein below detectable levels. However, levels of IL-1α protein in samples from sublethally and lethally irradiated mice at 5 min after exposure were minimally detectable and were significantly elevated in samples at 8 h postirradiation. Again, however, no statistical differences were observed between the levels of IL-1α protein in sublethally compared to lethally irradiated mice.

Total Splenic RNA and Splenic Cellularities

RNA yields per spleen in mice exposed to 7.75 and 9.75 Gy were comparable at the three times studied (Table I). Splenic RNA yields at 8 and 24 h after exposure in the mice exposed to 7.75 and 9.75 Gy were significantly less than yields from normal spleens ($P < 0.039$). In mice exposed to 7.75 Gy, RNA yields were reduced to 65.9 and 40.7% of control by 8 and 24 h postirradiation, respectively. In mice exposed to 9.75 Gy, yields were reduced to 63.5 and 32.6% of control for the same periods.

Total splenic cellularities in both sublethally and lethally irradiated mice were also significantly decreased at 8 and 24 h after irradiation (Table I). In mice exposed to 7.75 Gy, the cellularity of the spleens was were reduced to 34.3 and 12.0% of control by 8 and 24 h postirradiation, respectively. Similarly, in mice exposed to 9.75 Gy, the number of cells was reduced to 34.1 and 8.9% of normal by 8 and 24 h after exposure, respectively. Although in both radiation groups the cell numbers were comparable at 5 min and 8 h after exposure, by 24 h fewer cells were recovered in mice exposed to 9.75 Gy than in mice exposed to 7.75 Gy ($12.6 \pm 0.4 \times 10^6$ compared to $17.5 \pm 0.73 \times 10^6$ cells, $P < 0.001$).

According to differential cell counts, lymphocytes accounted for approximately 97% of the cells of normal

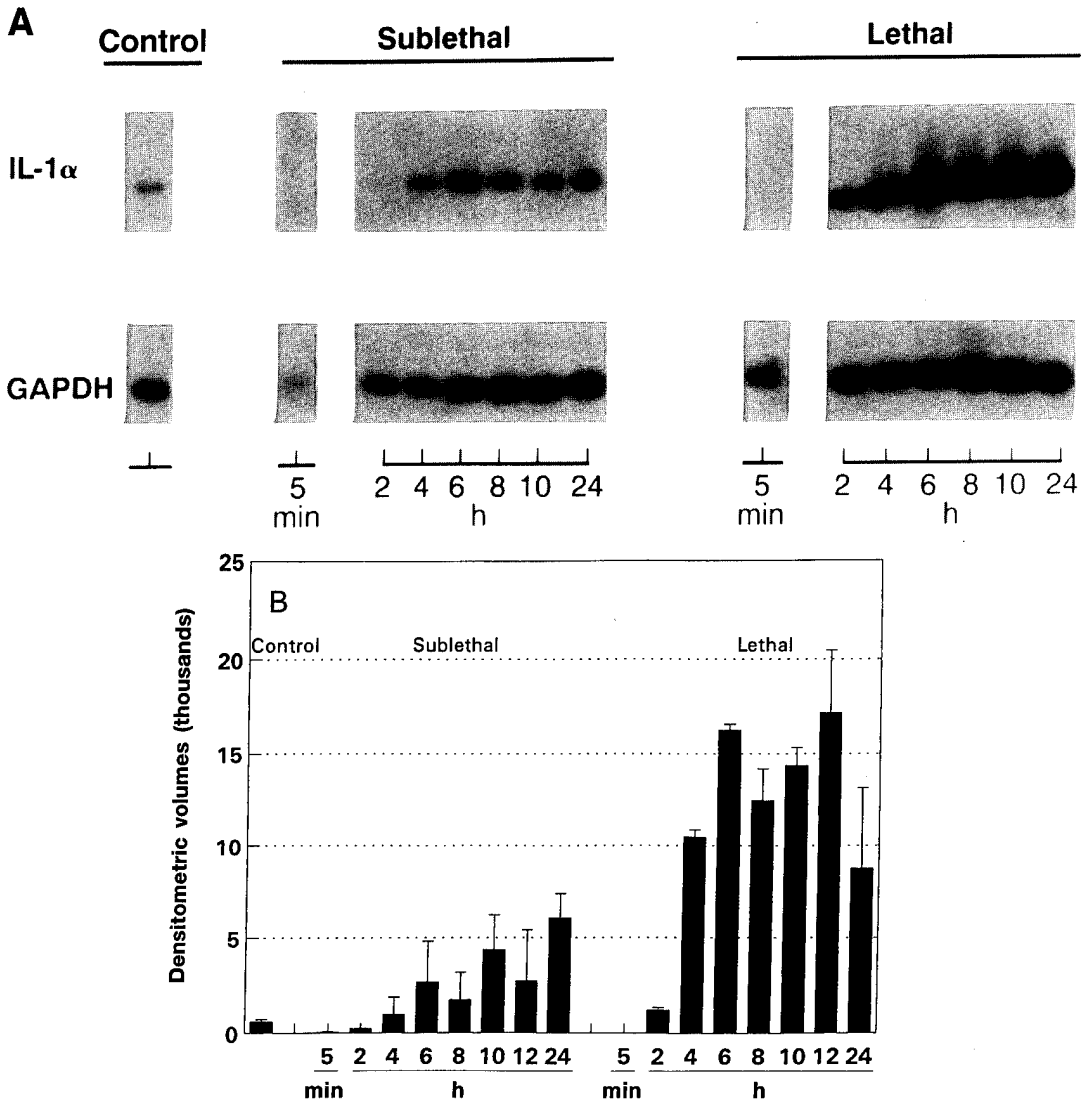

FIG. 2. Panel A: Autoradiographic image of RT-PCR products from whole spleens of control mice and sublethally (7.75 Gy) and lethally (9.75 Gy) irradiated mice harvested 5 min and 2, 4, 6, 8, 10 and 24 h after ^{60}Co irradiation. RNA was isolated, reverse-transcribed into cDNA and amplified with IL-1α or GAPDH specific primers. Panel B: Graphic display of IL-1α densitometric volumes generated from scanned autoradiographs of blotted and hybridized PCR products and normalized to GAPDH.

spleens. After sublethal and lethal exposures, lymphocyte counts declined at 5 min and 8 and 24 h to 99.3 ± 3.8, 69.5 ± 11.0 and 66.9 ± 12.3, respectively, for the 7.75-Gy group and 96.8 ± 3.8, 69.3 ± 11.2, and 56.5 ± 1.9, respectively, for the 9.75-Gy group.

DISCUSSION

Interleukin-1 is a polypeptide mediator of hematopoiesis and is involved in inflammation, immunity, and tissue and organ differentiation and development (*9, 10*). Administering IL-1 either before or after life-threatening radiation exposures in mice has been shown to improve survival (*11*). Furthermore, endogenous IL-1 has been demonstrated to be critical to postirradiation survival based on the detrimental effects of administration of anti-IL-1 receptor antibody both before and after irradiation (*2, 12*). Lethal effects of total-body exposure to ionizing radiation in these studies are manifest as damage to hematopoietic tissues, namely the bone marrow and the spleen in the mouse. *In vivo* responses of IL-1α mRNA in the mouse spleen after treatment with lipopolysaccharide (LPS) have been documented (*13*), but they have not been observed after radiation exposure. *In vitro* studies in Syrian hamster embryo cells have demonstrated that mRNA for IL-1 can be induced by X rays, γ rays and neutrons. Patterns of IL-1 induction by these three sources were similar, becoming evident at 3 h after exposure and decreasing to basal levels by 7 h after exposure (*3*).

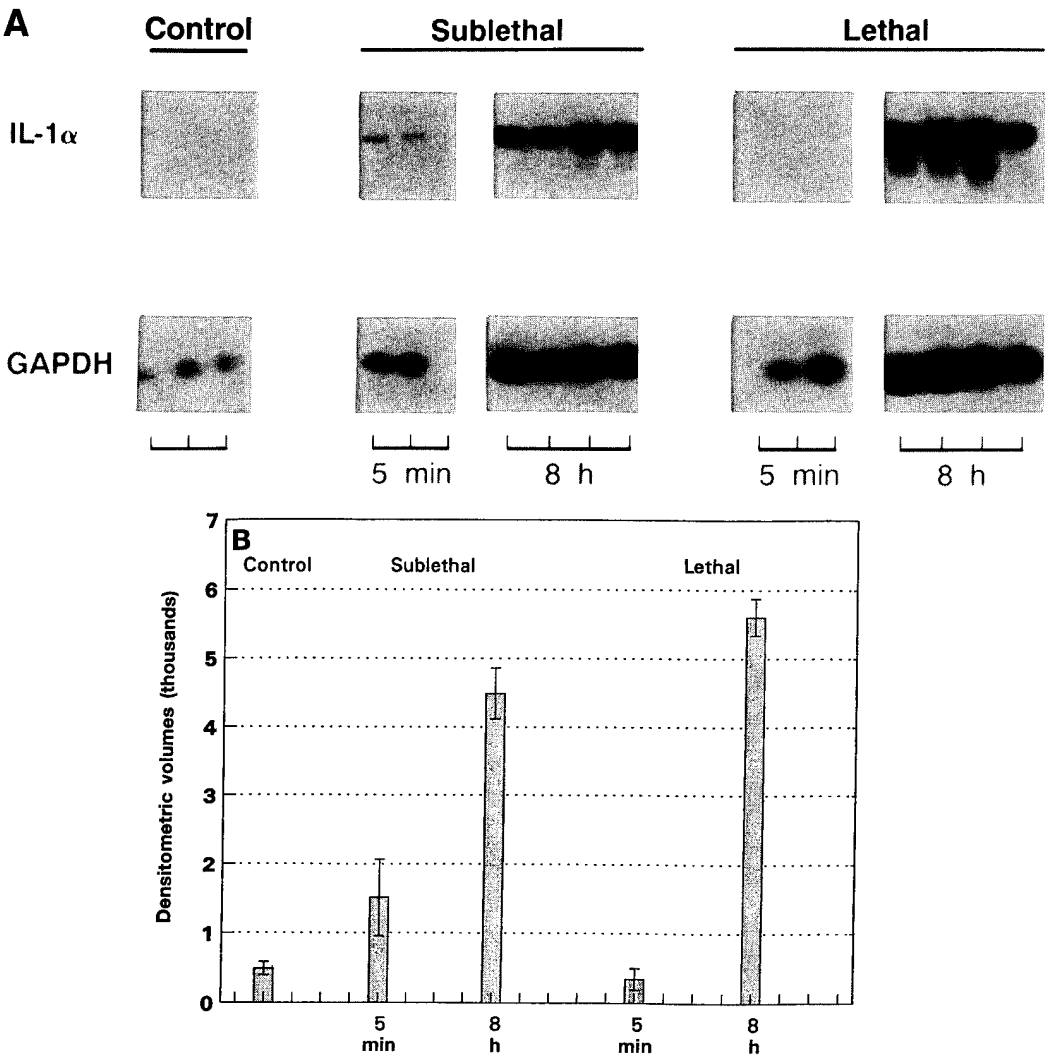

FIG. 3. Panel A: Autoradiographic image of RT-PCR products from whole spleens of control mice and sublethally (7.75 Gy) and lethally (9.75 Gy) irradiated mice harvested 5 min and 8 h after ^{60}Co irradiation. RNA was isolated, reverse-transcribed into cDNA and amplified with IL-1α or GAPDH specific primers. Panel B: Graphic display of IL-1α densitometric volumes generated from scanned autoradiographs of blotted and hybridized PCR products and normalized to GAPDH.

In our *in vivo* study, we have demonstrated an accumulation of splenic IL-1α message and an up-regulation of IL-1α protein production after sublethal and lethal exposure to total-body ionizing radiation. The accumulation of IL-1α mRNA at these doses was dependent on the time and radiation dose within the first 24 h after ^{60}Co irradiation, whereas the up-regulation of protein was dependent only on time. Contrary to our finding, Ishihara *et al.* (*6*) detected elevated accumulations of only IL-1β in whole spleens after exposure to ionizing radiation. Explanations for this discrepancy may in part be that (1) IL-1β, at least in some systems, predominates over IL-1α, and (2) they used Northern analysis for message detection rather than RT-PCR, a more sensitive technique for detecting low copy numbers of message. Compared to the *in vitro* observations noted above (*3*), our *in vivo* responses were more prolonged. This difference may be attributed to possible continued or secondary stimulation of production of IL-1 in splenic cells *in vivo* through either local paracrine or endocrine stimulation or through systemic stimulation associated with radiation damage. Longer-term experiments in our laboratory have documented elevated levels of IL-1α mRNA within the spleen beyond day 10 after sublethal irradiation (Baker, unpublished data, 1991). The effect of radiation damage may also be responsible in part for the graded increased accumulations of IL-1α message in spleens of sublethally compared to lethally exposed animals.

It could be argued that the increased levels of message specific for IL-1α observed in our study may result from a

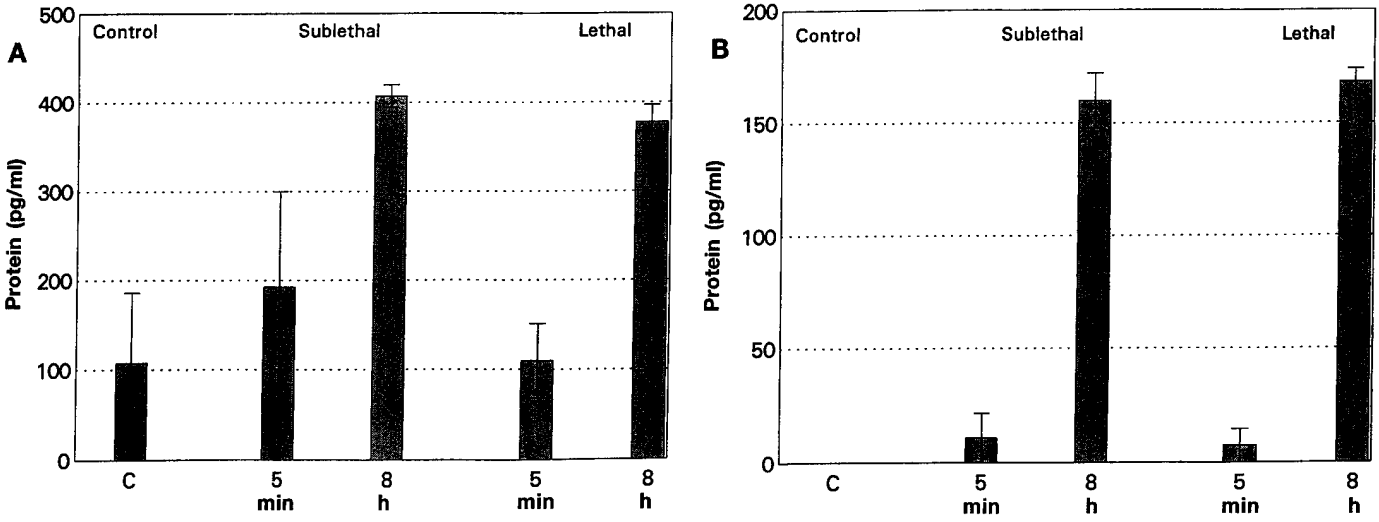

FIG. 4. Levels of IL-1α protein determined in (panel A) whole spleens and (panel B) spleen cell suspensions from control mice and from sublethally (7.75 Gy) and lethally (9.75 Gy) irradiated mice 5 min and 8 h after ^{60}Co irradiation. IL-1α was measured by ELISA. Each data point represents the mean ± standard error of values obtained from at least two observations.

selective concentration of splenic cells capable of producing IL-1α, if these cells were more radioresistant than other cells within the spleen. It is possible that some relatively radioresistant lymphocytes may be responsible for production of a fraction of the IL-1α measured (*14*); a greater portion of the IL-1α message and protein measured is likely produced by macrophages, as has been demonstrated by *in situ* hybridization in splenic red pulp, marginal zone and white pulp in normal mice and in mice after administration of LPS (*15*, *16*). Although concentration of these populations may occur, we suggest that it is not the only mechanism accounting for increased IL-1α mRNA postirradiation.

The normal mouse spleen, unlike most mammalian spleens, is an actively hematopoietic organ and a lymphoid organ as well. According to differential counts, lymphocytes constitute approximately 97% of the splenic cellularity of B6D2F$_1$ mice after sublethal or lethal ^{60}Co total-body irradiation, splenic cellularity is significantly reduced to approximately $^1/_3$ and $^1/_{10}$ of normal by 8 and 24 h, respectively. Based on differential counts, and corroborated at 24 h by FACS data in C3H/HeN mice (*17*), these changes reflect an absolute decrease in lymphocytes to $^1/_5$ and $^1/_{20}$ of normal levels by the same respective times. With reduction of cellularity by 8 h to $^1/_5$ of normal, even if all remnant cells were constitutively producing IL-1α, concentration could account for, at maximum, only a 5-fold increase in IL-1 message. Since we observed 9.1- to 11.4-fold increases in our PCR signal 8 h postirradiation, cell concentration alone does not appear to explain these changes. Additionally, the cellularity at 8 h and whole spleen RNA yields for sublethally and lethally irradiated mice were comparable, while at 8 h, IL-1α mRNA levels differed significantly.

TABLE I
Mean Splenic RNA Concentration and Cellularity in Sublethally and Lethally ^{60}Co-Irradiated Mice

	Control mice	Time after irradiation	^{60}Co irradiation 7.75 Gy (sublethal)	^{60}Co irradiation 9.75 Gy (lethal)
RNA concentration (μg)	375.4 ± 27.4	5 min	318.6 ± 61.0	374.7 ± 30.5
		8 h	247.3 ± 24.5[a]	238.3 ± 48.0[a]
		24 h	152.7 ± 15.3[a]	122.3 ± 13.1[a]
Cellularity (× 10^6)	146.2 ± 4.6	5 min	138.1 ± 5.9	144.5 ± 7.3
		8 h	50.2 ± 3.3[a]	47.0 ± 4.4[a]
		24 h	17.5 ± 0.73[a,b]	12.6 ± 0.4[a]

[a]Significantly less than normal ($P < 0.04$).
[b]Significantly greater than 9.75 Gy, 24 h observation ($P < 0.0001$).

Considering another factor that might concentrate message specific for IL-1α in our system, the 0.5-μg samples amplified by PCR represent 0.20, 0.21 and 0.13% of the total splenic RNA isolated from the 7.75 and 9.75 Gy-irradiated mice and controls, respectively. These figures represent concentrations 1.5- and 1.6-fold higher than normal levels and again are not representative of the increases in IL-1α message observed in samples at 8 h postirradiation, even when combined with the above estimates of concentration.

We therefore interpret these data to suggest that the majority of the change in IL-1α specific mRNA may be due to mechanisms over and above mere concentration of cells, such as increased IL-1α transcription and/or stabilization of IL-1α transcripts. Previous studies have reported self-induced accumulation of IL-1 mRNA in endothelial cells and fibroblasts post-transcriptionally by stabilizing RNA through activation of ribonuclease-inhibiting activity (*18*). Additional *in vitro* data have demonstrated that ionizing radiation increases levels of steady-state GM-CSF, IL-6 and IL-1β RNAs in CHU-2 and GCT cells (*19*) and levels of TNF RNAs in human myeloid leukemia cells and peripheral blood monocytes (*20*).

Regarding our data for the levels of IL-1α protein, although we detected increased levels in whole spleens, they were only three- to fourfold above control levels. Thus, although IL-1α message may stabilize and accumulate within this system, translation may not be similarly increased.

In conclusion, we have demonstrated *in vivo* accumulations of IL-1α mRNA in a time- and dose-dependent manner in the mouse spleen after sublethal and lethal exposures to γ radiation. Elevated IL-1 protein levels were likewise observed to be dependent on time, although the levels of protein expression were 1.5 to 2 magnitudes less than message accumulation. This apparent uncoupling of transcription and translation reinforces the need to examine the production of protein as well as message in such studies. Selective concentration of IL-1α-producing cells alone or other possible sources of bias considered do not appear to account for the magnitude of the change observed in levels of IL-1α mRNA in the mouse spleen in our *in vivo* system.

ACKNOWLEDGMENTS

The authors wish to thank Dr. Ueli Gubler of Hoffmann-LaRoche, Inc. for providing the murine IL-1α cDNA, M. Greenville for editorial assistance, and Roxanne Fischer and Isaac Aguilar for laboratory technical support. This research was supported by the Armed Forces Radiobiology Research Institute under work unit 00132. Views presented in this paper are those of the authors; no endorsement by the Department of Defense has been given or should be inferred. Research was conducted according to the principles enunciated in the *Guide for the Care and Use of Laboratory Animals* prepared by the Institute of Laboratory Animal Resources, National Research Council.

Received: June 22, 1994; accepted: April 24, 1995

REFERENCES

1. R. Neta, S. Douches and J. J. Oppenheim, Interleukin 1 is a radioprotector. *J. Immunol.* **138**, 2483–2485 (1986).
2. R. Neta, S. N. Vogel, J. M. Plocinski, N. S. Tare, W. Benjamin, R. Chizzonite and M. Pilcher, *In vivo* modulation with anti-interleukin-1 (IL-1) receptor (p80) antibody 35F5 of the response to IL-1. The relationship of radioprotection, colony-stimulating factor, and IL-6. *Blood* **76**, 57–62 (1990).
3. G. E. Woloschak, C-M. Chang-Liu, P. S. Jones and C. A. Jones, Modulation of gene expression in Syrian hamster embryo cells following ionizing radiation. *Cancer Res.* **50**, 339–344 (1990).
4. D. E. Hallahan, D. R. Spriggs, M. A. Beckett, D. W. Kufe and R. R. Weichselbaum, Increased tumor necrosis factor α mRNA after cellular exposure to ionizing radiation. *Proc. Natl. Acad. Sci. USA* **86**, 10104–10107 (1989).
5. R. R. Weichselbaum, D. E. Hallahan, V. Sukhatme, A. Dritschilo, M. L. Sherman and D. W. Kufe, Biological consequences of gene regulation after ionizing radiation exposure. *J. Natl. Cancer Inst.* **83**, 480–484 (1991).
6. H. Ishihara, T. K. Tsuneoka, A. B. Dimchev and M. Shikita, Induction of the expression of the interleukin-1β gene in mouse spleen by ionizing radiation. *Radiat. Res.* **133**, 321–326 (1993).
7. J. Schulz, P. R. Almond, J. R. Cunningham, J. G. Holt, R. Loevinger, N. Sunthralingam, K. A. Wright, R. Nath and D. Lempert, A protocol for the determination of absorbed dose from high energy photon and electron beams. *Med. Phys.* **10**, 741–771 (1983).
8. P. T. Lomedico, U. Gubler, C. P. Hellman, M. Dukovich, J. G. Giri, Y. C. Pan, K. Collier, R. Semionow, A. O. Chua and S. B. Mizel, Cloning and expression of murine interleukin-1 cDNA in *Escherichia coli. Nature* **312**, 458–461 (1984).
9. M. J. Fenton, Review: Transcriptional and post-transcriptional regulation of interleukin 1 gene expression. *Int. J. Immunopharmacol.* **14**, 401–411 (1992).
10. N. J. Rothwell, Functions and mechanisms of interleukin 1 in the brain. *Trends Pharmacol. Sci.* **12**, 430–436 (1991).
11. R. Neta, Cytokines in radioprotection and therapy of radiation injury. *Biotherapy* **1**, 41–45 (1988).
12. R. Neta, D. Williams, F. Selzer and J. Abrams, Inhibition of c-kit ligand/steel factor by antibodies reduces survival of lethally irradiated mice. *Blood* **81**, 324–327 (1993).
13. A. B. Troutt and F. Lee, Tissue distribution of murine hemopoietic growth factor mRNA production. *J. Cell. Physiol.* **138**, 38–44 (1989).
14. C. Cerdan, Y. Martin, H. Brailly, M. Courcoul, S. Flavetta, R. Costello, C. Mawas, F. Birg and D. Olive, IL-1α is produced by T lymphocytes activated via the CD2 plus CD28 pathways. *J. Immunol.* **146**, 560–564 (1991).
15. L. Takacs, E. J. Kovacs, M. R. Smith, H. A. Young and S. K. Durum, Detection of IL-1α and IL-1β gene expression by *in situ* hybridization. Tissue localization of IL-1 mRNA in the normal C57BL/6 mouse. *J. Immunol.* **141**, 3081–3095 (1988).
16. L. M. Duncan, L. S. Meegan and E. R. Unanue, IL-1 gene expression in lymphoid tissue. *J. Immunol.* **146**, 565–571 (1991).
17. J. L. Williams, M. L. Patchen, J. H. Darden and W. E. Jackson, Effects of radiation on survival and recovery of T lymphocyte subsets in C3H/HeN mice. *Exp. Hematol.* **22**, 510–516 (1994).
18. G. C. Bagby, Interleukin 1 and hematopoiesis. *Blood Rev.* **3**, 152–161 (1989).
19. M. Akashi, M. Hachiya, H. P. Koeffler and G. Suzuki, Irradiation increases levels of GM-CSF through RNA stabilization which requires an AU-rich region in cancer cells. *Biochem. Biophys. Res. Commun.* **189**, 986–993 (1992).
20. M. L. Sherman, R. Datta, D. E. Hallahan, R. R. Weichselbaum and D. W. Kufe, Regulation of tumor necrosis factor gene expression by ionizing radiation in human myeloid leukemia cells and peripheral blood monocytes. *J. Clin. Invest.* **87**, 1794–1797 (1991).

ARMED FORCES RADIOBIOLOGY RESEARCH INSTITUTE
SCIENTIFIC REPORT
SR95-23

Bone Marrow and Splenic Granulocyte-Macrophage Colony-Stimulating Factor and Transforming Growth Factor-β mRNA Levels in Irradiated Mice

By C.M. Chang, A. Limanni, W.H. Baker, M.E. Dobson, J.F. Kalinich, W. Jackson, and M.L. Patchen

The effects of a myeloablative sublethal 775 cGy ^{60}Co gamma radiation exposure on endogenous bone marrow (BM) and splenic granulocyte-macrophage colony-stimulating factor (GM-CSF) and transforming growth factor-β (TGF-β) mRNA levels were assayed in $B_6D_2F_1$ female mice. BM and spleen were harvested from normal mice and irradiated mice on days 2, 4, 7, 10, and 14 after exposure. Cytokine mRNA levels were determined using reverse transcription-polymerase chain reaction. After irradiation, GM-CSF mRNA levels were significantly increased in the BM from days 2 to 10 and in the spleen from days 4 to 10. However, when BM and splenic GM-CSF protein levels were measured using Western dot blot, no increased protein levels were detected. Serum GM-CSF levels were likewise unchanged. Radiation exposure did not affect BM or splenic TGF-β mRNA levels and this cytokine is known to be produced by cell populations similar to those that produce GM-CSF. These data suggest that radiation injury to hemopoietic tissues results in differential effects on GM-CSF and TGF-β mRNA levels and that, in the case of GM-CSF, increased mRNA levels are not matched by increased protein production.

THE BONE MARROW (BM) and the spleen have been recognized as important hematopoietic organs in the mouse containing both multipotential stem cells and a variety of committed progenitor cells. It is known that endogenously produced cytokines regulate hematopoietic stem and progenitor cell proliferation, differentiation, and function. Granulocyte-macrophage colony-stimulating factor (GM-CSF) is a hematopoietic cytokine with a specific ability to stimulate proliferation and maturation of granulocyte and macrophage myeloid cells.[1] A number of different cell types are able to synthesize and release GM-CSF, such as macrophages, endothelial cells, fibroblasts and stromal cells.[2] Transforming growth factor-β (TGF-β) is a multifunctional cytokine that has the ability to inhibit or stimulate the proliferation of hematopoietic progenitor cells. Goey et al[3] showed that femoral artery infusion of TGF-β_1 into normal animals partially inhibited interleukin-3 (IL-3)–induced colony-forming unit-erythroid (CFU-e) and completely prevented IL-3-induced colony-forming unit-granulocyte, erythroid, monocyte, megakaryocyte (CFU-GEMM) formation. On the other hand, Keller et al[4] showed that TGF-β can increase the differentiation of neutrophils in suspension cultures when used in combination with GM-CSF and also showed that the same combination increases granulocyte-macrophage colony-forming cells (GM-CFC) in 5-fluorouracil–treated BM. This cytokine is also known to be produced by a number of different cell types, including endothelial cells, monocytes, fibroblasts, epidermis, chondrocytes, and epithelial cells.[5]

In in vitro systems, expression of GM-CSF mRNA and production of GM-CSF protein have been shown to increase in response to stimulation with chemical and physical agents. In the MLA-144 T-cell line, which does not exhibit a detectable basal GM-CSF mRNA level, an increase in GM-CSF mRNA level was detected when cells were stimulated with phorbol 12-myristate 13-acetate.[6] Murine BM cells treated with the tumor-promoting phorbol ester 12-0-tetradecanoylphorbol-13-acetate (TPA) and lipopolysaccharide (LPS) have been shown to exhibit increased levels of GM-CSF protein.[7] Very high levels of TGF-β mRNA were also shown to be induced in mouse epidermal cells treated with TPA.[8] Furthermore, increases in the production of GM-CSF protein have been observed in murine long-term BM cultures[9,10] and in spleen cell cultures[11] after in vitro irradiation. Increases in the production of TGF-β protein have also been found in rabbit lung alveolar macrophage cell cultures after irradiation.[12] Using a murine radiation model in which a high sublethal radiation exposure was used to induce severe hematopoietic hypoplasia, we have evaluated the effects of radiation on endogenous GM-CSF and TGF-β mRNA levels in vivo.

MATERIALS AND METHODS

Mice. $B_6D_2F_1$ female mice (approximately 20 g) were purchased from Jackson Laboratories (Bar Harbor, ME). Mice were maintained in a facility accredited by American Association for the Accreditation of Laboratory Animal Care (AAALAC) in Micro-Isolator cages on hardwood-chip contact bedding and were provided commercial rodent chow and acidified water (pH 2.5) ad libitum. Animal rooms were equipped with full-spectrum light from 0600 to 1800 hours and were maintained at 21°C ± 1°C and 50% ± 10% relative humidity with at least 10 air changes per hour of 100% conditioned fresh air. On arrival, all mice were tested for *Pseudomonas* and quarantined until test results were obtained. Only healthy mice were released for experimentation. All animal experiments were approved by the Institute Animal Care and Use Committee before they were performed.

Irradiation. The ^{60}Co source at the Armed Forces Radiobiology Research Institute (AFRRI) was used to administer bilateral total-body gamma radiation. Mice were placed in ventilated Plexiglas containers and sublethally irradiated at a dose of 775 cGy. Dosimetry was performed using ionization chambers as previously described,[13] with calibration factors traceable to the National Institute of Stan-

From the Departments of Experimental Hematology, Radiation Biochemistry, and Computer and Electronics, Armed Forces Radiobiology Research Institute, Bethesda, MD.

Submitted November 10, 1994; accepted May 8, 1995.

Supported by the Armed Forces Radiobiology Research Institute, Defense Nuclear Agency, under research work unit no. 00132. Research was conducted according to the principles enunciated in the "Guide for the Care and Use of Laboratory Animals" prepared by the Institute of Laboratory Animal Resources, National Research Council.

Address reprint requests to C.M. Chang, PhD, Department of Experimental Hematology, Armed Forces Radiobiology Research Institute, 8901 Wisconsin Ave, Bethesda, MD 20889-5603.

The publication costs of this article were defrayed in part by page charge payment. This article must therefore be hereby marked "advertisement" in accordance with 18 U.S.C. section 1734 solely to indicate this fact.

0006-4971/95/8606-0018$0.00/0

dards and Technology. Before experiments were initiated, the dose rate at the midline of an acrylic mouse phantom was measured with a 0.5-mL tissue-equivalent ionization chamber manufactured by Exradin (Lisle, IL). Before each experimental irradiation, the dose rate at the same location with the phantom removed was measured with a 50-mL ionization chamber fabricated at AFRRI. The ratio of these two dose rates, the tissue-air ratio (TAR), was then used to ensure delivery of the midline dose desired for each animal exposure. The TAR in these experiments was 0.96, and dose variation within the exposure field was less than 3%.

Cells and tissues. Femurs and spleens were harvested from normal and irradiated mice on days 2, 4, 7, 10, and 14 postirradiation after euthanization by cervical dislocation. Tissues from 3 to 7 mice were pooled to obtain sufficient cells for each specific assay. BM cells were flushed from femurs with 3.0 mL of McCoy's 5A medium (Flow Labs, McLean, VA) containing 10% heat-inactivated fetal bovine serum (Hyclone Labs, Logan, UT). In mRNA and protein studies, spleens were homogenized with a polytron homogenizer. For cell culture studies, spleens were pressed through a stainless steel mesh screen, and the cells were washed from the screen with 6.0 mL of McCoy's 5A medium. The number of nucleated cells in the BM and splenic suspensions was determined using a Coulter counter (Coulter, Hialeah, FL). To obtain serum from normal and irradiated mice on days 2, 4, 8, 10, 14, and 17 postexposure, animals were halothane-anesthesized and blood was drawn by cardiac puncture using a syringe attached to a 20-gauge needle.

Reverse transcription-polymerase chain reaction (RT-PCR) and Southern blotting. Total RNA was extracted from BM suspensions and homogenized spleens using the RNAzol method (Tel-Test Inc, Friendswood, TX) as modified from Chomczynski and Sacchi.[15] RNA concentrations were determined spectrophotometrically from absorbance at 260 nm. Total RNA of each sample was characterized by ethidium bromide staining of agarose gels to ensure use of only intact RNA. Intact total RNA was reversely transcribed into first-strand cDNA, which was then amplified using PCR. The final volume of 5 μL RT reaction mixture contained 0.1 μg BM total RNA or 0.5 μg splenic total RNA; 50 mmol/L Tris-HCl (pH 8.3); 3 mmol/L $MgCl_2$; 75 mmol/L KCl; 2.5 μg/mL oligo$(dT)_{12\text{-}18}$; 1 mmol/L each of dATP, dGTP, dTTP, and dCTP; and 10 U Moloney murine leukemia virus RT. The reaction mixture for RT was incubated at 37°C for 1 hour and at 90°C for 10 minutes and chilled on ice for 10 minutes. The PCR primers for GM-CSF, TGF-β, or glyceraldehyde-3-phosphate dehydrogenase (GAPDH) mRNA were purchased from Clontech Laboratories, Inc (Palo Alto, CA). The sequence of primers and expected product size are described in Table 1. The reaction mixture for PCR contained 5 μL cDNA template from the RT reaction; 10 mmol/L Tris-HCl (pH 8.3); 50 mmol/L KCl; 1.5 mmol/L $MgCl_2$; 0.8 mmol/L each of dATP, dGTP, dTTP, and dCTP; 1.0 μmol/L 5′-primer; 1.0 μmol/L 3′-primer; and 1.25 U Taq DNA polymerase. PCR was performed with a DNA Thermal Cycler (Perkin Elmer-Cetus, Norwalk, CT) at 94°C for 1 minute, at 60°C for 2 minutes, and at 72 °C for 3 minutes per cycle until the optimum number of cycles was reached. The amplified products were electrophoresed in a 1% agarose gel in the presence of 1 μg/mL ethidium bromide, transferred onto Nytran membrane (Schleicher & Schuell, Keene, NH), and hybridized with ^{32}P-labeled murine GM-CSF, TGF-β, and GAPDH probes. The probes were ^{32}P-labeled with a nick-translation commercial kit (Bethesda Research Laboratories, Gaithersburg, MD). The steps of hybridization were as follows. Prehybridization was performed in a solution containing 50% formamide solution, 6× SSC, 5× Denhardt's, 50 mmol/L Tris, 100 μg/mL salmon sperm DNA, and 1% sodium dodecyl sulfate (SDS) at 42°C; overnight hybridization was performed in the same solution after the addition of its respective ^{32}P-labeled cytokine probe. Subsequently, blots were washed three times at 42°C in a solution containing 2× SSC and 0.5% SDS and finally at 62°C in a solution containing 0.1× SSC and 0.1% SDS for 1 hour. Autoradiography was performed at −70°C using Kodak XAR film (Eastman Kodak, Rochester, NY).

Table 1. Sequence of Amplimer Set for Murine Cytokines

Cytokine	Sequence	Fragment (bp)
GM-CSF		
5′-primer	5′-TGTGGTCTACAGCCTCTCAGCAC-3′	368*
3′-primer	5′-CAAAGGGGATATCAGTCAGAAAGGT-3′	1964†
TGF-β		
5′-primer	5′-TGGACCGCAACAACGCCATCTATGAGAAAACC-3′	525
3′-primer	5′-TGGAGCTGAAGCAATAGTTGGTATCCAGGGCT-3′	
GAPDH		
5′-primer	5′-CCATGGAGAAGGCTGGGG-3′	195
3′-primer	5′-CAAAGTTGTCATGGATGACC-3′	

* Spliced
† Unspliced.

GM-CFC assay. BM and splenic hematopoietic progenitor cells committed to granulocyte and/or macrophage development were assayed using a double-layer agar GM-CFC assay.[14] Mouse endotoxin serum (5% vol/vol) was added to feeder layers as a source of colony-stimulating factors. Colonies (>50 cells) were counted after 10 days of incubation in a 37°C humidified environment containing 5% CO_2. Triplicate plates were cultured for each cell suspension, and experiments were repeated three times. A similar procedure was used to evaluate colony-stimulating activity in serum from normal and irradiated mice. In these studies 5% or 10% (vol/vol) of test serum was added to the feeder layers and cultured with 5×10^4 normal BM cells as the target population. Both GM-CFC colony (>50 cells) and cluster (<50 cells) formation was evaluated.

GM-CSF protein assays. BM and splenic GM-CSF protein were assayed using the Western dot blot technique. BM single-cell suspensions and splenic homogenates were placed on ice and disrupted by 5 seconds of sonication (Heat Systems Cell Disrupter with Microtip, Farmingdale, NY). The method of Bradford[16] was used to determine protein concentrations. A modification of the method of Hawkes et al[17] was used to determine the relative amounts of GM-CSF in the cell homogenates. Briefly, 10 μg of total cellular protein was blotted onto a 0.45-μm nitrocellulose membrane (Schleicher & Schuell) for 1 hour using a dot blotting apparatus (Bethesda Research Laboratories). After blocking the nitrocellulose by incubation for 60 minutes at room temperature with phosphate-buffered saline (PBS) containing 5% nonfat dried milk, the blot was incubated overnight at 4°C with a goat polyclonal antibody against recombinant murine GM-CSF (R & D Systems, Minneapolis, MN) at 10 μg/mL in PBS/5% bovine serum albumin (BSA) containing 0.1% thimerosal. The blot was washed three times (10 minutes each) in PBS/0.1% Tween-20 before incubating for 60 minutes at room temperature with a 1,000x dilution of rabbit antigoat IgG horseradish peroxidase conjugate (Sigma, St Louis, MO) in 1% gelatin. The blot was then washed six times (5 minutes each) in PBS/0.1% Tween-20 before detection of the peroxidase activity using the substrate 4-chloro-1-naphthol (Sigma) in the presence of hydrogen peroxide. After completion of the color reaction, the blots were washed with distilled water and dried. Serum GM-CSF protein was measured using a commercial enzyme-linked immunosorbent assay (ELISA) kit (Endogen, Inc, Boston, MA). Sera obtained from 10 normal or irradiated mice were pooled for use in this assay. Assays were performed according to the manufacturer's instructions after twofold dilution of the sera using the standard diluent supplied with the kit.

Quantitation. Each sample's densitometric volume was measured using a scanning laser densitometer (Model 300B; Molecular Dynamics, Sunnyvale, CA) by measuring the gray density of the entire PCR product band in each lane or color intensity of dot blot in each well. The images were analyzed using ImageQuant software version 3.2

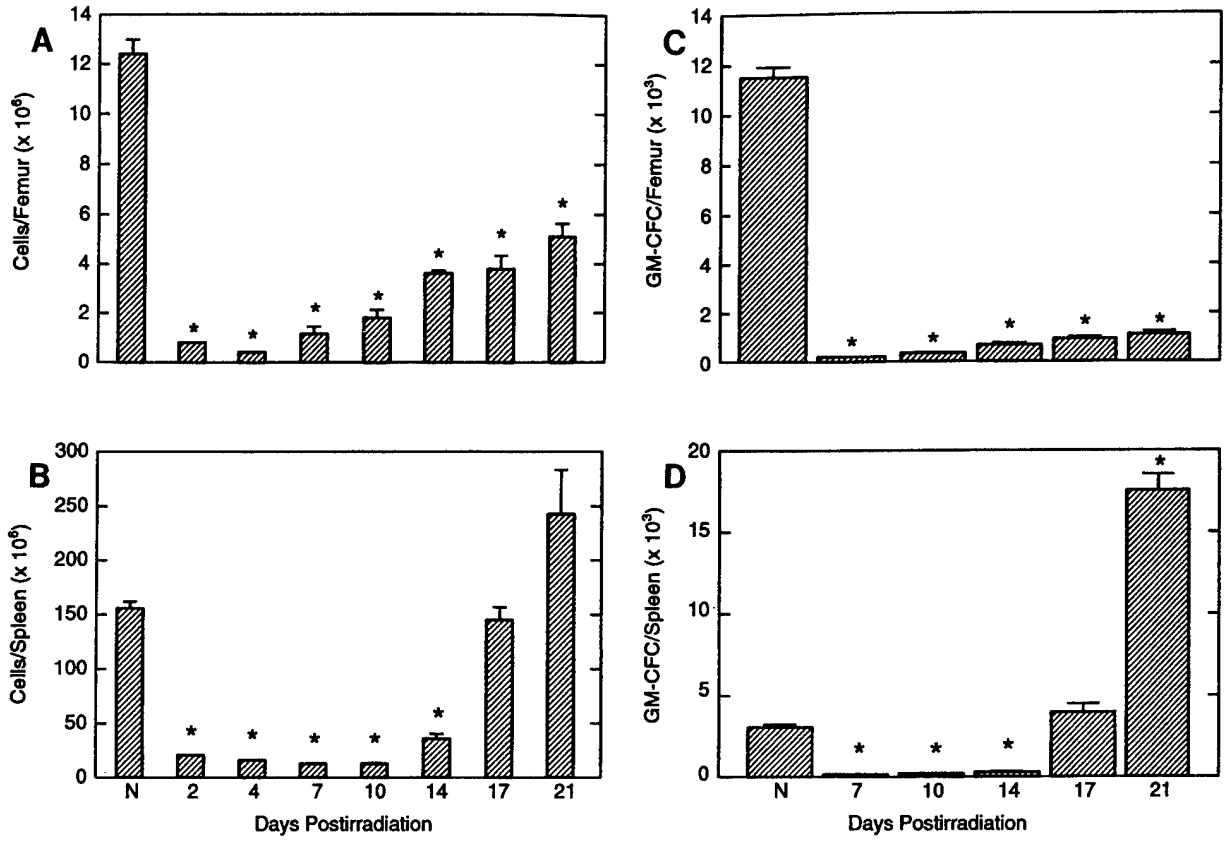

Fig 1. BM (A) and splenic (B) cellularity in normal mice (N) and in irradiated mice on days 2, 4, 7, 10, 14, 17, and 21. GM-CFC recovery in BM (C) and spleen (D) in normal (N) and irradiated mice at days 7, 10, 14, 17, and 21 after 775 cGy ^{60}Co gamma exposure. Data represent the mean ± SEM of values obtained from three experiments. *$P < .05$ with respect to normal control values.

(Molecular Dynamics), which was supplied with the densitometer. PCR product and protein comparisons were then based on relative expression differences between irradiated and control samples.

Statistics. *t*-tests were used to analyze all data. Data from mRNA and protein experiments are expressed as a percentage of the control value for each experiment (ie, percentage of normal). Data were then log transformed before calculating means and standard errors and *t*-tests were performed (in log units) comparing each mean with 100% (normal controls). All *P* values were Bonferroni corrected. *P* values of less than .05 were considered to be statistically significant.

RESULTS

Radiation-induced changes in cellularity. Changes in BM and splenic cellularity after radiation are illustrated in Fig 1A and B. The number of BM cells at days 2 and 4 decreased to approximately 5.8% and 3.0% of control mice, respectively. On subsequent days, a gradual recovery toward normal levels was observed; however, even at day 21 postirradiation, BM cell numbers recovered to only 41.2% of normal controls. In the spleen, cellularity decreased to 13.3% of control values by day 2 postirradiation and remained at approximately this level through day 10. However, between days 14 and 17 a dramatic recovery to normal levels occurred and progressed to supranormal levels at day 21 (156% of control values).

Radiation-induced changes in GM-CFC progenitor cells. After irradiation, dramatic decreases in the number of GM-CFC progenitor cells in the BM and the spleen also occurred (Fig 1C and D). BM GM-CFC numbers were reduced to almost undetectable levels by day 7; by day 21 postirradiation, they had recovered to only 9.6% of normal. Splenic GM-CFC numbers were also reduced to almost undetectable levels by day 7; however, between days 14 and 17 a dramatic recovery to normal GM-CFC levels occurred that overshot normal levels by 5.8-fold on day 21 postirradiation.

Effects of radiation on GM-CSF mRNA levels. Autoradiographs of RT-PCR–amplified GM-CSF mRNA transcripts of BM and spleen from one representative experiment are shown in Fig 2. The average relative GM-CSF mRNA levels obtained from four BM experiments and three spleen experiments are shown in Fig 3. BM GM-CSF mRNA levels were significantly increased by day 2 and remained elevated through day 10 postirradiation. By day 14, BM GM-CSF mRNA levels had decreased to within the normal range. GM-CSF mRNA levels in the spleen were also significantly increased from day 4 to day 10 and also returned to normal levels by day 14 postirradiation. GAPDH mRNA levels were measured by simultaneous RT-PCR of aliquots of RNA from each specimen (data not shown). GAPDH mRNA levels did increase significantly to about 2.5 times normal at day 4 and 7 after irradiation, but correction for these changes failed to explain the larger increases in GM-CSF transcript levels.

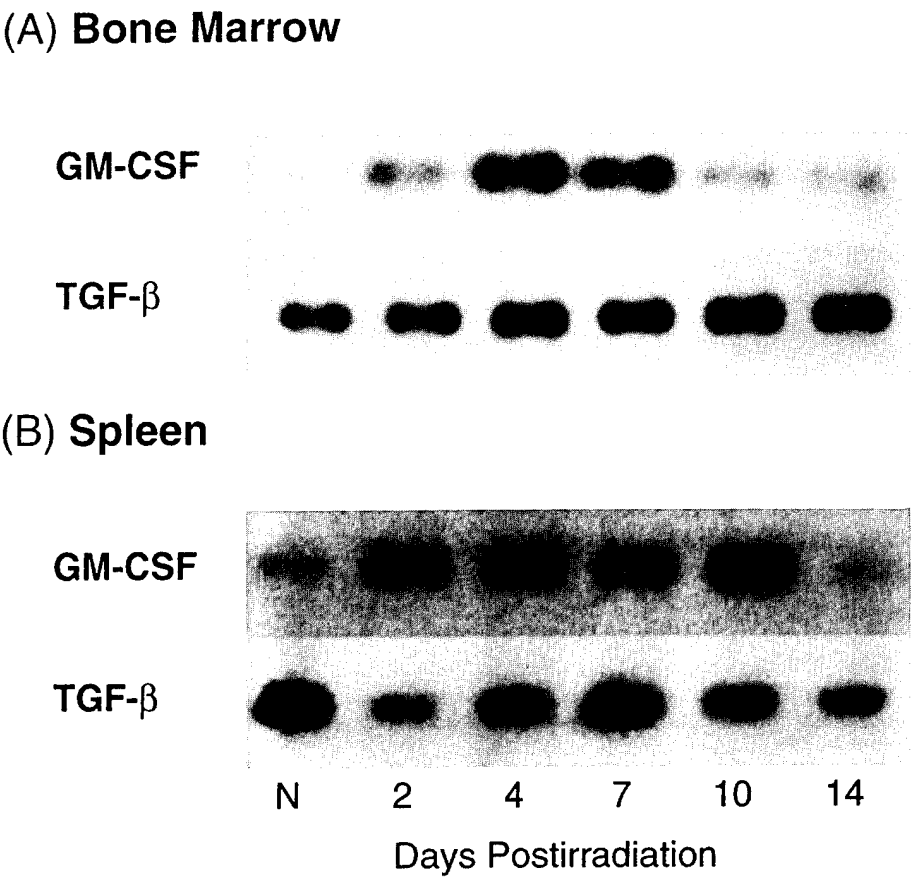

Fig 2. Representative autoradiographs of RT-PCR–amplified mRNA transcripts of GM-CSF and TGF-β in BM (A) and spleen (B) of normal mice (N) and of irradiated mice on days 2, 4, 7, 10, and 14 after 775 cGy ^{60}Co gamma radiation exposure. Each blot represents only one of three or four experiments performed for each gene in each tissue.

Effects of radiation on TGF-β mRNA levels. Autoradiographs of RT-PCR–amplified TGF-β mRNA transcripts of BM and spleen from one representative experiment are also shown in Fig 2. The average relative TGF-β mRNA levels obtained from three BM and spleen experiments are shown in Fig 4. Compared with normal controls, no significant differences in either BM or splenic TGF-β mRNA levels were detected at any recovery day after irradiation.

Effects of radiation on GM-CSF protein production. Because increased GM-CSF mRNA levels were observed after irradiation, it was thought that GM-CSF protein levels would also be increased. Using the Western dot blot technique, BM and splenic GM-CSF protein levels of normal mice and irradiated mice on days 2, 4, 7, 10, and 14 postexposure are shown in Table 2. Surprisingly, BM and splenic GM-CSF protein levels were not significantly different from normal controls at any recovery day after irradiation. GM-CSF levels were also evaluated in serum from normal mice and irradiated mice on days 2, 4, 8, 10, 14, and 17 postexposure using an ELISA assay capable of detecting down to 3.9 pg/mL of murine GM-CSF. In this assay, serum GM-CSF protein was also not detected (data not shown). However, sera from irradiated mice were able to support GM-CFC colony and cluster formation to a much greater extent than normal serum (Fig 5).

DISCUSSION

Hematopoietic recovery after sublethal myeloablative injury is presumed to be mediated by endogenously produced hematopoietic growth factors. In this study, we evaluated the effects of a sublethal radiation exposure on GM-CSF and TGF-β mRNA levels. Because increases in GM-CSF message levels were detected, GM-CSF protein levels were also evaluated. To perform message evaluations, detection and semiquantitation for GM-CSF and TGF-β mRNA levels using the RT-PCR method and Southern blot analysis were established using as little as 0.1 μg of total RNA. This was critical for evaluations in radiation studies in which cell numbers and RNA concentrations were extremely low at days 2, 4, and 7 postirradiation, thus obviating the use of traditional techniques such as Northern blot and RNase protection assays.

Significant increases from basal GM-CSF mRNA levels occurred during the period of postirradiation hematopoietic regeneration, with BM responses being more dramatic than those in the spleen. At days 2, 4, 7, and 10 postirradiation, BM GM-CSF mRNA levels increased approximately 11.6-, 12.1-, 16.1-, and 6.9-fold over normal controls, whereas splenic GM-CSF mRNA levels at days 4, 7, and 10 increased about 3.6-, 3.7-, and 5.5-fold over normal controls, respectively. By 2 weeks after irradiation, GM-CSF mRNA levels in both tissues had returned to normal levels.

Because it was not until day 14 or later that significant BM or splenic GM-CFC recovery was detected in irradiated mice, it appeared that GM-CSF mRNA expression preceded hematopoietic regeneration. However, despite the increase in the levels of GM-CSF mRNA in both BM and spleen, no increase in the levels of GM-CSF protein in BM, spleen, or

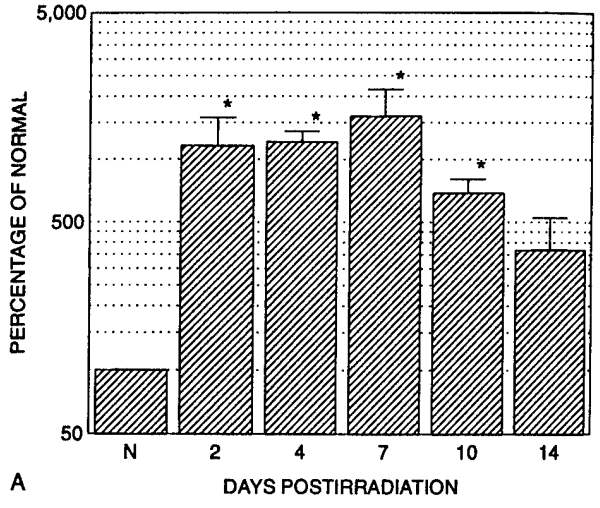

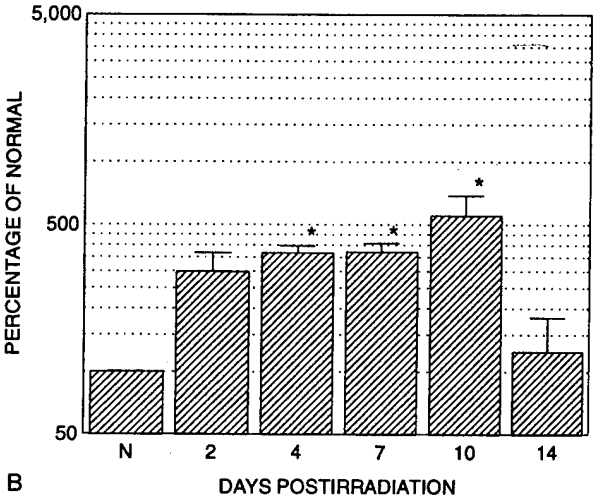

Fig 3. BM (A) and splenic (B) GM-CSF mRNA levels in normal mice (N) and in irradiated mice on days 2, 4, 7, 10, and 14 after 775 cGy ^{60}Co gamma exposure. Data are presented as the percentage of normal control levels and represent the mean ± SEM of values obtained from four BM experiments and three splenic experiments. *$P < .05$ with respect to normal control values.

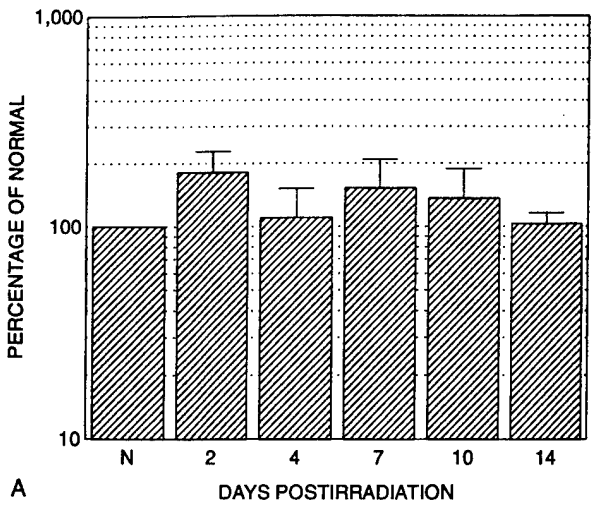

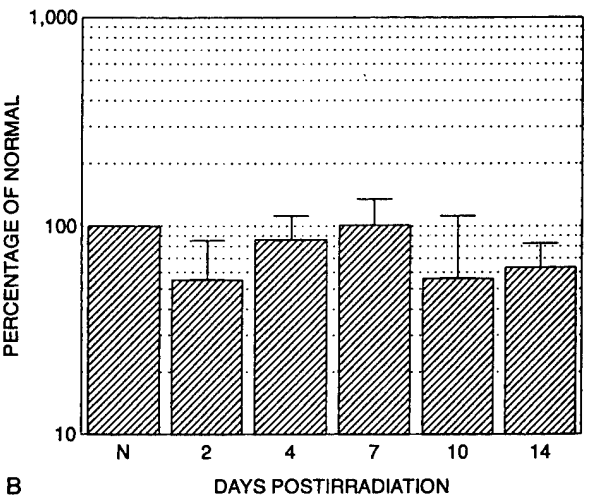

Fig 4. BM (A) and splenic (B) TGF-β mRNA levels in normal mice (N) and in irradiated mice on days 2, 4, 7, 10, and 14 after 775 cGy ^{60}Co gamma exposure. Data are presented as the percentage of normal control levels and represent the mean ± SEM of values obtained from three experiments.

serum could be detected using Western dot blot and ELISA assays. These data suggest that GM-CSF mRNA levels have been increased after irradiation without an increase in protein production. Using human monocytes stimulated with recombinant C5a, Geiger et al[18] have shown that two signals are necessary for the induction of IL-1β: one signal for transcriptional activation and another signal for translational activation. It is possible that a similar mechanism is used for GM-CSF production. It is also possible that the increases in GM-CSF mRNA levels observed in our experiments were due simply to message stabilization. After irradiating CHU-2 and GCT cell cultures, Akashi et al[19] showed that the levels of GM-CSF mRNA in these cells increased at least partially due to stabilization of the GM-CSF mRNA and were specifically associated with the multiple repeated AUUUA motif found in the 3′ untranslated region of the GM-CSF mRNA. The lack of increased GM-CSF protein production after irradiation in our studies may also be the result of altered posttranscriptional processing. The absence of high molecular weight RT-PCR GM-CSF products (data not shown) using primers that span introns rules out altered splicing mechanisms. Simi-

Table 2. Effects of a 775 cGy ^{60}Co Gamma Radiation Exposure on BM and Splenic GM-CSF Protein Levels in Mice

Day Postirradiation	BM	Spleen
2	100.6 ± 1.6	102.2 ± 1.2
4	100.3 ± 1.3	101.8 ± 2.0
7	97.9 ± 2.5	99.2 ± 1.2
10	102.3 ± 1.6	97.9 ± 1.5
14	98.9 ± 2.6	98.0 ± 0.9

Results are from densitometric analyses of Western dot blot. The values of GM-CSF protein are expressed as a percentage of normal control values. Data represent the mean ± SEM of values obtained from three experiments.

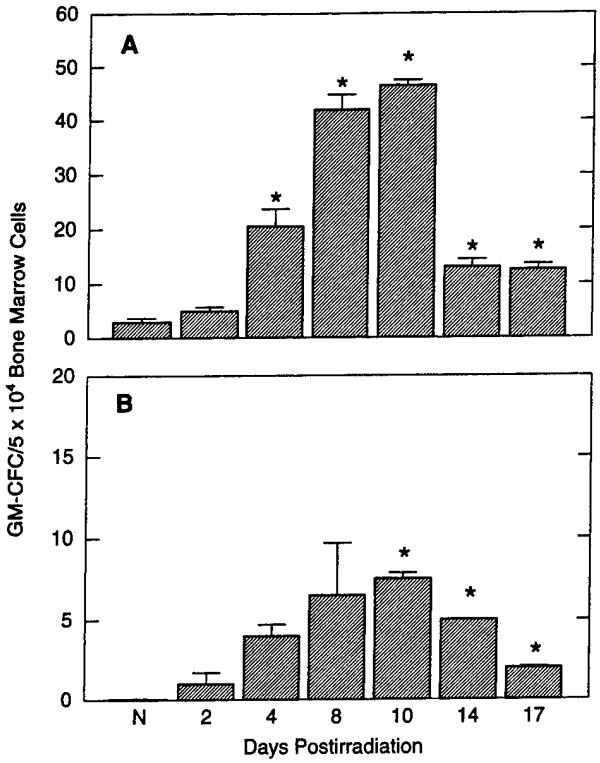

Fig 5. Colony-stimulating activity of 100 μL of serum from normal (N) and irradiated mice on days 2, 4, 8, 10, 14, and 17 after 775 cGy ^{60}Co gamma radiation exposure. Total GM-CFC colony and cluster formation (A) versus GM-CFC colony formation (B). Data represent the mean ± SEM of values from triplicate plates in a single experiment.

larly, the use of poly dT for priming of the reverse transcriptase reaction indicates that proper polyadenylation of the mRNA has taken place. Alternatively, GM-CSF protein may be produced but is secreted so rapidly that intracellular pools do not appear to change. However, if that were the case, it is likely that we would have observed increased levels of GM-CSF in the sera when assayed by ELISA, which we did not. This then would leave the remote possibility that the secreted GM-CSF is rapidly bound to the target cells and turned over in a manner that makes it undetectable by the assays used. Although we did not detect GM-CSF proteins in the serum of irradiated mice using the ELISA assay, we did detect colony-stimulating activity using a GM-CFC bioassay. However, increases in the levels of a number of other cytokines could have produced this effect even in the absence of GM-CSF.[20,21] Finally, it is possible that GM-CSF may play a minor role in the postirradiation recovery of hematopoietic cells. Studies by Neta et al[22] evaluating the radioprotective effects of LPS and IL-1 in the mouse have shown that treatment with GM-CSF antibodies does not detrimentally affect LPS- and IL-1–induced hematopoietic recovery and mouse survivability after irradiation.

In contrast to the results given above, we observed no change in the levels of TGF-β mRNA in either the BM or the spleen after irradiation when compared with unirradiated controls. Because both GM-CSF and TGF-β are produced by similar cell types, these results suggest that the observed increases in the levels of GM-CSF mRNA in both BM and spleen after irradiation are not due to an increase in the percentage of cells producing GM-CSF in these organs but rather represent a genuine increase in the levels of mRNA present in the cells. Although we cannot rule out the level of GM-CSF mRNA per cell remaining constant with the level of TGF-β mRNA decreasing, we consider this explanation to be unlikely given the nearly identical levels of TGF-β in the control and experimental cell populations and the known effects of increased stability of GM-CSF mRNA after irradiation in in vitro studies.

In conclusion, we have shown that (1) using RT-PCR we can detect quantitative changes in the levels of GM-CSF mRNA but not TGF-β mRNA in the BM and spleen of irradiated mice relative to unirradiated mice; (2) the changes observed in the levels of GM-CSF mRNA vary in a tissue- and time-specific manner; and (3) the levels of GM-CSF protein in the BM, spleen, and serum do not appear to increase after sublethal irradiation relative to controls.

ACKNOWLEDGMENT

The authors are grateful to Dr Su Wen Qian for the rat TGF-β cDNA plasmid DNA; to Ruth Seeman, Roxanne Fischer, and Drusilla Hale for technical assistance; to Dr David McClain, James Speicher, and Linda Tiller for assistance in using the laser densitometer; and to Modeste Greenville for editorial assistance.

REFERENCES

1. Metcalf D: The granulocyte-macrophage colony-stimulating factors. Science 229:16, 1985

2. Demetri GD: Hematopoietic growth factors: Current knowledge and future prospects. Curr Probl Cancer 16:178, 1992

3. Goey H, Keller JR, Back T, Longo DL, Ruscetti FW, Wiltrout RH: Inhibition of early murine hemopoietic progenitor cell proliferation after in vivo locoregional administration of transforming growth factor-β_1. J Immunol 143:877, 1989

4. Keller JR, Jacobson SEW, Sill KT, Ellingsworth LR, Ruscetti FW: Stimulation of granulopoiesis by transforming growth factor β: Synergy with granulocyte/macrophage colony-stimulating factor. Proc Natl Acad Sci USA 88:7190, 1991

5. Thompson NL, Flanders KC, Smith JM, Ellingsworth LR, Roberts AB, Sporn MB: Expression of transforming growth factor-β_1 in specific cells and tissues of adult and neonatal mice. J Cell Biol 108:661, 1989

6. Gilliland G, Perrin S, Blanchard K, Bunn HF: Analysis of cytokine mRNA and DNA: Detection and quantitation by competitive polymerase chain reaction. Proc Natl Acad Sci USA 87:2725, 1990

7. Pluznik DH, Mergenhagen SE: Synergistic action of lipopolysaccharide and tumor-promoting phorbol esters: Two-signal requirement for colony-stimulating factor production by murine bone marrow cells. Exp Hematol 14:1029, 1986

8. Akhurst RJ, Fee F, Balmain A: Localized production of TGF-β mRNA in tumor promoter-stimulated mouse epidermis. Nature 331:363, 1988

9. Hall BM: The effects of whole body irradiation on serum colony stimulating factor and in vitro colony-forming cells in the bone marrow. Br J Haematol 17:553, 1969

10. Naparstek E, Donnelly T, Kase K, Greenberger JS: Biologic effects of in vitro X-irradiation of murine long-term bone marrow cultures on the production of granulocyte-macrophage colony-stimulating factors. Exp Hematol 13:701, 1985

11. Onoda M, Shinoda M, Tsuneoka K, Shikita M: X-ray-induced production of granulocyte-macrophage colony-stimulating factor (GM-CSF) by mouse spleen cells in culture. J Cell Physiol 104:11, 1980

12. Rubin P, Finkelstein J, Shapiro D: Molecular biology mechanisms in the radiation induction of pulmonary injury syndromes: Interrelationship between the alveolar macrophage and the septal fibroblast. Int J Radiat Oncol Biol Phys 24:93, 1992

13. Schulz J, Almond PR, Cunningham JR, Holt JG, Loevinger R, Suntharalingam N, Wright KA, Nath R, Lempert D: A protocol for the determination of absorbed dose for high-energy photon and electron beams. Med Physiol 10:741, 1983

14. Patchen ML, MacVittie TJ: Hemopoietic effects of intravenous soluble glycan administration. J Immunopharmacol 8:407, 1986

15. Chomczynski P, Sacchi N: Single-step method of RNA isolation by acid guanidinium thiocyanate-phenol-chloroform extraction. Anal Biochem 162:156, 1987

16. Bradford M: A rapid and sensitive method for the quantitation of microgram quantities of protein utilizing the principle of protein-dye binding. Anal Biochem 42:248, 1976

17. Hawkes R, Niday E, Gordon J: A dot-immunobinding assay for monoclonal and other antibodies. Anal Biochem 119:142, 1982

18. Geiger T, Rordorf C, Galakatos N, Seligmann B, Henn R, Lazdin J, Erard F, Vosbeck K: Recombinant human C5a induces transcription but not translation of interleukin-1β mRNA in human monocytes. Lymphokine Cytokine Res 11:55, 1992

19. Akashi M, Hachiya M, Koeffler HP, Suzuki G: Irradiation increases levels of GM-CSF through RNA stabilization which requires an AU-rich region in cancer cells. Biochem Biophys Res Commun 189:986, 1992

20. Ogawa M: Differentiation and proliferation of hematopoietic stem cells. Blood 81:2844, 1993

21. Metcalf D: Hematopoietic regulators: Redundancy or subtlety? Blood 82:3515, 1993

22. Neta R, Williams D, Selzer F, Abrams J: Inhibition of c-kit ligand/steel factor by antibodies reduces survival of lethally irradiated mice. Blood 81:324, 1993

INT. J. RADIAT. BIOL., 1995, VOL. 68, NO. 3, 311–320

Mixed-field neutrons and γ photons induce different changes in ileal bacteria and correlated sepsis in mice

T. B. ELLIOTT*, G. D. LEDNEY, R. A. HARDING, P. L. HENDERSON, H. M. GERSTENBERG†, J. R. ROTRUCK‡, M. H. VERDOLIN‡, C. M. STILLE§, and A. G. KRIEGER¶

(Received 6 February 1995; revision received 11 May 1995; accepted 24 May 1995)

Abstract. High doses of radiation induce septicaemia, from bacterial translocation, and death in animals. Mice were exposed to either comparable lethal ($LD_{90/30}$) or sublethal ($LD_{0/30}$) doses of mixed-field [$n/(n+\gamma) = 0{\cdot}67$] or pure ^{60}Co γ-photon radiation. The relative biological effectiveness of these comparable doses of radiation was 1·82, determined by probit analysis. Mice given a lethal dose of mixed-field radiation developed a significant ($p < 0{\cdot}01$), 10^9-fold increase in Gram-negative facultative bacteria in their ilea over values in control mice. In contrast, mice given a lethal dose of γ-photon radiation developed a significant ($p < 0{\cdot}01$) increase in only Gram-positive bacteria in their ilea, while the number of Gram-negative bacteria remained near values in control mice. Data correlated with bacteria that were isolated and identified from the livers of mice that were given comparable lethal doses ($LD_{99/30}$) of mixed-field or γ-photon radiation. In sublethally irradiated mice, fluctuation in the total number of bacteria was detected in their ilea during the first week following irradiation, after which the number approximated the value in control mice. This difference in the predominant facultative bacteria in ilea resulting from different qualities of radiation has important implications for the treatment of septicaemic-irradiated hosts.

1. Introduction

Exposure to neutron or γ-photon radiation results in an antimicrobial defense system compromised severely enough to lead to sepsis and death (Lawrence and Tennant 1937, Miller *et al.* 1951, Vogel *et al.* 1954, Ledney *et al.* 1991). Bacterial microflora of the intestine are probably responsible for septicaemia in irradiated animals (Miller *et al.* 1951, Guzman-Stein *et al.* 1989) and in animals subjected to other forms of stress, including burns (Berg 1992) and wound trauma (Ledney *et al.* 1991). Although Miller *et al.* (1951) suggested that the caecum is the probable source of bacteraemia after X-irradiation (600 r) in mice, Vincent *et al.* (1955) found the major source in X-irradiated (650 r) rats was the small intestine, indicated by the parallel between the quantity and kind of bacteria in the small intestine and the quantity and kind in their bacteraemic samples. The number of bacteria that translocate systemically in unirradiated animals, as measured by appearance of bacteria in the mesenteric lymph nodes, is directly related to the numbers of intestinal bacteria (Wells *et al.* 1988, Ledney *et al.* 1991).

In recent studies of qualitative microbiology in B6D2F1 and C3H/HeN mice, the cause of sepsis correlated with the quality of radiation to which they were exposed (Brook *et al.* 1993, Ledney *et al.* 1994). Specifically, mixed-field irradiation [$n/(n+\gamma) = 0{\cdot}67$] resulted in predominantly Gram-negative sepsis, whereas ^{60}Co γ-photon irradiation resulted in sepsis from predominantly Gram-positive bacteria (Ledney *et al.* 1994). However, the sources of translocating bacteria following different types of radiation exposure were not studied. In the present work, we determine the numbers and identities of predominant genera of the bacteria found in the ilea of B6D2F1/J mice following exposure to mixed-field and γ-photon radiation.

The results corroborated previous and concurrent studies. We found that lethal mixed-field irradiation leads to significant increases in the number of both Gram-negative and -positive enteric bacteria in the ileum, whereas lethal γ-photon irradiation results in marked increases in the number of only Gram-positive enteric bacteria in the ileum.

2. Materials and methods

2.1. *Animals*

Research was conducted in a facility accredited by the American Association for Accreditation of Laboratory Animal Care. All procedures involving animals were reviewed and approved by our

*Author for correspondence.
Wound and Infection Management Program, Experimental Hematology Department, and †Radiation Biophysics Department, Armed Forces Radiobiology Research Institute, Bethesda, MD 20889-5603, USA.
‡Present address: University of Miami School of Medicine, Miami, FL 33101, USA.
§Present address: University of Iowa School of Medicine, Iowa City, IA 52246, USA.
¶Present address: University of Wyoming, Laramie, WY 82070, USA.

0955–3002/95 $10·00

institutional animal-care-and-use committee. Two shipments of female, B6D2F1/J mice (*Mus musculus*), 9–10 weeks of age, were obtained from Jackson Laboratories (Bar Harbor, ME) 1 year apart. (There may be slight differences in sensitivity of mice in different shipments to radiation.) The mice were held in quarantine for 2 weeks. Representative samples were examined by microbiology, serology, and histopathology to assure the absence of specific bacteria, particularly *Pseudomonas aeruginosa*, and common murine diseases. Up to 10 mice were housed in sanitized 46 × 24 × 15-cm polycarbonate boxes with a filter cover (MicroIsolator, Lab Products, Inc., Maywood, NJ, USA) on hard-wood-chip bedding. The animal holding rooms were maintained at approximately 70°F and 50% (± 10%) relative humidity with a 12-h light/dark, full-spectrum lighting cycle. Conditioned fresh air was changed at least 10 times per h. The mice were given feed (Wayne Lab Blox, Continental Grain Co., Chicago, IL, USA) and acidified (pH 2·5) water freely, and were used when 19–20 weeks of age.

2.2. *Irradiation*

2.2.1. *Mixed-field irradiation.* Mice (shipment 1) were exposed to mixed fission-neutron and γ-photon radiation in an exposure room of the AFRRI TRIGA Mark-F reactor. We document in the Appendix the current detailed characteristics and dosimetry because they have not been published in full. Mice were placed in well-ventilated aluminum holders that rotated at a speed that was no greater than 1·5 rpm. Mice were arranged in an arc 225 cm from the wall lobe and 120 cm above the exposure room floor. Rotation assured that the depth–dose distribution was as uniform as possible to allow an optimal comparison with a bilateral photon irradiation. All doses were at midline tissue (MLT). At the position of irradiation, the measured ratio of the neutron dose to the total dose (neutron plus γ) was $n/(n+\gamma) = 0{\cdot}67$, delivered at a nominal dose rate of 40 cGy/min MLT. The uniformity of the radiation field was within 3% of the dose at the center of the array.

To study colonization of bacteria in the terminal ileum, 70 mice received 350 cGy ($LD_{0/30}$) and 70 mice received 535 cGy ($LD_{90/30}$). Twenty mice were separated from the two groups and observed for 30 days to record survival.

2.2.2. *Gamma irradiation.* Mice (shipment 2) were placed in ventilated acrylic plastic boxes and exposed bilaterally to γ-photon radiation in the AFRRI ^{60}Co Whole-body Irradiation Facility (Carter and Verrelli 1973). The boxes were designed to minimize the air gap between the mouse and the plastic and were placed on a stationary platform. The MLT dose rate for mice was measured before irradiation of animals under conditions that were identical to those for irradiating mice by placing a 0·5-cm^3 tissue-equivalent ionization chamber in the center of a 2·5-cm diameter, cylindrical, acrylic mouse phantom at a known distance from the ^{60}Co source. The ratio of the dose-rate measured in the phantom to the dose-rate in free air, for this array, was 0·98. Exposure time was adjusted so that animals received the desired dose at a nominal dose-rate of 40 cGy/min. Variation of dose within the exposure field was $< 3\%$. The average energy of γ photons was 1·25 MeV. The techniques used for these measurements were performed in accordance with the protocol of the American Association of Physicists in Medicine for the determination of absorbed dose from high-energy photon and electron beams (American Association of Physicists in Medicine 1983).

To study colonization of bacteria in the terminal ileum, 70 mice received 700 cGy ($LD_{0/30}$) and 70 mice received 1000 cGy ($LD_{90/30}$). Twenty mice were separated from each group and observed for 30 days to record survival.

2.2.3. *Radiation dose–responses.* Mice were given graduated doses of mixed-field or γ-photon radiation in order to determine a current relative biological effectiveness (*RBE*) and biologically comparable, or isoeffective, doses of the two qualities of radiation. The current $LD_{50/30}$ and $LD_{90/30}$ for the B6D2F1/J strain of mouse were calculated by probit analysis (Finney 1978) from complete radiation dose–response mortality data.

2.3. *Tissues*

2.3.1. *Quantitation of bacteria in ileum.* Five unirradiated mice from each shipment were included as initial controls at day 0 without apparent difference in microbiology between shipments. On postirradiation days 1, 3, 5, 7, 10, 12, 14, 17 and 21, five mice from each experimental group were randomly selected and killed by cervical dislocation. The ventral surface was rinsed with 70% ethanol; the peritoneal cavity was aseptically opened; and 5 cm of terminal ileum and contents were removed and weighed to the nearest mg. The ilea were homogenized individually in a volume of cold 0·9% NaCl solution adequate to prepare a 1:5 dilution (w/v) in a sterile 5-ml Potter-Elvehjem tissue homogenizer. The suspension of homogenate was diluted serially and dilutions were inoculated with a Spiral Plater™ (Spiral Systems, Inc., Cincinnati, OH, USA) on to Columbia Sheep Blood Agar (SBA), Phenylethyl Alcohol Agar (PEA), and MacConkey's Agar (MAC) (BBL, Cockeysville, MD, USA). Total numbers of facultative bacteria were counted on SBA.

PEA, which minimizes the growth of Gram-negative bacterial colonies, was used to enumerate Gram-positive bacteria. MAC, which inhibits the growth of Gram-positive bacteria, was used to enumerate Gram-negative bacteria. Cultures were incubated for 24 h at 35°C in 5% CO_2. After counting of colonies in the spiral growth, the predominant facultative colonies were identified with a Vitek Jr automated system (Vitek Systems, Inc., Hazelwood, MO, USA).

2.4. *Data analysis*

The numbers of colonies of the two predominant morphologies on each medium per mg tissue were calculated. The geometric means and standard errors of the means were calculated from log-transformed data, compared by *t*-test, and plotted graphically for each experimental set of five mice. The mass of excised ileum in these experiments varied from 170 to 416 mg in unirradiated mice, from 156 to 312 mg in γ-irradiated mice, and from 162 to 403 mg in mixed-field-irradiated mice.

3. Results

3.1. *Enumeration and identification of bacteria in the terminal ileum*

Quantitative and qualitative changes in the intestinal microflora were determined in mice that were irradiated with comparable lethal and sublethal doses of mixed-field and γ-photon radiation. Figure 1 illustrates the numbers of bacteria isolated on PEA (Gram-positive) and MAC (Gram-negative). Figure 2 illustrates the total numbers of bacteria on SBA from the mixed-field- and γ-photon-irradiated mice. Table 1 shows the predominant species found on each culture day. The facultative ileal microorganisms in five control mice from the two shipments were sufficiently similar in species and numbers at day 0 (Table 1). A 10-fold difference in numbers of Gram-negative bacteria between the two control groups on day 0 seems negligible, when considering the overlap of standard errors of the means and the preponderate range of biological difference from day 0 that was observed later in irradiated mice (Figure 1).

The number of Gram-negative microorganisms from ilea that grew on MAC increased continuously through day 12 following a lethal dose of 535 cGy mixed-field radiation (Cox and Stuart test for trend, $p = 0{\cdot}0156$; Figure 1A). A definite shift towards predominance of Gram-negative bacteria began on day 3 that continued to day 12. A straight-line regression on log values shows a very significant ($p < 0{\cdot}001$) upward trend. In those mice that were given a lethal dose of mixed-field radiation, the numbers of Gram-negative bacteria in ilea increased more than 10^5-fold on day 3 and 10^9-fold by day 12 compared with control animals at day 0 (Figure 1A).

Numbers of Gram-positive bacteria cultured on PEA, meanwhile, appeared to decrease without statistical significance in these mice on days 1–5, and then numbers of colonies on PEA returned to the initial numbers, which were isolated from unirradiated control mice at day 0. During days 5–12, in the ilea there was a sustained shift in predominance from Gram-positive bacteria (*Lactobacillus.* sp.) to a preponderately high proportion of total isolated bacteria that were Gram-negative (*E. coli* and *Proteus*

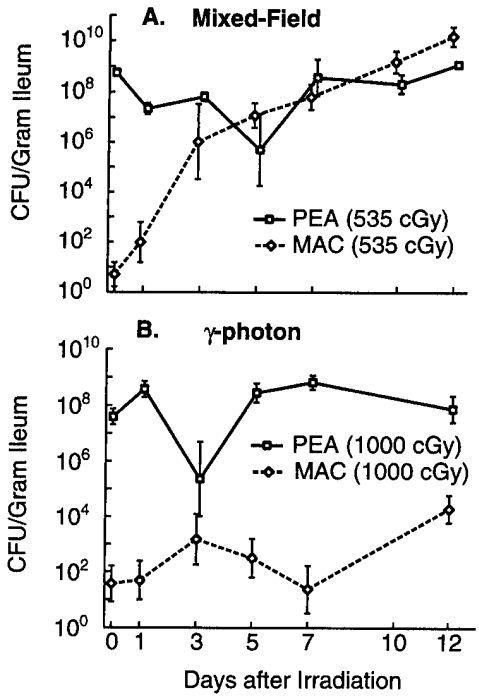

Figure 1. (A) Numbers of facultative bacteria cultured from ilea of the B6D2F1 mouse ($n = 5$) that received 535 cGy mixed-field radiation. Numbers of Gram-negative bacteria cultured on MAC (◇) increased continuously compared with initial numbers of bacteria cultured at day 0 from the unirradiated control mouse on MAC ($p < 0{\cdot}01$). A very significant shift towards Gram-negative predominance began on day 3 that continued to day 12 ($p < 0{\cdot}001$). Meanwhile, numbers of Gram-positive bacteria cultured on PEA (□) appeared to decrease without statistical significance days 1–5, and return by day 7 to initial numbers at day 0 from the unirradiated control mouse. (B) Numbers of facultative bacteria cultured from ilea of the B6D2F1 mouse ($n = 5$) that received 1000 cGy γ-photon radiation. Numbers of Gram-negative bacteria cultured on MAC (◇) remained essentially stable and were no more than 10^2-fold greater through day 12 than in the unirradiated control mouse at day 0. Numbers of Gram-positive bacteria cultured on PEA (□) remained essentially near initial concentrations at day 0 from the unirradiated control mouse.

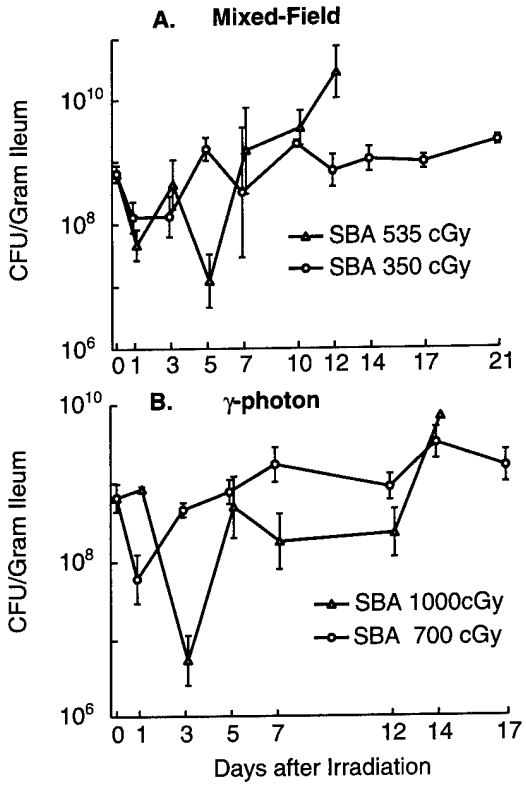

Figure 2. (A) Total numbers of facultative bacteria cultured on SBA from ilea of the B6D2F1 mouse ($n = 5$) that received 535 (△) or 350 cGy (○) of mixed-field radiation decreased on day 1 from initial concentrations at day 0 in the unirradiated control mouse. Numbers of bacteria from 350-cGy-irradiated mice remained near the initial concentration from days 5 to 21, whereas those from 535-cGy-irradiated mice increased, following the lowest numbers, on days 5–12. The remaining 535-cGy-irradiated mice died by day 14. (B) Total numbers of facultative bacteria cultured on SBA from ilea of mice ($n = 5$) that received 1000 (△) or 700 cGy (○) γ-photon radiation decreased early, on days 3 and 1 respectively. Numbers of bacteria from 700-cGy-irradiated mice returned on day 3 and remained through day 17 near the initial concentration at day 0; but numbers of bacteria from 1000-cGy-irradiated mice remained lower than the initial concentration through day 12, then increased on day 14. The remaining 1000-cGy-irradiated mice died by day 17.

mirabilis) (Table 1, Figures 1A and 2A). After day 5, the predominant small bacterial colonies that grew on PEA were identified as inhibited *E. coli* and *P. mirabilis* (Figure 1A), which closely paralleled the increase in Gram-negative bacteria on MAC (Figure 1A) and the total numbers of bacteria found on SBA (Figure 2A).

In contrast, following a lethal dose of 1000 cGy γ-photon radiation, numbers of Gram-negative bacteria that were isolated on MAC remained essentially stable and were no more than 10^2-fold greater through day 12 than in controls at day 0 (Figure 1B). In these mice, numbers of bacteria that were isolated on PEA remained near initial concentrations, which were isolated at day 0 from unirradiated control mice, except for a decrease on day 3 that corresponded to a slight increase of colonies isolated on MAC. That is, the 1000-cGy γ-photon-irradiated mice (Figure 1B) did not exhibit the trend towards Gram-negative predominance found in the 535-cGy mixed-field-irradiated mice. In 1000-cGy γ-photon-irradiated mice, the numbers of Gram-negative microorganisms ($2{\cdot}3 \times 10^1$ to $1{\cdot}9 \times 10^4$ CFU/g of ileum) remained comparatively near the initial numbers isolated from unirradiated control mice.

Total numbers of ileal bacteria that were cultured on SBA (Figure 2) decreased on days 1 and 5 in mice that were given 535 cGy mixed-field radiation and then increased above the initial concentration through day 12. Total numbers decreased on day 3 in mice given 1000 cGy of γ photons and remained somewhat below the initial concentration through day 12, then increased above the initial concentration on day 14. Total

Table 1. Predominant bacterial species in ilea of mice after 1000-cGy γ-photon or 535-cGy mixed-field irradiation.

Day	Radiation quality[a]	No. of mice	Sheep blood agar	MacConkey agar
0	None	20	*Lactobacillus* sp.[b]	*Escherichia coli*
1	γ	5	*Lactobacillus* sp.	*E. coli*[c]
			Bacillus sp.	
	n + γ	5	*Lactobacillus* sp.[b]	*E. coli*
			Staphylococcus aureus	
3	γ	5	*Lactobacillus* sp.	*E. coli*
	n + γ	5	*E. coli*	*E. coli*
5	γ	5	*Lactobacillus* sp.	*E. coli*
			Staphylococcus xylosus	
	n + γ	5	*E. coli*	*E. coli*
			Proteus mirabilis	*P. mirabilis*
7	γ	5	*Lactobacillus* sp.	*E. coli*[c]
			S. xylosus	*P. mirabilis*[c]
	n + γ	5	*E. coli*	*E. coli*
10	γ	5	*Lactobacillus* sp.	*E. coli*
			S. xylosus	*P. mirabilis*
			E. coli	
	n + γ	5	*E. coli*	*E. coli*
			P. mirabilis	*P. mirabilis*
12	γ	5	*Lactobacillus* sp.	*E. coli*
			E. coli	
	n + γ	5	*E. coli*	*E. coli*
14	γ	1	*Lactobacillus* sp.	*E. coli*[c]
	n + γ	2	*E. coli*	*E. coli*
			P. mirabilis	*P. mirabilis*

[a] γ photon (1000 cGy), n + γ = mixed field [n/(n + γ) = 0·67] (535 cGy).

[b] Non-spore-forming, facultative, Gram-positive rods.

[c] Only one mouse exhibited these bacteria on this day. On all other days, at least two mice from each group had these species.

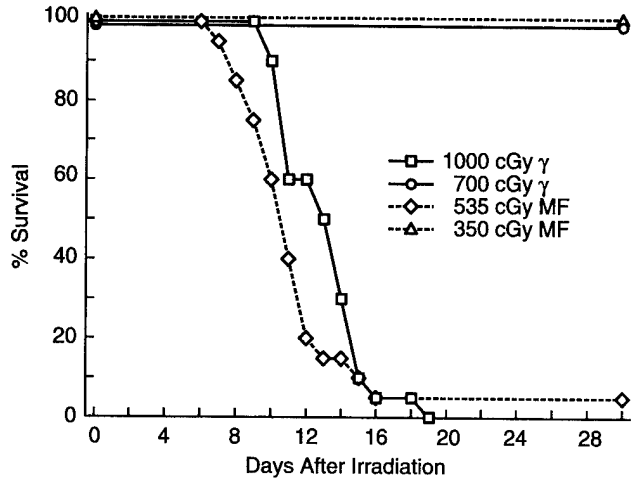

Figure 3. Survival of the B6D2F1/J female mice ($n = 20$) that were given lethal and sublethal doses of mixed-field [n/(n + γ) = 0·67] (MF) or ^{60}Co γ-photon (γ) radiation.

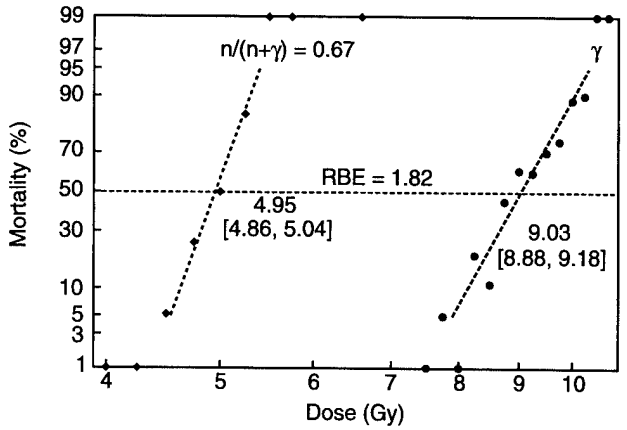

Figure 4. Dose–response by probit analysis of mortality of B6D2F1/J mice given mixed-field [n/(n + γ) = 0·67] or ^{60}Co γ-photon radiation ($n = 20$ mice/dose). Numbers are corresponding $LD_{50/30}$ [95% confidence interval].

numbers of isolated ileal bacteria in 350-cGy mixed-field- and the 700-cGy γ-photon-irradiated mice decreased on day 1, but returned to and remained near initial concentrations, which were isolated from unirradiated control mice at day 0, throughout the study.

3.2. *Dose–responses of mice*

Mice received comparable lethal (1000 cGy γ photon versus 535 cGy mixed-field) and sublethal (700 cGy γ photon versus 350 cGy mixed-field) doses of radiation based on a previous calculation of the *RBE* at the $LD_{50/30}$ and probit analysis for mixed-field irradiation (Ledney *et al.* 1991, 1992). Mortality occurred from day 7 to 16 in mice given 535-cGy mixed-field radiation and day 10–19 in those given 1000-cGy γ photons, the period of hematopoietic syndrome. Mean survival times of mice were 11·9 ± 1·1 days ($n = 20$, including one survivor at 30 days) in those given 535-cGy mixed-field radiation and 13·2 ± 0·5 days ($n = 20$) in those given 1000-cGy γ photons (NS, Behrens–Fischer *T*-test). A comparison of daily survival data by the generalized Savage (Mantel–Cox) procedure showed that there was no significant difference between the two sets ($p = 0·13$; Figure 3). Figure 4 illustrates the mortality of mice given graduated doses of γ-photon or mixed-field radiation. The $LD_{50/30}$ for γ-photon irradiation was 9·03 Gy ($LCL = 8·88$; $UCL = 9·18$). The $LD_{50/30}$ for mixed-field was 4·95 Gy ($LCL = 4·86$; $UCL = 5·04$). Therefore, the *RBE* for the mixed-field- compared with the γ photon-irradiated mice was 1·82 ($LD_{50/30}$ γ photon/$LD_{50/30}$ mixed field).

4. Discussion

This report addresses implications for effective treatment involved in the management of septicaemia, because of selective bacterial translocation in animals given lethal isoeffective doses of two qualities of radiation, mixed-field neutrons and γ photons. Gram-negative facultative bacteria increased to a higher magnitude than Gram-positive bacteria in the ilea of mixed-field-irradiated mice. This trend was not found in γ-photon-irradiated mice. That is, ileal cultures showed either a predominance of Gram-negative or -positive microorganisms, depending upon the quality of radiation the host received, an important distinction for effective therapy of sepsis. This observation is consistent with previous observations in CF1 mice (Vogel *et al.* 1954, Hammond *et al.* 1955) and correlates, as well, with the qualitative incidence of bacteria in livers and blood of septic mice (Brook *et al.* 1993, Ledney *et al.* 1994). Previous studies in this laboratory showed that incidence of bacteria in livers correlated best with sepsis in irradiated mice (Brook *et al.* 1984, Brook and Elliott 1991), but quantitation of bacteria in liver does not sufficiently improve the correlation. In animals that were given $LD_{99/30}$ of radiation (Ledney *et al.* 1994), more liver cultures demonstrated bacteria in mixed-field-irradiated mice than in mice given a comparable dose of γ photons ($p < 0·05$; Figure 5). In mixed-field-irradiated animals, the predominant (93%) microorganisms cultured from the liver were Gram-negative (*E. coli*, *Proteus* sp.). In γ-photon-irradiated animals, 92% of the microorganisms cultured from the liver were Gram-positive (*Streptococcus* sp., *Staphylococcus* sp., *Enteroccoccus* sp.).

The reason remains unclear for the increased

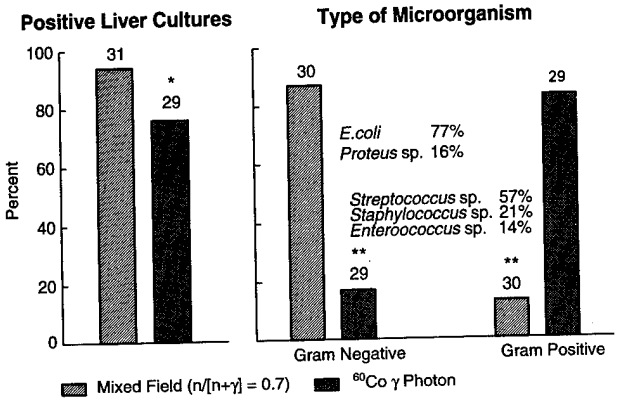

Figure 5. Incidence of bacteria in livers of B6D2F1 within 21 days after 1025 cGy ^{60}Co γ-photon or 560 cGy mixed-field [n/(n + γ) = 0·67] radiation. Statistical differences were determined by chi-square analysis (*$p < 0{\cdot}05$; **$p < 0{\cdot}01$). The number above each bar indicates the number of mice tested.

numbers of Gram-negative bacteria in ilea and the correlated selective translocation of Gram-negative bacteria that were observed in lethally, but not sublethally, mixed-field-irradiated mice, compared with the selective translocation of Gram-positive bacteria in lethally γ-photon-irradiated mice. Although there may be slight differences in sensitivity of mice in different shipments to radiation, the biological difference in results reported here overwhelms those slight differences in sensitivity. We suspect that the selective translocation of bacteria depends upon the degree of injury to intestinal cells caused by neutrons compared with γ photons. Lawrence and Tennant (1937) concluded that, for the same amount of ionization, neutrons are more biologically destructive than X-rays. The gastrointestinal tract is the source of translocating bacteria (Miller *et al.* 1951, Berg and Garlington 1979), against which the mice have no active defense, because of injury to hematopoietic stem cells (Hammond *et al.* 1954). The oral cavity does not appear to be a source of infection in irradiated mice (Quastler *et al.* 1956).

Several possible mechanisms for translocation have been postulated including passage of bacteria between or through intestinal epithelial cells (Deitch and Berg 1987, Wells *et al.* 1990), as well as the uptake of enteric bacteria by macrophages (Wells *et al.* 1987a, 1988). Radiation damage to the intestinal mucosa may lead to a disruption in the integrity of the epithelial lining and villi, thereby allowing enteric bacteria to translocate systemically (Lawrence and Tennant 1937, Hamlet *et al.* 1981, Geraci *et al.* 1985). Onset of mortality and bacteraemia occurred earlier with a lower dose of radiation in neutron- compared with γ-photon-irradiated mice (Vogel *et al.* 1954). A similar apparent difference that we observed was not statistically significant, when we used isoeffective doses of the two qualities of radiation. Based upon quantitative regeneration of crypt cells, neutrons cause greater damage to intestinal villi than do X-rays (Carr *et al.* 1984) and changes in the villous topography and the stromal pericryptal plate were different after high doses of γ photons and neutrons (Carr *et al.* 1985). Also, the sensitivity of the small intestine of B6CF1 mice *in vitro* was greater than hematopoietic cells to neutrons, based upon the *RBE* = 2·8 for jejunal microcolonies and 1·9 for spleen CFU at the D_0s (Hanson *et al.* 1984).

Vincent *et al.* (1955) found that decreased numbers of intestinal lactobacilli, which provide antimicrobial activity and natural competition for other bacteria, especially *Enterobacteriaceae* (Vincent *et al.* 1959), could account for Gram-negative bacteraemia in X-irradiated rats. However, this role for lactobacilli alone would not explain the difference that we saw between mixed-field- and γ-photon-irradiated mice, unless lactobacilli are adversely effected by neutrons, but not by γ photons. Spear (1944) showed that neutrons and γ photons had similar effects on survival of bacteria and bacterial spores.

Furthermore, our results suggest that the efficacy of antimicrobial treatment is time dependent after lethal doses of mixed-field-neutron or γ-photon radiation. The shift to predominantly Gram-negative microorganisms in mice that were lethally irradiated with mixed-field neutrons began 3 days after irradiation, followed by the death of the first mouse on day 7. The time-related nature of this shift in predominant bacteria implies that antimicrobial therapy should begin earlier than 72 h after exposure to neutrons to inhibit exponential growth of Gram-negative microorganisms, thus slowing translocation and the development of sepsis.

Our data indicate more clearly for mixed-field-neutron-irradiated hosts than for γ-photon-irradiated hosts when to initiate treatment, because of the distinctive early increase in enteric Gram-negative rods in neutron-irradiated mice, but antimicrobial therapy in γ-photon-irradiated hosts should probably commence before day 5. Liver cultures of lethally γ-photon-irradiated mice showed colonization by Gram-positive microorganisms by day 5, followed by the initial deaths on day 10 (Ledney *et al.* 1994). Similarly, Vogel *et al.* (1954) recovered α-hemolytic streptococci from most cultures of heart blood of mice beginning 7 days after 900–942 r ^{60}Co γ-photon irradiation, which was later than enteric Gram-negative rods were detected in neutron-irradiated mice.

Selection of an antimicrobial agent should take into account its toxicity to endogenous gastrointestinal anaerobic microflora, which inhibit colonization by

opportunistic microorganisms (Vincent *et al.* 1955, 1959, van der Waaij 1968, Brook 1988), as well as its activity against Gram-negative bacteria in neutron-irradiated animals. Antimicrobial agents, which act against the endogenous anaerobic gastrointestinal microflora, may actually promote translocation of Gram-negative rods such as *E. coli* (Berg 1981, Wells *et al.* 1987b). Therefore, these antimicrobial agents should be avoided, despite their application in cases of abdominal trauma in unirradiated humans (van Rensburg *et al.* 1991).

In addition to use of antimicrobial agents, it is crucial in the irradiated host to stimulate the non-specific phagocytic cells, the production of which is compromised by direct injury to hematopoietic stem cells in bone marrow (Lamerton 1966, Fu *et al.* 1975). Combined therapy with an antimicrobial agent and a non-specific immunomodulator can increase survival more than either agent alone (Madonna *et al.* 1989, Brook *et al.* 1992).

The focus of this study was limited to correlating the quantitation of bacteria in ilea with qualitative bacteriology in livers (Ledney *et al.* 1994) of lethally irradiated mice. Results show the need for different treatments for anticipated sepsis, depending upon the quality of radiation in the low lethal range of doses. Further studies in other mammals, such as baboon, monkey, or dog, would determine whether this phenomenon occurs among species. Although the exact functional basis for selective translocation of bacteria has yet to be determined, particularly in neutron-irradiated animals, it is clear that different qualities of radiation given at low lethal doses effect translocation of different bacteria. Most importantly, therapies that combine antimicrobial agents and immunomodulators can improve survival of irradiated hosts. Based on these principles, development of definitive treatment regimens after exposure to different qualities of radiation is appropriate.

Appendix: Neutron dosimetry in TRIGA Mark-F reactor

The AFRRI TRIGA Mark-F reactor (Moore and Elsasser 1986) has a movable core that is suspended in a pool of water. During irradiation, the core was positioned at one end of the pool in a semicylindrical lobe in the wall, which projects into the exposure room. In this configuration, neutrons that stream from the core encounter minimal moderating material, that is, $< 2{\cdot}5$ cm of water between the core and the exposure room. The spectrum of intense γ-photon radiation (Verbinski *et al.* 1981b), which is emitted from the core in the direction of the array, is attenuated by placing a 15-cm lead shield in the room between the wall lobe and the position of the exposure array. The effect on the photon spectrum in the exposure room is to increase the proportion of low-energy γ photons by removing high-energy γ photons that emanate from the core. The implication of this effect is discussed below. The shield not only reflects low-energy neutrons back to the array, but it also softens the fission-neutron spectrum to a lower energy by inelastically scattering neutrons that have energies > 1 MeV (Verbinski *et al.* 1981a).

The exposure array, constructed of aluminum, consisted of 12 vertical columns of four ventilated cylinders. The columns were uniformly spaced along a 23-cm arc, which had a radius of 285 cm from the center of the reactor core in the wall lobe. The array was positioned 255 cm from the wall lobe and 120 cm above the floor of the exposure room. During all exposures, acrylic mouse phantoms were placed in the columns at both ends of the arc to ensure a more uniform irradiation field. Each cylinder contained one mouse or acrylic phantom. This arrangement allowed up to 40 mice to be irradiated simultaneously. A motorized gear system rotated each column of cylinders around their vertical long axis at 1·5 rpm. Rotation assured a uniform depth–dose distribution to allow an optimal comparison with bilateral ^{60}Co γ-photon irradiation. Details of a similar exposure array in which 20 mice were irradiated in a lead cave was described previously (Stewart *et al.* 1982).

Mixed-field dosimetry for each run was passively monitored by using sulphur activation tablets and actively monitored by using fission and ionization chambers in the exposure room. Paired ion chambers were used to allow a separate determination of dose due to γ-photon and neutron radiations (Meulders 1988). The paired chambers, available commercially, were a tissue-equivalent chamber filled with tissue-equivalent gas and a magnesium chamber filled with argon gas (Goodman 1985, Musk 1993). The volume of each chamber was 0·5 cm^3. Chamber calibrations for mixed fields, as well as those for ^{60}Co fields, are traceable to national standards maintained by the National Institute of Standards and Technology (NIST).

With the paired-chamber technique, determination of the fractional parts of the total dose due to both neutrons and γ photons requires the knowledge of four constants—k_t, k_u, h_t and h_u—that relate to the sensitivities of the chambers to the γ-photon and neutron radiations. Of the four constants, the determination of the fractional dose parts is strongly dependent upon h_u, the response of the magnesium chamber to γ photons in the mixed field relative to the 1·25-MeV ^{60}Co γ photons that were used for calibration of chambers. A weaker dependency is shown by h_t, the response of the tissue-equivalent chamber of the calibration radiation. h_t and h_u are 1·0, except where

the energies of the γ photons in the mixed field are considerably lower than energies of the γ photons in the calibration field.

h_u was determined at NIST from chamber calibration factors (Lamperti 1992) for several γ-photon sources that have energies below the ^{60}Co calibration energy. These studies indicated that, for γ photons with energies < 200 keV, $h_u > 1{\cdot}0$ and increases rapidly with decreasing energy. This is important because the experimental configuration in our experiment included a 15-cm lead shield between the core and the array. At the position of the array, the shield reduced γ photons that emanated directly from the core, but increased the relative contribution of wall-generated lower-energy γ photons. Calculations (Eisenhauer 1993), which were based upon a simplified model of the exposure room, indicated that most of these lower-energy photons arose from higher-energy photons, which were degraded by Compton scattering in the wooden walls.

An estimate of the effective h_u for the mixed field was made by folding the measured h_u response, as described above, with the reactor photon spectrum calculated (Verbinski *et al.* 1981b) for our experimental configuration. Although the calculation of the photon spectrum was based upon a distance of 70 cm between the array and the wall lobe, rather than 255 cm in this experiment, the result is considered valid for any reasonable distance within the room. The analysis (C. M. Eisenhauer, personal communication) determined that the value for the effective h_u was 1·37, which is consistent with the fact that 35% of the photon fluence spectrum is < 200 keV. A similar analysis also determined that the effective h_t was 0·97. These calculated effective paired-chamber constants, together with k_t (0·941) and k_u (0·054), were then used to determine the fractional parts of total dose due to γ photon and neutron radiations. The ratio of neutron to total dose $[n/(n+\gamma)]$ was $0{\cdot}67(\pm 10\%)$. Future measurements of the γ-photon spectrum in the exposure room will determine the accuracy and precision of these calculations. All doses, which were delivered at a nominal dose rate of 40 cGy/min, were determined at midline tissue (MLT) by placing each chamber at the center of a 2·5-cm-diameter, cylindrical acrylic mouse phantom, which, in turn, was placed in an aluminum cylinder in the array. Uniformity of the radiation field was within 3% of the dose at the center of the array. Mean energies of the neutron spectrum, weighted for fluence and kerma, were 0·96 and 1·69 MeV respectively. The fluence-weighted mean energy of the direct photon spectrum was 0·92 MeV (Ferlic and Zeman 1983, Eisenhauer 1991). These values were determined from the calculated spectra for a distance of 70 cm from the array to the wall-lobe (Verbinski *et al.* 1981a, b).

Acknowledgements

We are grateful to William E. Jackson III for expert statistical analyses. We also thank Lorelei Dacquel and Alyssa Hong for technical assistance. Identification of bacteria was performed by the Clinical Laboratory of the Uniformed Services University of the Health Sciences. This work was supported by the Armed Forces Radiobiology Research Institute (AFRRI), Defense Nuclear Agency, under Work Unit 4440-00129. ENSs Rotruck, Stille, and Verdolin, MC, USNR, were under the authority of the US Navy Health Sciences Education and Training Command and were associated with AFRRI as a part of their Armed Forces Health Professions Scholarship Program. C1C Krieger, USAF, was under the authority of the US Air Force Academy Cadet Summer Research Program. Views presented in this paper are those of the authors; no endorsement by the Defense Nuclear Agency, the US Navy, or the US Air Force has been given or should be inferred.

References

AMERICAN ASSOCIATION OF PHYSICISTS IN MEDICINE, TASK GROUP 21, RADIATION THERAPY COMMITTEE, 1983, A protocol for the determination of absorbed dose from high-energy photon and electron beams. *Medical Physics*, **10,** 741–771.

BERG, R. D., 1981, Promotion of the translocation of enteric bacteria from the gastrointestinal tracts of mice by oral treatment with penicillin, clindamycin, or metronidazole. *Infection and Immunity*, **33,** 854–861.

BERG, R. D., 1992, Translocation of enteric bacteria in health and disease. In *Gut-Derived Infectious-Toxic Shock (GITS). Current Studies in Hematology and Blood Transfusion.* Edited by H. Cottier and R. Kraft (Karger, Basel), **59,** pp. 44–65.

BERG, R. D. and GARLINGTON, A. W., 1979, Translocation of certain indigenous bacteria from the gastrointestinal tract to the mesenteric lymph nodes and other organs in a gnotobiotic mouse model. *Infection and Immunity*, **23,** 403–411.

BROOK, I., 1988, Use of antibiotics in the management of postirradiation wound infection and sepsis. *Radiation Research*, **115,** 1–25.

BROOK, I. and ELLIOTT, T. B., 1991, Quinolone therapy in the prevention of mortality after irradiation. *Radiation Research*, **128,** 100–103.

BROOK, I., LEDNEY, G. D., MADONNA, G. S., DEBELL, R. M. and WALKER, R. I., 1992, Therapies for radiation injuries: research perspectives. *Military Medicine*, **157,** 130–136.

BROOK, I., MACVITTIE, T. J. and WALKER, R. I., 1984, Recovery of aerobic and anaerobic bacteria from irradiated mice. *Infection and Immunity*, **46,** 270–271.

BROOK, I., TOM, S. P. and LEDNEY, G. D., 1993, Quinolone and glycopeptide therapy for infection in mouse following exposure to mixed-field neutron-γ-photon radiation. *International Journal of Radiation Biology*, **64,** 771–777.

CARR, K. E., HAMLET, R., NIAS, A. H., BOYLE, F. C. and FIFE, M. G., 1985, Stromal damage in the mouse small intestine after ^{60}Co gamma or D-1 neutron irradiation. *Scanning Electron Microscopy*, **4,** 1615–1621.

CARR, K. E., HAMLET, R., NIAS, A. H. and WATT, C., 1984, Morphological differences in the response of mouse small intestine to radiobiologically equivalent doses of X and neutron irradiation. *Scanning Electron Microscopy*, **1,** 445–454.

CARTER, R. E. and VERRELLI, D. M., 1973, AFRRI cobalt whole-body irradiator. Technical Note 73-3 (Armed Forces Radiobiology Research Institute, Bethesda).

DEITCH, E. A. and BERG, R. D., 1987, Bacterial translocation from the gut: a mechanism of infection. *Journal of Burn Care and Rehabilitation*, **8,** 475–482.

EISENHAUER, C. M., 1991, *AFRRI Neutron Spectrum Directory* (National Institute of Standards and Technology, Gaithersburg).

EISENBAUER, C. M., 1993, *Response of Mg–Ar Chamber in Ledney Fields*. NIST Memorandum (National Institute of Standards and Technology, Gaithersburg).

FERLIC, K. P. and ZEMAN, G. H., 1983, *Spectrum-Averaged Kerma Factors for Reactor Dosimetry with Paired Ion Chambers*. Technical Report TR83-2 (Armed Forces Radiobiology Research Institute, Bethesda).

FINNEY, D. J., 1978, *Statistical Methods in Biological Assay*, 3rd edn (Macmillan, New York).

FU, K. K., PHILLIPS, T. L., KANE, L. J. and SMITH, V., 1975, Tumor and normal tissue response to irradiation *in vivo*: variation with decreasing dose rates. *Radiology*, **114,** 709–716.

GERACI, J. P., JACKSON, K. L. and MARIANO, M. S., 1985, The intestinal radiation syndrome: sepsis and endotoxin. *Radiation Research*, **101,** 442–450.

GOODMAN, L., 1985, *A Practical Guide to Ionization Chamber Dosimetry at the AFRRI TRIGA Reactor*. AFRRI Contract Report CR85-1 (Armed Forces Radiobiology Research Institute, Bethesda).

GUZMAN-STEIN, G., BONSACK, M., LIBERTY, J. and DELANEY, J. P., 1989, Abdominal radiation causes bacterial translocation. *Journal of Surgical Research*, **46,** 104–107.

HAMLET, R., CARR, K. E., NIAS, A. H. W. and WATT, C., 1981, Surface damage in the small intestine of the mouse after X- or neutron irradiation. *Scanning Electron Microscopy*, **4,** 73–78.

HAMMOND, C. W., TOMPKINS, M. and MILLER, C. P., 1954, Studies on susceptibility to infection following ionizing radiation. I. The time of onset and duration of the endogenous bacteremias in mice. *Journal of Experimental Medicine*, **99,** 405–410.

HAMMOND, C. W., VOGEL, H. H., JR, CLARK, J. W., COOPER, D. B. and MILLER, C. P., 1955, The effect of streptomycin therapy on mice irradiated with fast neutrons. *Radiation Research*, **2,** 354–360.

HANSON, W. R., CROUSE, D. A., FRY, R. J. M. and AINSWORTH, E. J., 1984, Relative biological effectiveness measurements using murine lethality and survival of intestinal and hematopoietic stem cells after Fermilab neutrons compared to JANUS reactor neutrons and ^{60}Co gamma rays. *Radiation Research*, **100,** 290–297.

LAMERTON, L. F., 1966, Cell proliferation under continuous irradiation. *Radiation Research*, **27,** 119–138.

LAMPERTI, P. J., 1992, *Report of Calibration and Photon Kerma Measurements*. NIST Report, DG 9549/92 (National Institute of Standards and Technology, Gaithersburg.

LAWRENCE, J. H. and TENNANT, R., 1937, The comparative effects of neutrons and X-rays on the whole body. *Journal of Experimental Medicine*, **66,** 667–688.

LEDNEY, G. D., ELLIOTT, T. B., LANDAUER, M. R., VIGNEUELLE, R. M., HENDERSON, P. L., HARDING, R. A. and TOM, S. P., JR, 1994, Survival of irradiated mice treated with WR-151327, synthetic trehalose dicorynomycolate, or ofloxacin. *Advances in Space Research*, **14,** 583–586.

LEDNEY, G. D., ELLIOTT, T. B. and MOORE, M. M., 1992, Modulation of mortality by tissue trauma and sepsis in mice after radiation injury. In *The Biological Basis of Radiation Protection Practice*. Edited by K. L. Mossman and W. A. Mills (Williams & Wilkins, Baltimore), ch. 13, pp. 202–217.

LEDNEY, G. D., MADONNA, G. S., ELLIOTT, T. B., MOORE, M. M. and JACKSON, W. E., III, 1991, Therapy of infections in mice irradiated in mixed neutron/photon fields and inflicted with wound trauma: a review of current work. *Radiation Research*, **128,** S18–28.

MADONNA, G. S., LEDNEY, G. D., ELLIOTT, T. B., BROOK, I., ULRICH, J. T., MYERS, K. R., PATCHEN, M. L. and WALKER, R. I., 1989, Trehalose dimycolate enhances resistance to infection in neutropenic animals. *Infection and Immunity*, **57,** 2495–2501.

MEULDERS, J.-P., 1988, Dosimetry in mixed n + γ field. In *Ionizing Radiation: Protection and Dosimetry*. Edited by G. Paić (CRC Press, Boca Raton), ch. 11, pp. 203–216.

MILLER, C. P., HAMMOND, C. W. and TOMPKINS, M. 1951, The role of infections in radiation injury. *Journal of Laboratory and Clinical Medicine*, **38,** 331–343.

MOORE, M. L. and ELSASSER, S., 1986, *The TRIGA Reactor Facility at the Armed Forces Radiobiology Research Institute: A Simplified Technical Description*. AFRRI Technical Report TR86-1 (Armed Forces Radiobiology Research Institute, Bethesda).

MUSK, J. H., 1993, *Memorandum on Dosimetry Protocol for the Mouse Rotator Array*. Protocol Number R-93-02 (Armed Forces Radiobiology Research Institute, Bethesda).

QUASTLER, H., AUSTIN, M. K. and MILLER, M., 1956, Oral radiation death. *Radiation Research*, **5,** 338–353.

SPEAR, F. G., 1944, The action of neutrons on bacteria. *British Journal of Radiology*, **17,** 348–351.

STEWART, D. A., LEDNEY, G. D., BAKER, W. H., DAXON, E. G. and SHEEHY, P. A., 1982, Bone marrow transplantation of mice exposed to a modified fission neutron (n/g—30:1) field. *Radiation Research*, **92,** 268–279.

VAN RENSBURG, L. C. J., WARREN, B., WARREN, V. and MÜLLER, R., 1991, Ceftriaxone (Rocephin) in abdominal trauma. *Journal of Trauma*, **31,** 1490–1494.

VAN DER WAAIJ, D., 1968, The persistent absence of Enterobacteriaceae from the intestinal flora of mice following antibiotic treatment. *Journal of Infectious Diseases*, **118,** 32–38.

VERBINSKI, V. V., CASSAPAKIS, C. G., HAGAN, W. K., FERLIC, K. and DAXON, E., 1981a, *Radiation Field Characterization for the AFRRI TRIGA Reactor*, vol. 1, *Baseline Measurements and Evaluation of Baseline Data*. Defense Nuclear Agency Report, DNA 5793F-1 (Armed Forces Radiobiology Research Institute, Bethesda).

VERBINSKI, V. V., CASSAPAKIS, C. G., HAGAN, W. K., FERLIC, K. and DAXON, E., 1981b, *Calculation of the Neutron and Gamma-ray Environment in and Around the AFRRI TRIGA Reactor*. vol. 2, *Baseline Measurement and Evaluation of Baseline Data*. Defense Nuclear Agency Report, DNA 5793-2 (Armed Forces Radiobiology Research Institute, Bethesda).

VINCENT, J. G., VEOMETT, R. C. and RILEY, R. F., 1955, Relation of the indigenous flora of the small intestine of the rat to post-irradiation bacteremia. *Journal of Bacteriology*, **69,** 38–44.

VINCENT, J. G., VEOMETT, R. C. and RILEY, R. F., 1959, Antibacterial activity associated with *Lactobacillus acidophilus*. *Journal of Bacteriology*, **78,** 477–484.

VOGEL, H. H., JR, CLARK, J. W., HAMMOND, C. W., COOPER, D. B. and MILLER, C. P., 1954, Endogenous infection in mice irradiated with fast neutrons or gamma rays. *Proceedings of the Society for Experimental Biology and Medicine*, **87,** 114–119.

WELLS, C. L., JECHOREK, R. P. and ERLANDSEN, S. L., 1990, Evidence for the translocation of *Enterococcus faecalis* across the mouse intestinal tract. *Journal of Infectious Diseases*, **162,** 82–90.

WELLS, C. L., MADDAUS, M. A., REYNOLDS, C. M., JECHOREK, R. P. and SIMMONS, R. L., 1987b, Role of anaerobic flora in the translocation of aerobic and facultatively anaerobic intestinal bacteria. *Infection and Immunity*, **55,** 2689–2694.

WELLS, C. L., MADDAUS, M. A. and SIMMONS, R. L., 1987a, Role of the macrophage in the translocation of intestinal bacteria. *Archives of Surgery*, **122,** 48–53.

WELLS, C. L., MADDAUS, M. A. and SIMMONS, R. L., 1988, Proposed mechanisms for the translocation of intestinal bacteria. *Reviews of Infectious Diseases*, **10,** 958–979.

ARMED FORCES RADIOBIOLOGY RESEARCH INSTITUTE
SCIENTIFIC REPORT
SR95-25

Trolox inhibits apoptosis in irradiated MOLT-4 lymphocytes

DAVID E. McCLAIN,[1] JOHN F. KALINICH, AND NARAYANI RAMAKRISHNAN

Applied Cellular Radiobiology Department, Armed Forces Radiobiology Research Institute, Bethesda, Maryland 20889-5603, USA

ABSTRACT **MOLT-4 cells, a human lymphocytic leukemia line, undergo apoptosis in response to a variety of stimuli, including exposure to ionizing radiation. Very little is known of the molecular mechanisms by which radiation induces apoptosis. Morphology changes and chromatin cleavage at internucleosomal sites accompany apoptosis in these cells. We found that trolox, a water-soluble derivative of vitamin E that penetrates biomembranes and protects mammalian cells from oxidative damage, blocks DNA fragmentation in irradiated MOLT-4 cells. Levels of DNA fragmentation in cells not treated with trolox were directly related to both radiation dose and time postirradiation. Preincubation of cells with trolox or incubation with trolox only during irradiation did not protect cells. A 4 h postirradiation incubation with trolox was sufficient to completely block fragmentation measured at 24 h, indicating the processes triggered by radiation to induce DNA fragmentation occur early after irradiation. Removal of cells from trolox earlier than 4 h resulted in progressively less inhibition. Trolox preserves the integrity of irradiated cells as judged by increased viability and thymidine incorporation. Radiation induces an uptake of extracellular Ca^{2+} into MOLT-4 cells that was blocked by a postirradiation incubation with trolox. These results suggest that membrane-associated oxidations triggered by radiation are responsible for radiation-induced apoptosis in MOLT-4 cells.—McClain, D. E., Kalinich, J. F., Ramakrishnan, N. Trolox inhibits apoptosis in irradiated MOLT-4 lymphocytes. *FASEB J.* 9, 1345–1354 (1995)**

Key Words: radiation · apoptosis

IT HAS BEEN SHOWN THAT MANY KINDS of cells, including thymocytes (1), lymphocytes (2), parotid serous cells (3), and intestinal crypt cells (4), undergo apoptosis after exposure to clinically relevant doses of radiation. Apoptosis is a programmed form of cell death characterized by a variety of morphological, biochemical, and genetic markers (5), but very little is known of the mechanisms by which apoptosis is triggered in such cells.

MOLT-4 lymphocytes, a human leukemic cell line originally isolated in 1971 by Minowada et al. (6), were first studied extensively by Szekeley and co-workers (7, 8) and shown to be very radiosensitive. They found that exposure of MOLT-4 cells to low doses of radiation induced changes in cell morphology, including cell shrinkage, plasma membrane perturbations, and nuclear pyknosis (7), that we now know are characteristics of radiation-induced apoptosis. More recently, two studies by Shinohara and Nakano (9, 10) characterized various aspects of X-ray-induced cell death in MOLT-4 cells and concluded on the basis of morphologic and clonogenic evidence that radiation induces mixed characteristics of interphase death and reproductive death in irradiated MOLT-4 cells. However, these studies indicated that apoptosis appeared to be the underlying mechanism in both cases.

Radiation exerts its primary effect on the cell by the generation of reactive free radicals. Cellular membranes have long been postulated to be one of the most radiation-sensitive regions of the cell (11). Free radical damage initially induced by radiation can be propagated and magnified by lipid peroxidation chain reactions (12). Our laboratory has previously shown that membrane damage appears to play a role in radiation-induced apoptosis (13). The specific sites or functions damaged are not well characterized, but membrane lipid peroxidation has been shown to lead to a variety of membrane alterations, including structural damage (14) and changes in membrane permeability (15). Functions associated with membranes such as expression of IgG on the surface of B cells and protein kinase C activity (16) are also sensitive to radiation.

In this study we have characterized aspects of apoptotic death in irradiated MOLT-4 cells and have demonstrated the protective effects of the antioxidant drug trolox, a water-soluble analog of vitamin E. Trolox is a peroxyl radical scavenger that rapidly penetrates biological membranes (12). It is a powerful inhibitor of membrane damage that has been shown to protect cells both in vivo (17) and in vitro (18). The protective effect of trolox appears to be based on its capacity to inhibit membrane lipid peroxidations (18). The results of our experiments with trolox sup-

[1]To whom correspondence and reprint requests should be addressed, at: Applied Cellular Radiobiology Department, Armed Forces Radiobiology Research Institute, 8901 Wisconsin Ave., Bethesda, MD 20889-5603, USA.

[2]Abbreviations: trolox, 6-hydroxy-2,5,7,8-tetramethylchroman-2-carboxylic acid; HBSS, Hanks' balanced salt solution.

0892-6638/95/0009-1345/$01.50.

port the hypothesis that lipid peroxidations play an important role in radiation-induced apoptosis.

MATERIALS AND METHODS

Cells

MOLT-4 cells were obtained from American Type Culture Collection (ATCC, Rockville, Md.) and grown in RPMI 1640 medium containing 10% fetal bovine serum, 3 mM glutamine, and 100 U/ml penicillin/streptomycin (all Gibco/BRL, Grand Island, N.Y.) in an atmosphere of 5% CO_2 in air at 37°C. Cell cultures were maintained at densities not exceeding 1–1.5 × 10^6 cells/ml because higher densities tended to affect cell viability. Only cells with viabilities greater than 94% (trypan blue dye exclusion) were used for experiments.

Irradiation

Cells were suspended (approximately 1 × 10^7 cells/ml) in normal growth medium and irradiated at room temperature, using the AFRRI ^{60}Co Facility at a dose rate of 1 Gy/min. After irradiation, cells were pelleted by centrifugation (750 × g, 5 min at room temperature) and resuspended (approximately 1 × 10^6 cells/ml) in warm, fresh medium with or without reagents to be tested.

Trolox treatment

Trolox (Aldrich Chemical Co., Milwaukee, Wis.) was dissolved in 1 M $NaHCO_3$ at a concentration of 300 mM and the pH was adjusted to 7.0. For experiments, the solution was diluted to the desired concentration with medium. The viability of cells incubated with 10 mM trolox demonstrated no significant decrease during 24 h of incubation, but cells were routinely exposed to trolox for no longer than 8 h. All cell suspensions not treated with trolox were brought to a concentration of $NaHCO_3$ equivalent to that delivered with the trolox.

Microscopy

Cells (0.5–1.5 × 10^7) were pelleted by centrifugation (750 × g, 5 min), resuspended in 1 ml of freshly prepared 3% formaldehyde in HBSS, and refrigerated for a sufficient time to allow cells to settle to the bottom of tube (about 2 h). Centrifugation to pellet cells was avoided because it appeared to contribute to distorted cell morphology. Fixed cells could be kept refrigerated for several weeks without any apparent degradation.

For bright-field and fluorescence microscopy, all but about 0.1 ml of the fixing buffer overlaying the cells was removed and the cells were gently resuspended in the remaining buffer. A 20 µl aliquot (approximately 1–3 × 10^6 cells) was removed and mixed with 20 µl of a 0.1 mg/ml solution of ethidium bromide in HBSS (final concentration: 50 µg/ml). The stained suspension was kept in the dark on ice until used. Ten microliters of suspension were placed on a microscope slide and gently covered with a 20 mm square coverslip. The coverslip was sealed with cement to prevent drying. Cells were allowed to settle onto the surface of the slide for 5–10 min before observation began.

Photomicroscopy was performed with an Olympus AHBT3 Research microscope with Nomarski-type differential interference contrast and reflected-light fluorescence. Images were preserved on high-speed Polaroid Type 57 film.

DNA agarose gel electrophoresis

Electrophoresis of DNA was performed essentially according to the method used by Gong et al. (19). This method is rapid, uses nontoxic reagents, and permits the selective extraction of fragmented, smaller molecular weight DNA from unfragmented DNA. The removal of high molecular weight DNA from the sample enhances the detection of apoptotic DNA, whose appearance in the gel is an indication of the degree of apoptosis. Briefly, 5 × 10^6 cells were pelleted from the growth medium, washed once with HBSS, resuspended in 1 ml HBSS, diluted with 10 ml of ice-cold 70% ethanol, and then stored refrigerated at least 24 h. Cells fixed in this way could be stored for weeks without any apparent degradation. The cells were pelleted by centrifugation (750 × g, 5 min) and the ethanol completely removed, then resuspended in 50 µl of phosphate-citrate buffer (192 parts 0.2 M Na_2HPO_4 and 8 parts 0.1 M citric acid, pH 7.8) and transferred to a 0.5 ml Eppendorf-style microcentrifuge tube in which they were allowed to stand at room temperature for 45 min. After centrifugation (750 × g, 5 min), the supernatant was transferred to a new tube and the volume reduced in a SpeedVac concentrator (Savant Instruments, Farmingdale, N.Y.) for 15 min. A 4 µl aliquot of RNase A (1 mg/ml in water, Sigma, St. Louis, Mo.) was added to each sample, which was then incubated at 37°C for 45 min. A 4 µl aliquot of proteinase K (1 mg/ml in water, Boehringer Mannheim, Indianapolis, Ind.) was then added and the sample was incubated an additional 45 min at 37°C. After the incubations, samples were mixed with 5 µl of 6X loading buffer (0.25% bromophenol blue, 40% sucrose in water) and the entire volume was loaded onto a 0.8% agarose gel containing 0.5 µg/ml ethidium bromide. Electrophoresis was performed at 2 V/cm of gel length for about 16 h. DNA bands were visualized using UV transillumination and photographs of the gels were obtained using Polaroid Type 665 positive/negative film.

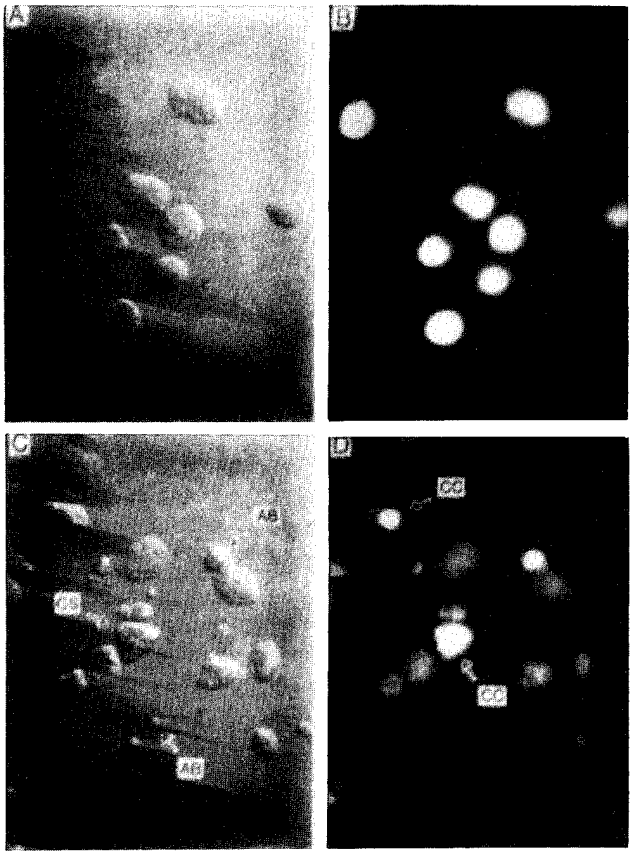

Figure 1. Representative bright-field and ethidium bromide DNA fluorescence images of MOLT-4 cells 24 h after exposure to 0 Gy or 3 Gy ^{60}Co-gamma radiation. Cells were prepared for microscopy as described in Methods. A comparison of bright-field images of unirradiated (*A*) and irradiated (*C*) cells clearly demonstrates marked alterations in cell morphology that accompany radiation-induced apoptosis, including cell shrinkage (CS) and production of apoptotic bodies (AB). DNA staining of unirradiated (*B*) and irradiated (*D*) cells demonstrates presence of pronounced chromatin condensation (CC) and other nuclear disruptions in irradiated cells.

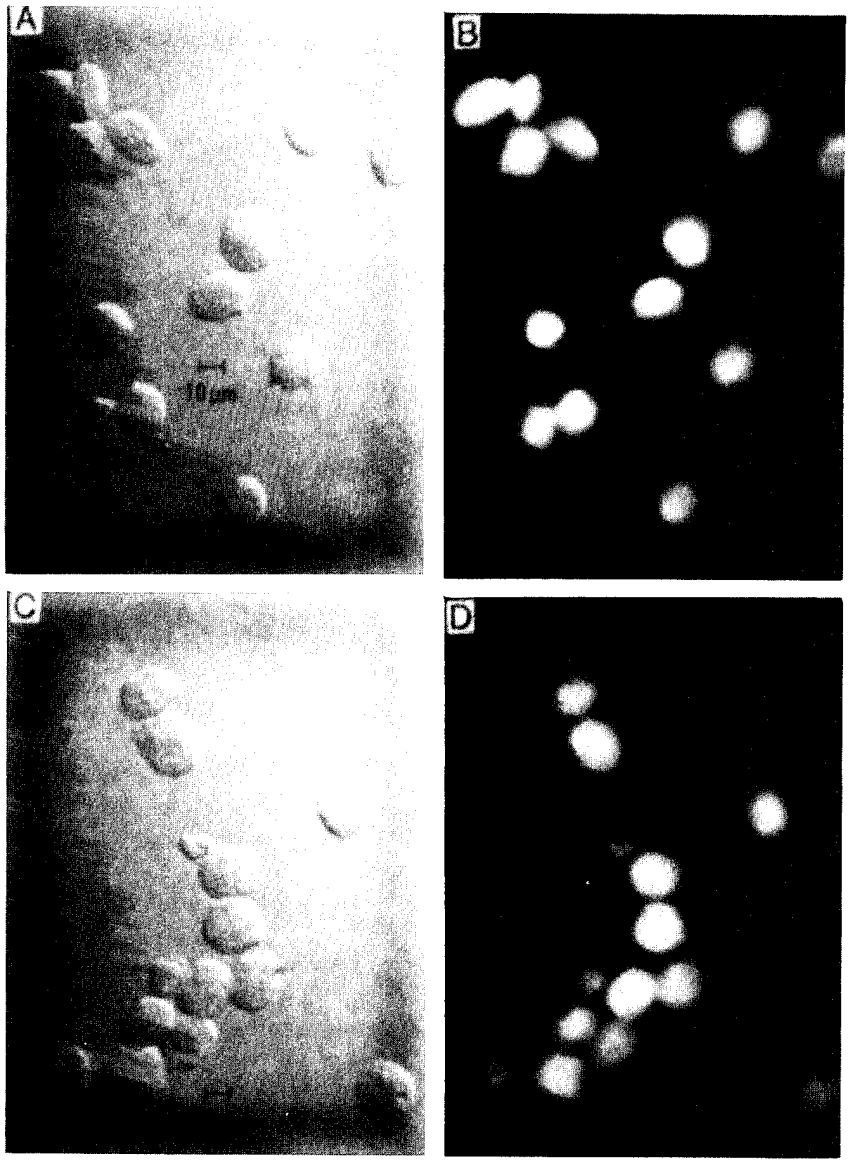

Figure 2. Images analogous to those in Fig. 1, except cells were treated with trolox (10 mM) for 8 h after irradiation, before cells were prepared for microscopy 24 h postirradiation. Trolox treatment of unirradiated cells caused no significant disruption of morphology apparent in either representative bright-field (*A*) or fluorescence (*B*) images, compared to cells not treated (Fig. 1*A–B*). Trolox treatment of irradiated cells resulted in sharp decrease in number of cells manifesting apoptotic morphology (C, D).

DNA fragmentation assay

Cells (1–2 × 10^6) were collected by centrifugation and lysed with ice-cold lysis buffer containing 10 mM Tris-HCl (pH 7.5), 1 mM EDTA, and 0.2% Triton X-100 and then pelleted by centrifugation (14,000 × *g*, 4°C, 20 min) to separate intact from fragmented DNA. The pellet was resuspended in lysis buffer and sonicated for 10 s at 4°C. DNA in both the supernatant and pellet fractions was determined by means of an automated fluorometric protocol that we designed using AutoAnalyzer II components (Technicon, Tarrytown, N.Y.) and the DNA-specific fluorescent probe Hoechst 33258 (13). Percent DNA fragmentation was calculated by dividing the amount of DNA in the supernatant by the total DNA in the sample (supernatant + pellet DNA) and multiplying by 100.

Thymidine incorporation

Cells were irradiated as described. Immediately after irradiation cells were resuspended (5 × 10^5 cells/ml) in medium containing 0.25 μCi [^{3}H]thymidine/ml (Dupont/NEN, Boston, Mass.) with or without trolox. After exposure to trolox for 8 h, cells were transferred to warm, fresh medium containing [^{3}H]thymidine without trolox, and the incubation was continued. At selected times, 3 ml of suspension (1.5 × 10^6 cells) was removed, the cells pelleted by centrifugation (750 × *g*, 5 min), washed twice with HBSS, and resuspended with 10% TCA to precipitate DNA (at least 1 h at 4°C). The precipitate was then harvested on glass-fiber filters (GF/C), which were then washed twice with 5 ml of ice-cold 5% TCA and once with 5 ml ice-cold 70% ethanol to remove unincorporated [^{3}H]thymidine. Incorporated radioactivity was determined by scintillation counting (LS5801, Beckman Instruments, Palo Alto, Calif.) in 5 ml Ecoscint-A cocktail (National Diagnostics, Manville, N.J.).

Calcium uptake

Ca^{2+} uptake studies were performed by a method modified from McClain et al. (20). Cells (3 × 10^6/ml) were incubated at 37°C for 30 min before radiation exposure in medium containing 10 μCi $^{45}Ca^{2+}$/ml

($^{45}CaCl_2$, Dupont/NEN). This preincubation time was sufficient to equilibrate intracellular Ca^{2+} stores with the isotope (unpublished observations). After irradiation the cell suspension was returned to 37°C and incubated with gentle mixing. At selected times postirradiation aliquots of the cell suspension (50 µl, 1.5×10^5 cells) were removed and layered over 150 µl of a silicone oil mixture [Versilube F50, General Electric, Waterford, N.Y., with 8% (v/v) light mineral oil (Fisher Scientific, Pittsburgh, Pa.)] in a 0.6 ml microcentrifuge tube. The sample was centrifuged in a microfuge (13,500 × *g*, 45 s) to pellet the cells through the oil and separate them from the radioactive medium. The aqueous and oil layers were carefully aspirated and the cell pellet resuspended in HBSS containing 1% Triton X-100. Suspensions were transferred to 7 ml scintillation vials, 5 ml Ecoscint-A was added, the vial contents were vigorously shaken, and the radioactivity in the samples was determined with a scintillation counter.

The amount of Ca^{2+} associated with the cells was calculated from the cpm in the cell pellet divided by the specific activity of $^{45}Ca^{2+}$ in the incubation medium. The specific activity was calculated by dividing the cpm in 10 µl of the radioactive cell suspension by the Ca^{2+} concentration in the incubation medium (0.42 mM). Ca^{2+} associated with the cell pellet was expressed as pmol/10^6 cells.

Lipid peroxidation measurements

Cell suspensions in medium were preincubated with 5 µM *cis*-parinaric acid (Molecular Probes, Eugene, Oreg.) for 1 h before irradiation. Cells were resuspended in fresh medium without *cis*-parinaric acid immediately before irradiation. Fluorescence measurements were carried out at room temperature in an SLM Model 8000 spectrofluorometer (SLM Instruments, Urbana, Ill.), using a stirred cuvette, with excitation and

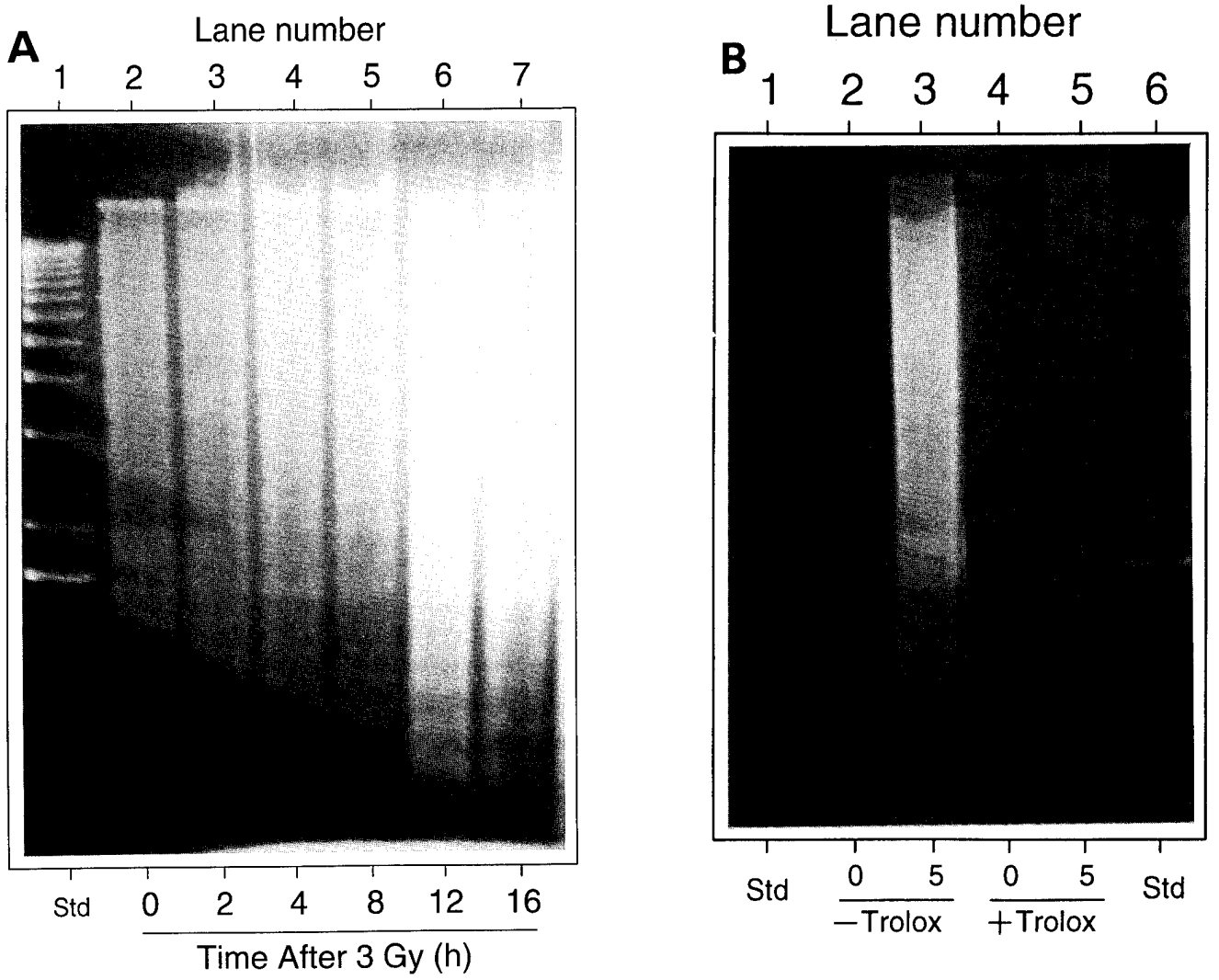

Figure 3. DNA agarose gels of chromatin extracted from MOLT-4 cells at various times after exposure to 5 Gy, without and with trolox treatment. Cells were irradiated and electrophoresis performed as described in Methods. *A*) Lane 1 is standard 1 kb DNA ladder. There is a very low level of internucleosomal DNA cleavage in unirradiated cells (lane 2). The ladder pattern becomes increasingly evident at 2, 4, and 8 h postirradiation (lanes 3–5). At 12 and 16 h (lanes 6, 7) there is an abrupt increase in amount of DNA in ladder, which appears to result from superposition of both internucleosomal and randomly fragmented DNA. *B*) Effect of trolox. Lanes 1 and 6: standard DNA ladders. Lanes 2 and 3: DNA from unirradiated ("0") and irradiated ("5," 5 Gy) cells not treated with trolox. Lanes 4 and 5: DNA from unirradiated and irradiated cells treated with trolox for 8 h, beginning immediately after irradiation. DNA was extracted in all samples 16 h postirradiation. (The figure is a composite of lanes run on the same gel.) In irradiated cells, trolox blocked both the appearance of ladder pattern of DNA in irradiated sample and inhibited amount of randomly fragmented DNA seen in irradiated cells not exposed to trolox.

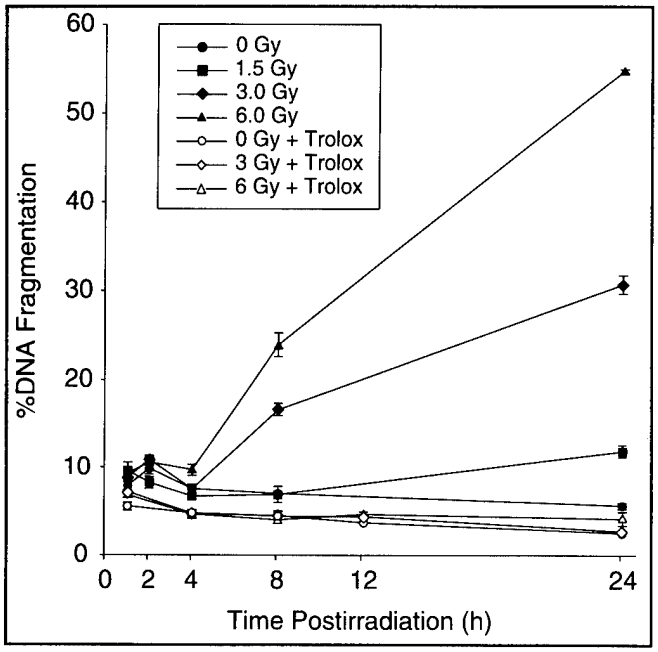

Figure 4. Time course of DNA fragmentation observed in unirradiated and irradiated cells with and without trolox. DNA fragmentation in all irradiated samples remains low for first 4 h postirradiation. After 4 h there is a steady increase in quantity of fragmented DNA in irradiated samples not treated with trolox, related to both radiation dose and time postirradiation. Both unirradiated and irradiated cells treated with trolox demonstrate even less fragmentation than observed in unirradiated, untreated cells. Data represent mean ± SEM of three experiments.

emission wavelengths at 324 nm and 425 nm, respectively (band widths 4 nm).

RESULTS

Irradiated MOLT-4 cells exhibit morphological characteristics that are typical of apoptosis (**Fig. 1**). Figures 1*A*, *B* show bright-field and ethidium bromide DNA fluorescence images, respectively, of unirradiated MOLT-4 cells. Figures 1*C* and *D* represent images of cells 24 h after exposure to 3 Gy ^{60}Co-gamma radiation. A comparison of the bright-field images of unirradiated and irradiated cells clearly demonstrates the marked alterations in cell morphology that accompany radiation-induced apoptosis, including cytoplasmic shrinkage, nuclear disruption, plasma membrane perturbations, and the production of apoptotic bodies. DNA staining with ethidium bromide (Figs. 1*B*, *D*) indicates the presence of pronounced chromatin condensation and other nuclear disruptions in the irradiated cells. Typically, both apoptotic and normal morphologies are present in cell populations examined at this time after irradiation.

Figures 2*A–D* are images analogous to those in Fig. 1, except the cells were treated with the vitamin E analog trolox during and for 8 h after irradiation before the cells were prepared for microscopy 24 h postirradiation. Both the bright-field and DNA-stained fluorescence images of irradiated cells reflect a decrease in the relative numbers of cells with apoptotic morphology, suggesting that trolox prevents the appearance of those characteristics.

Figure 3*A* shows an agarose gel of DNA extracted from MOLT-4 cells at various times after exposure to 5 Gy. The method used here recovers only fragmented DNA from the mixture of fragmented and unfragmented DNA in the sample. The amount of DNA in each lane is thus not necessarily constant, but is a reflection of the degree of fragmentation that has occurred. Immediately after irradiation (0 h, lane 2), there is only barely discernable evidence of internucleosomal DNA cleavage (the so-called "ladder" pattern of DNA fragments that are multiples of approximately 200 base pairs). The intensity of the ladder pattern increases through 2, 4, and 8 h postirradiation (lanes 3–5, respectively). At 12 and 16 h postirradiation (lanes 6 and 7), there is an abrupt increase in the amount of total DNA in the ladder, which appears to result from a combination of both internucleosomal and randomly fragmented DNA, identifiable as a smear in the sample lanes.

Figure 3*B* indicates the effect of trolox on internucleosomal DNA fragmentation in irradiated MOLT-4 cells. As a reference, lanes 2 and 3 contain, respectively, DNA from unirradiated and irradiated cells not treated with trolox.

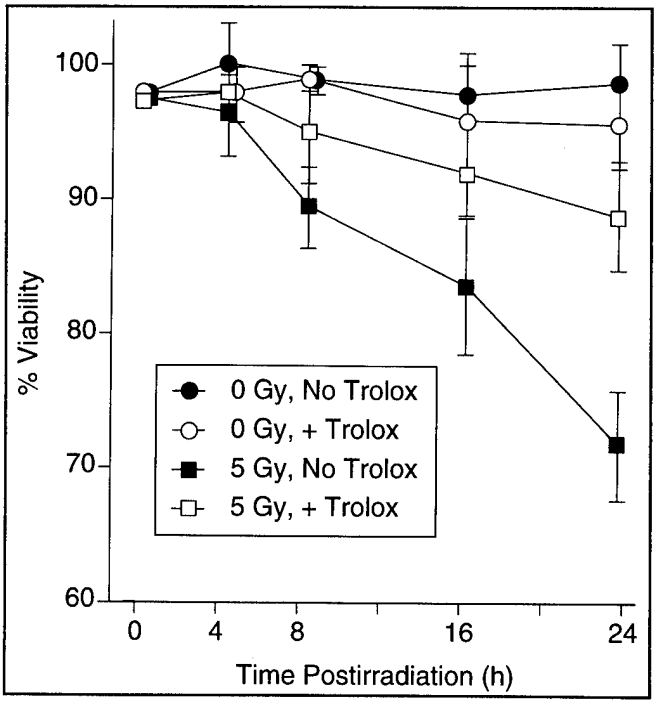

Figure 5. Effect of radiation and trolox on MOLT-4 cell viability. Cells were irradiated with 5 Gy and viability determined as described in Methods. Unirradiated cultures maintained high percentage of viable cells throughout course of these experiments. Trolox treatment of unirradiated cells decreased cell viability slightly. Irradiation without trolox treatment resulted in steady decrease in viability, but viability of irradiated cells treated with trolox was significantly better than irradiated cells not treated with trolox. Data represent mean ± SEM; of four measurements

Lanes 4 and 5 contain DNA from unirradiated and irradiated (5 Gy) cells exposed to trolox for 8 h after irradiation before the extraction of DNA 16 h postirradiation. The figure indicates that trolox treatment not only blocked the appearance of a ladder pattern of DNA in the irradiated sample but also reduced the amount of randomly fragmented DNA present in irradiated cells not exposed to trolox. Trolox appeared also to eliminate even the light background of fragmentation seen in unirradiated cells.

Figure 4 shows the results of experiments to measure more quantitatively the time course of the DNA fragmentation observed in cells irradiated with 0, 1.5, 3, and 6 Gy, and trolox-treated cells irradiated with 0, 3, and 6 Gy. This method calculates fragmentation by comparing the amount of DNA that does not pellet after a 14,000 × *g* centrifugation (fragmented DNA) with the total DNA in the supernatant and pellet fractions. We have previously used this procedure to quantitate apoptosis in thymocytes (13). The total amount of DNA present in unirradiated or irradiated cells did not differ significantly over the course of these experiments (data not shown). There were no significant changes in fragmentation in the first 4 h postirradiation. After 4 h, DNA fragmentation increased steadily for the duration of the measurements in a manner related to radiation dose. In marked contrast, irradiated cells treated with trolox demonstrated a degree of fragmentation no different than that observed in trolox-treated unirradiated cells. Trolox treatment of irradiated and unirradiated cells appeared to lower DNA fragmentation to levels even lower than that observed in unirradiated cells not treated with trolox. This result is consistent with the results from the DNA agarose gels, where trolox treatment by itself was also seen to lower the amount of background fragmentation in unirradiated cells.

To assess the effect of radiation and trolox treatment on the viability of MOLT-4 cells, we measured the capacity of these cells to exclude the vital dye trypan blue. **Figure 5** shows percent viability determined in cells various times after exposure to 5 Gy. Unirradiated cells remained about 98% viable under the conditions of the incubations in these experiments. Radiation caused a relatively steady decrease in viability over time, with about 70% of the cells retaining their capacity to exclude trypan blue 24 h postirradiation. Unirradiated cells treated with trolox exhibited a small decrease in viability compared to untreated cells, but irradiated cells treated with trolox retained a significantly greater capacity to exclude trypan blue 24 h postirradiation than did cells not treated with trolox.

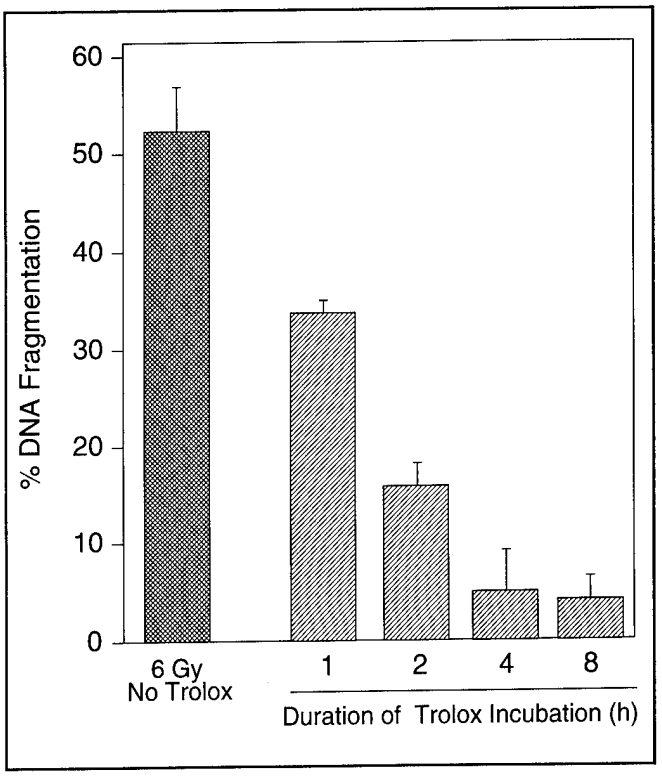

Figure 6. Optimal duration of trolox exposure after irradiation. Trolox was added to irradiated cells immediately after irradiation then removed at indicated times postirradiation. DNA fragmentation was calculated 24 h postirradiation. A 4 h incubation with trolox appears to be sufficient to reduce fragmentation to unirradiated levels (5.2 ± 0.6%, data not shown). Data represent mean ± SEM of 3 experiments.

We also counted the total numbers of cells present after trolox treatment, with or without irradiation, to ensure that decreases in the quantity of fragmented DNA observed in agarose gels of irradiated, trolox-treated cells were not related to a drop in absolute cell numbers. The number of irradiated cells incubated with trolox for 8 h, followed by an additional 16 h incubation without trolox, did not differ significantly from either the numbers of unirradiated cells incubated with trolox or that of cells receiving no treatment (data not shown).

We performed several experiments to determine the optimal time of administration of trolox relative to radiation exposure. **Table 1** shows the results of experiments in which cells were incubated with trolox only before, only during, or only after irradiation (6 Gy). DNA fragmentation in cells incubated with trolox only before or only during irradiation was reduced somewhat but did not differ greatly from the fragmentation measured in irradiated cells receiving no drug treatment. However, the addition of trolox immediately after irradiation completely inhibited DNA

TABLE 1. *Incubation with trolox before or during irradiation does not inhibit DNA fragmentation*[a]

Treatment	DNA Fragmentation, %
6 Gy (no trolox)	56.2 ± 2.1
Trolox incubation only before 6 Gy	48.9 ± 3.7
Trolox only during 6 Gy	51.3 ± 4.6
Trolox incubation only after 6 Gy	7.2 ± 0.4

[a]Cells were irradiated with 6 Gy as described in Methods. Cells were either preincubated with 10 mM trolox for 30 min before removing the trolox immediately before irradiation, incubated with trolox during irradiation before removing it, or incubated with trolox for 8 h beginning only after irradiation. DNA fragmentation was then determined 24 h postirradiation.

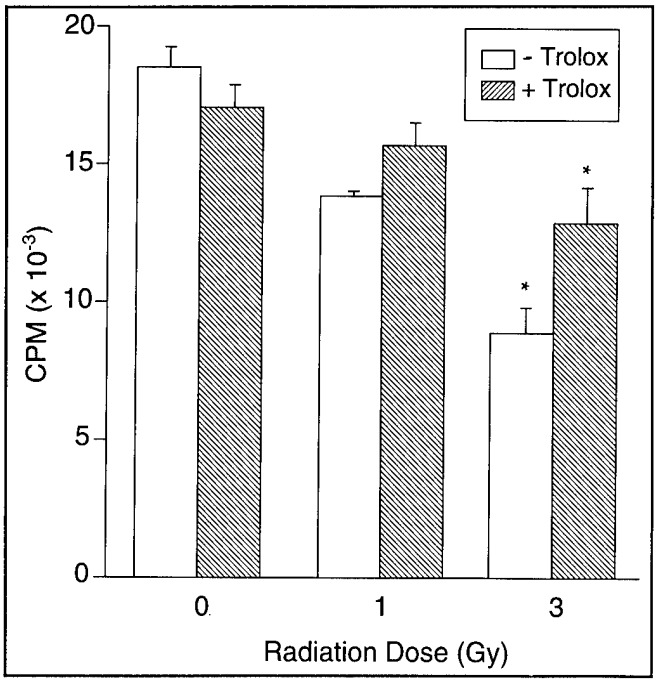

Figure 7. Increased thymidine incorporation in irradiated MOLT-4 cells treated with trolox. Cells were exposed to radiation with or without trolox treatment and [^{3}H]thymidine incorporation (0.25 μCi/ml) determined 24 h postirradiation, as described in Methods. Radioactivity in trolox-treated cells exposed to 3 Gy was significantly greater ($P > .05$, indicated by asterisk) than cells not treated, indicating trolox preserves functional integrity of irradiated cells. Data represent mean ± SEM of two independent experiments.

fragmentation, which shows that trolox inhibits events that are active only after exposure.

If trolox protects MOLT-4 cells by inhibiting membrane lipid peroxidation chain reactions triggered at the time of irradiation, then it would seem more important to have trolox present at times soon after irradiation than at later times. **Figure 6** shows the results of experiments in which trolox was added immediately after irradiation (6 Gy) and then removed at various times postirradiation. Incubations were continued until 24 h postirradiation in medium without trolox before measurements of DNA fragmentation. A 1 h incubation significantly decreased fragmentation, and a 2 h incubation reduced fragmentation further, to about one-third of that measured in untreated irradiated cells. A 4 h incubation reduced fragmentation to unirradiated control levels (5.2 ± 0.6%).

If trolox prevents radiation-induced apoptosis, we might expect that cells treated with trolox would have greater capacity to take up thymidine from the medium than those untreated. To test this possibility, we measured the incorporation of thymidine into DNA of irradiated cells (1 and 3 Gy) with or without trolox treatment. **Figure 7** shows a significantly greater incorporation of radiolabeled thymidine in the irradiated (3 Gy), trolox-treated cells 24 h postirradiation than in irradiated cells not treated with trolox ($P > 0.05$), suggesting that trolox-treated cells have greater functional viability than those not treated.

Our initial efforts to measure viability by thymidine incorporation using a specific activity of 1 μCi/ml showed a significant decrease in incorporation in all cells, including unirradiated controls, at 48 and 72 h postirradiation (data not shown). This suggested experimental conditions were affecting cell viability, which we confirmed using trypan blue dye exclusion. We believe this was an experimental artifact that reflects a sensitivity of MOLT-4 cells to internal irradiation by the radiolabeled probe itself, a factor previously noted by others using other radiolabels and cell models (21, 22). Decreasing the specific activity of radiolabled thymidine in our experiments (from 1 μCi/ml to 0.25 μCi/ml) preserved viability and enhanced our capacity to measure differences in thymidine incorporation between trolox-treated and -untreated cells (data not shown).

In initial studies to determine the role of Ca^{2+} in radiation-induced apoptosis in MOLT-4 cells, we measured the time course of Ca^{2+} uptake in irradiated cells either not treated or treated with trolox (**Fig. 8**). Beginning around 12 h postirradiation (5 Gy), there is a marked increase in the uptake of extracellular Ca^{2+} in cells not treated with trolox, which reached a plateau at 16 h and remained elevated for the duration of the measurements. Trolox treatment exerted a pronounced effect on Ca^{2+} uptake in irradiated cells by preventing the sharp rise seen at 12 h in untreated cells.

The known sensitivity of biological membranes to radiation combined with the effectiveness of the membrane antioxidant trolox at inhibiting radiation-induced changes in

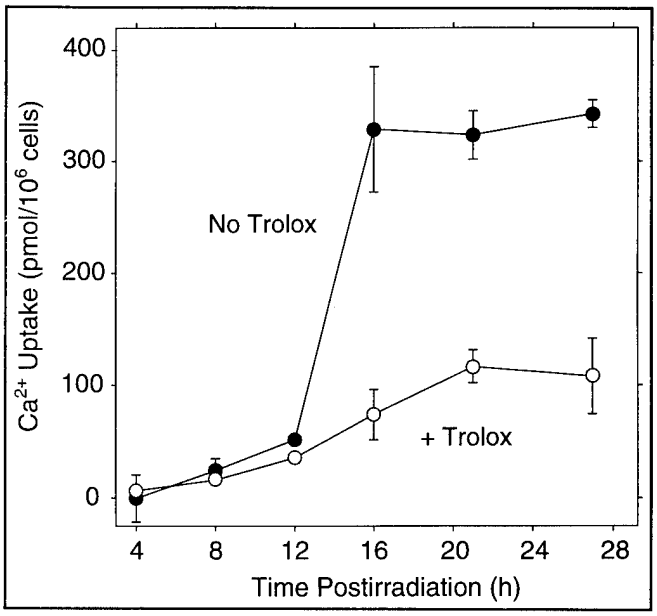

Figure 8. Ca^{2+} uptake in irradiated MOLT-4 cells. Cellular Ca^{2+} stores were equilibrated with $^{45}Ca^{2+}$ before irradiation (5 Gy) and Ca^{2+} uptake measured at various times postirradiation, as described in Methods. Trolox treatment led to inhibition of radiation-induced Ca^{2+} uptake. Radioactivity associated with unirradiated cells treated or not treated with trolox was subtracted from irradiated cells before calculation of pmol uptake to give net uptake depicted in the graph. Data represent mean ± SEM of two independent experiments.

MOLT-4 cells led us to determine whether measurable lipid peroxidation was occurring in the irradiated cells. For these studies we used the sensitive lipid probe *cis*-parinaric acid, a naturally fluorescent fatty acid. *cis*-Parinaric acid readily incorporates into the lipid bilayer of biomembranes and loses its fluorescence properties when oxidized (23). The results of these experiments are summarized in **Fig. 9**. Cells were incubated with 5 μM *cis*-parinaric acid for 1 h before irradiation (5 Gy) and then resuspended in fresh medium immediately before irradiation. Measurements of lipid peroxidation then began immediately after exposure. Unirradiated controls demonstrated a slight decrease in *cis*-parinaric acid fluorescence, probably due to the autoxidation of the probe in air (24). Radiation, however, induced a pronounced, rapid decrease in *cis*-parinaric acid fluorescence within the first 5 min postirradiation that continued throughout the 30 min postirradiation measurements. These experiments indicate lipid peroxidation is an early consequence of irradiation that appears to precede all other known indicators of apoptosis.

DISCUSSION

Radiation induces apoptosis in many different kinds of cells, but little is understood of the mechanisms by which it occurs. The rapidly growing body of literature on apoptosis supports the view that apoptosis is a process that uses normal, intracellular, biochemical pathways. This suggests that there is potential for the development of pharmacological approaches to modify not only the cellular response to radiation but also the role apoptosis plays in a variety of other physiological processes.

In this study we have used the membrane-soluble, peroxyl radical scavenger drug trolox to protect MOLT-4 cells from radiation-induced apoptosis. Our experiments to understand how trolox exerts its protective effect have in turn provided us insight into the mechanisms of apoptosis in these cells. We selected trolox for these studies based on our previous experience with the compound in inhibiting DNA fragmentation in irradiated mouse thymocytes (13). Trolox is superior to its parent compound, vitamin E, for such studies for two reasons: it is markedly more soluble in aqueous solution, and it can be up to 8 times more effective as an antioxidant than vitamin E (12).

MOLT-4 lymphocytes irradiated with clinically relevant doses of ionizing radiation demonstrate the classic morphological characteristics of apoptosis, including cellular condensation, nuclear pyknosis, and the generation of apoptotic bodies (Fig. 1). Chromatin extracted from apoptotic MOLT-4 cells shows the typical ladder pattern of DNA fragmentation after agarose gel electrophoresis (Fig. 3*A*). Quantitative measurements of fragmentation indicate that irradiation leads to increases in fragmentation that depend on both the radiation dose and time postirradiation (Fig. 4). Radiation also induces an abrupt uptake of extracellular Ca^{2+} around 12 h postirradiation (Fig. 8).

Trolox effectively inhibits these responses in MOLT-4 cells. Prompt treatment with trolox inhibits the morphological (Fig. 2) and chromatin changes (Fig. 3*B*) as well as

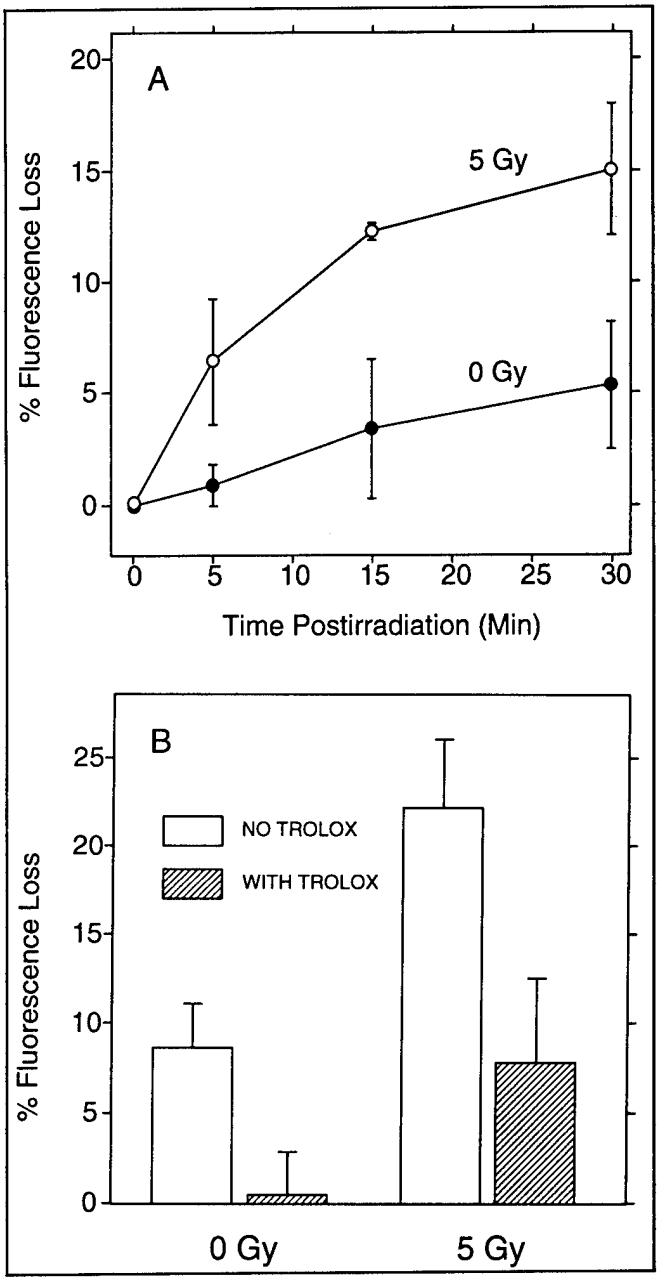

Figure 9. Time course of lipid peroxidation in irradiated MOLT-4 cells and effect of trolox treatment. Cells were incubated with 5 μM *cis*-parinaric acid for 1 h before irradiation (5 Gy), then resuspended in fresh medium without probe immediately before irradiation. *A*) Time course: fluorescence measurements performed in irradiated and unirradiated cells at indicated times postirradiation, as described in Methods (no trolox treatment). Data represent mean ± SEM of two independent experiments. *B*) Effect of trolox: cells were treated as above, but trolox was added immediately after irradiation (as described in Methods) and fluorescence determined 30 min postirradiation. Data represent mean ± SEM of four independent experiments. Data in each panel represent percent loss of natural *cis*-parinaric acid fluorescence in each respective sample relative to the level detected immediately before irradiation. Differences between means of data in panels *A* and *B* at 30 min are a reflection of typical experimental variation.

the uptake of extracellular Ca^{2+} (Fig. 8). This inhibition does not appear to result from any impairment of normal cell function caused by trolox toxicity, because the viability of unirradiated or irradiated cells treated with trolox was not significantly different from those cells not treated with trolox (as judged by counts of viable and unviable cells) (Fig. 5). Trolox treatment reduced the background levels of DNA fragmentation that are detected normally in MOLT-4 cells (Fig. 3*A*, *B*, and Fig. 4). Trolox also appears to rescue irradiated cells based on our experiments that showed a greater incorporation of thymidine in irradiated, trolox-treated cells than in irradiated cells not treated with trolox (Fig. 7).

We have shown here that radiation induces a rapid rise in the oxidation of membrane lipids (Fig. 9). If our observations of the effect of trolox are the result of an inhibition of lipid peroxidation chain reactions triggered by radiation, then we might expect that the presence of trolox only before or only during irradiation would be less effective than having trolox present only after irradiation, when chain reactions are propagating and magnifying the damage. This appears to be the case. Our results show that a postirradiation incubation is clearly the most effective at inhibiting radiation-induced apoptosis. Those events occurring after exposure are therefore the most significant for the induction of apoptosis in irradiated cells. A preincubation with trolox, followed by its removal before irradiation, apparently results in a decrease in the concentration of trolox in the membranes of cells to levels that are no longer protective. It is not known whether such a decrease results from the diffusion of trolox out of the membrane after the cells are placed into trolox-free medium or the inactivation by radiation of the trolox present in the membrane. The same reasons can be used to explain the observation that having trolox present only during the period of irradiation had little effect on the development of apoptotic characteristics. Also, the relatively short period the cells are exposed to trolox in such experiments (10–15 min) might not allow enough time for trolox to build to protective levels in the membrane.

We found that the duration of trolox treatment after irradiation plays an important role in the extent of protection provided to the cells. The capacity of trolox to inhibit apoptosis was greatest when the drug was incubated with the cells beginning immediately after irradiation and continuing for not less than 4 h. Longer incubations with trolox produced no significant enhancement of protection. These results indicate that radiation-induced lipid peroxidation chain reactions persist in MOLT-4 cells for hours after irradiation. However, once the chain reactions are blocked, trolox can then be safely removed from the incubation medium. All these characteristics of trolox actions are consistent with the idea that lipid peroxidation plays a key role in the induction of apoptosis in irradiated MOLT-4 cells.

The reactions that link the events of membrane lipid peroxidation and the induction of characteristics of apoptosis in irradiated MOLT-4 cells are not known. It has been shown that plasma membrane integrity plays an important role in maintaining cellular Ca^{2+} homeostasis (25). An elevation of cytosolic Ca^{2+} derived from extracellular sources has been proposed to be responsible for the activation of a nuclear Ca^{2+}-dependent endonuclease thought to be responsible for the internucleosomal fragmentation of chromatin during apoptosis (13, 26), though the requirement for Ca^{2+} in this process is apparently not clear (27). It does not appear that an increased permeability to extracellular Ca^{2+}, resulting possibly from radiation-induced structural damage to the plasma membrane, plays a direct role in the induction of apoptosis in irradiated MOLT-4 cells. In our experiments, Ca^{2+} uptake appears to be an event secondary to DNA fragmentation. Fragmentation begins to increase at about 4 h postirradiation (Fig. 4) and continues to increase steadily with time. DNA agarose gels show a faint, early appearance of a DNA ladder beginning as early as 2 h postirradiation, which increases with time. Ca^{2+} uptake, on the other hand, does not increase significantly until an abrupt rise around 12 h postirradiation, becoming maximal at 16 h (Fig. 8). The lack of a good correlation between the time courses of DNA fragmentation and Ca^{2+} uptake suggests extracellular Ca^{2+} does not activate the nuclear endonuclease. This of course does not discount an important role for Ca^{2+} in the process of DNA fragmentation that is observed in most apoptotic cells. We are currently investigating how various intracellular Ca^{2+} stores are involved in radiation-induced apoptosis.

It is interesting that the increased uptake of extracellular Ca^{2+} is much more closely correlated with the increased background of randomly fragmented DNA observed on agarose gels around 12 h postirradiation (Fig. 3*A*) than it is with the induction of internucleosomal fragmentation. The presence of randomly cleaved DNA is thought to be a consequence of necrotic death pathways that are often associated with an elevation of intracellular Ca^{2+} to toxic levels (28). It is possible that the Ca^{2+} uptake we observe around 12 h is responsible for triggering the characteristics of necrotic death that we and others (9, 10) have observed in irradiated MOLT-4 cells. We are in the process of obtaining data to determine more precisely the temporal correlation between Ca^{2+} uptake and the random scission of DNA induced by radiation.

Regardless of whether the radiation-induced uptake of extracellular Ca^{2+} is involved in apoptotic or necrotic pathways (or both), trolox treatment completely prevents its occurrence (Fig. 8). This implies that the uptake is a consequence of damage to cellular membranes by radiation. The 12 h lag in the manifestation of the damage supports the hypothesis that a build-up of membrane oxidations postirradiation may be responsible. We do not know why an analogous surge of extracellular Ca^{2+} occurs after only 2–3 h in irradiated mouse thymocytes (13). One possibility might be that endogenous antioxidant levels are higher in MOLT-4 cells, providing a longer period of defense against the radiation-induced free radical reactions before the defenses are overwhelmed and the damage progresses. Much interesting work remains to be done to assess the role of intracellular and extracellular Ca^{2+} in apoptosis in irradiated MOLT-4 cells. Understanding

what specific events trolox blocks will undoubtedly help our understanding of the mechanisms of radiation-induced apoptosis.

In conclusion, we have characterized, using morphological and biochemical evidence, MOLT-4 apoptosis induced by exposure to clinically relevant doses of ionizing radiation. We have described the capacity of the membrane penetrating antioxidant drug trolox to block the appearance of characteristics typical of apoptosis and necrosis in these cells. These experiments clearly implicate membrane lipid peroxidation as playing a key role in the process. We are currently involved in studies to characterize further the nature of the damage that occurs in irradiated membranes and the signals such damage produce that result in the induction of genetic mechanisms of self destruction involved in apoptosis. FJ

This work was supported by the Armed Forces Radiobiology Research Institute Work Unit 00150. We thank Ms. Consuella R. Matthews for her dedicated assistance throughout these studies.

REFERENCES

1. Yamada, T., and Ohyama, H. (1988) Radiation-induced interphase death of rat thymocytes is internally programmed (apoptosis). *Int. J. Radiat. Biol.* **53**, 65–75
2. Ashwell, J. D., Schwartz, R. H., Mitchell, J. B., and Russo, A. (1987) Effect of gamma irradiation on resting B lymphocytes. *J. Immunol.* **136**, 3649–3656
3. Stephens, L. C., Schultheiss, T. E., Ang, K. K., and Peters, L. J. (1989) Response of parotid organ culture to radiation. *Radiat. Res.* **120**, 140–153
4. Potten, C. S., Chwalinski, S., Swindell, R., and Palmer, M. (1982) The spatial organization of the heirarchical proliferative cells of the crypts of the small intestines into clusters of "synchronized" cells. *Cell Tissue Kinet.* **15**, 351–370
5. Wyllie, A. H., Kerr, J. F. R., and Currie, A. R. (1980) Cell death: the significance of apoptosis. *Int. Rev. Cytol.* **68**, 251–262
6. Minowada, J., Ohnuma, T., and Moore, G. E. (1972) Rosette-forming human lymphoid cell lines. I. Establishment and evidence for origin of thymus-derived lymphocytes. *J. Natl. Cancer Inst.* **49**, 891–895
7. Szekeley, J. G., Raaphorst, G. P., Lobreau, A. U., and Copps, T. P. (1982) Effect of X-irradiation and radiation modifiers on cellular ultrastructure. *Scan Electron Microsc.* **82**, 335–347
8. Szekeley, J. G., Lobreau, A. U., Einspinner, M., and Raaphorst, G. P. (1985) The use of flow cytometry to measure X-ray survival in cultured T lymphocytes. *Int. J. Radiat. Biol.* **47**, 681–688
9. Shinohara, K., and Nakano, H. (1993) Interphase and reproductive death in X-irradiated MOLT-4 cells. *Radiat. Res.* **135**, 197–205
10. Nakano, H., and Shinohara, K. (1994) X-ray-induced cell death: apoptosis and necrosis. *Radiat. Res.* **140**, 1–9
11. Bacq, Z. M., and Alexander, P. (1961) *Fundamentals of Radiobiology, 2nd ed*, Pergamon Press, New York
12. Castle, L., and Perkins, M. J. (1986) Inhibition kinetics of chain-breaking phenolic antioxidants in SDS micelles. Evidence that intermicellar diffusion may be rate-limiting for hydrophobic inhibitors such as alpha-tocopherol. *J. Am. Chem. Soc.* **108**, 6381–6382
13. Ramakrishnan, N., McClain, D. E., and Catravas, G. N. (1993) Membranes as sensitive targets in thymocyte apoptosis. *Int. J. Radiat. Biol.* **63**, 693–701
14. Purohit, S. C., Bisby, R. H., and Cundall, R. B. (1980) Structural modification of human erythrocyte membranes following gamma-radiation. *Int. J. Radiat. Biol.* **38**, 147–158
15. Nakazawa, T., and Nagatsuka, S. (1980) Radiation-induced lipid peroxidation and membrane permeability in liposomes. *Int. J. Radiat. Biol.* **38**, 537–544
16. Ojeda, F., Andrade, J., Maldonado, C., Guarda, M. I., and Fulch, H. (1991) Radiation-induced surface IgG modulation: protein kinase C involvement. *Int. J. Radiat. Biol.* **59**, 53–58
17. Mickle, D. A. G., Li, R.-K., Weisel, R. D., Birnbaum, P. L., Wu, T.-W., Jackowski, G., Madonik, M., Burton, G., and Ingold U. (1989) Myocardial salvage with trolox and ascorbic acid for an acute evolving infarction. *Ann. Thor. Surg.* **47**, 553–557
18. Wu, T.-W., Hashimoto, N., Wu, J., Carey, D., Li, R.-K., Mickle, D. A. G., and Weisel, R. D. (1990) The cytoprotective effect of trolox demonstrated with three types of human cells. *Can. J. Biochem. Cell Biol.* **68**, 1189–1194
19. Gong, J., Traganos, F., and Darzynkiewicz, Z. (1994) A selective procedure for DNA extraction from apoptotic cells applicable for gel electrophoresis and flow cytometry. *Anal. Biochem.* **218**, 314–319
20. McClain, D. E., Donlon, M. A., Hill, T. A., and Catravas, G. N. (1984) Early kinetics of Ca^{2+} fluxes and histamine release in rat mast cells stimulated with compound 48/80. *Agents Actions* **15**, 279–284
21. Forster, T. H., Allan, D. J., Gobé, G. C., Harmon, B. V., Walsh, T. P., and Kerr, J. F. R. (1992) Beta-radiation from tracer doses of ^{32}P induces massive apoptosis in Burkitt's lymphoma cell line. *Int. J. Radiat. Biol.* **61**, 365–367
22. Solary, E., Bertrand, R., Jenkins, J., and Pommier, Y. (1992) Radiolabeling of DNA can induce its fragmentation in human promyelocytic leukemic HL-60 cells. *Exp. Cell Res.* **203**, 495–498
23. Kuypers, F. A., van den Berg, J. J. M., Schalkwijk, C., Roelofsen, B., and Op den Kamp, J. A. F. (1987) Parinaric acid as a sensitive fluorescent probe for the determination of lipid peroxidation. *Biochim. Biophys. Acta* **921**, 266–274
24. Hedley, D., and Chow, S. (1992) Flow cytometric measurements of lipid peroxidation in vital cells using parinaric acid. *Cytometry* **13**, 686–692
25 Pascoe, G. A., and Reed, D. J. (1989) Cell calcium, vitamin E, and the thiol redox system in cytotoxicity. *Free Rad. Biol. Med.* **6**, 209–224
26. McConkey, D. J., Nicotera, P., Hartzell, P., Bellomo, G., Wyllie, A. H., and Orrenius, S. (1989) Glucocorticoids activate a suicide process in thymocytes through an elevation of cytosolic Ca^{2+} concentration. *Arch. Biochem. Biophys.* **269**, 365–370
27. Zhivotovsky, B., Nicotera, P., Bellomo, G., Hanson, K., and Orrenius, S. (1993) Ca^{2+} and endonuclease activation in radiation-induced lymphoid cell death. *Exp. Cell Res.* **207**, 163–170
28. Boobis, A. R., Fawthrop, D. J., and Davies, D. S. (1989) Mechanisms of cell death. *Trends Physiol. Sci.* **10**, 275–280

Received for publication June 9, 1995

Accepted for publication July 10, 1995.

NeuroToxicology® 16(3): 497-510, 1995

Gamma Radiation-Induced Disruption in Schedule-Controlled Performance in Rats[1]

PAUL C. MELE[2] AND JOHN H. MCDONOUGH[3]

Behavioral Sciences Department Armed Forces Radiobiology Research Institute, Bethesda, Maryland 20889-5145 USA; [2]Current address: Office of Research and Technology Applications, Walter Reed Army Institute of Research, Washington, DC 20307-5100; and [3]Current address: Biochemical Pharmacology Branch, U.S. Army Medical Research Institute of Chemical Defense, Aberdeen Proving Ground, Maryland 21010-5425

Abstract: PAUL C. MELE AND JOHN H. MCDONOUGH. Gamma Radiation-Induced Disruption in Schedule-Controlled Performance in Rats. *Neurotoxicology* **16**(3): 497-510, 1995. *Adult male rats responded under a multiple fixed-interval 2-min, fixed-ratio 50 (multiple FI FR) schedule of milk delivery. Four groups of rats were given acute whole-body doses of 2.25, 4.5, 6.75, or 9.0 gray (Gy) of ^{60}Co gamma-photon radiation; a fifth group of rats received sham irradiation. During the session that began 10 min after exposure (day 1), multiple FI FR performance was not significantly affected in any treatment group. Neither the sham nor the 2.25-Gy irradiation produced significant alterations in performance over 6 weeks postexposure. Over days 2-4 postexposure, the 4.5-Gy and 6.75-Gy doses reduced response rates approximately 50% and increased postreinforcement pause durations under both the FI and FR schedules. The 9.0-Gy dose produced a progressive decline in both FI and FR responding over the first week postexposure, with response rates decreasing to approximately 10% of pre-irradiation control levels on day 5. Frequently, FI rates decreased more than FR rates after exposure to 4.5-9.0 Gy. Substantial recovery of pre-irradiation response rates was evident in all treatment groups over weeks 2-4 postexposure; behavioral recovery was essentially complete during postexposure weeks 5 and 6. Eight weeks after irradiation, two groups of rats were irradiated a second time. In the group given two 6.75-Gy exposures, performance decrements were similar after each exposure. In the group given two 9.0-Gy exposures, performance declined more rapidly and showed less recovery after the second exposure than after the first. Re-irradiation produced a dose-dependent increase in the incidence of lethality. Overall, gamma radiation disrupted schedule-controlled responding in a dose-related manner; both the magnitude and time course of this disruption varied as a function of dose. Exposure to higher doses of gamma radiation resulted in residual damage that was expressed following re-irradiation challenge.* © *1995 Intox Press, Inc.*

Key Words: Gamma Radiation, Operant Behavior, Behavioral Recovery, Re-irradiation Challenge, Residual Damage

INTRODUCTION

Early effects of whole-body exposure to ionizing radiation in humans are characterized by dose-dependent and time-dependent sequelae known collectively as the acute radiation syndrome (Anno *et al.*, 1989). As the delivered dose of radiation increases, there is a reduction in the latency to onset and an increase in the severity and duration of the different components of the syndrome. Of these components, behavioral and

Please send requests for reprints to Dr. Paul C. Mele, Office of Research and Technology Applications, Walter Reed Army Institute of Research, Washington, DC 20307-5100 USA.

[1]Early studies used the roentgen as the unit of ionizing radiation (x ray photons) measured free in air. More recent studies have used the rad or the gray (Gy), which are units of absorbed dose in tissue, as the unit of measurement for both photon (x rays and gamma rays) and particle (*e.g.*, proton and neurton) radiation (International Commission on Radiation Units and Measurement, 1980). To facilitate comparison between results reported in the present study with those reported previously, all radiation doses cited have been converted to Gy. To convert roentgen to rad, a quasi-conversion factor of 0.96 was used. Rad was converted to Gy by multiplying by 0.01.

Submitted: February 16, 1994. Accepted: June 6, 1995.

neurological endpoints are among the most sensitive indicators of exposure. Anorexia, for example, is one of the first symptoms to appear after exposure to relatively low, sublethal doses of radiation. Nausea, vomiting, weakness, and fatigue become manifest at similar or successively higher doses. These effects typically last for hours or days after irradiation, although mild weakness and fatigue may persist for weeks or even months after low-level exposures. As the level of exposure is increased, additional behavioral and neurological dysfunctions such as headache, dizziness, disorientation, and fainting may occur.

Animal studies have shown that schedule-controlled operant behavior provides a sensitive means of identifying and quantifying dose-related and time-related effects of ionizing radiation. Early studies demonstrated that acute exposure to photon radiation (either 250-kilovolt peak, kVp, x rays or ^{60}Co gamma rays) produced a dose-dependent reduction in responding under fixed-ratio (FR) (Brown *et al.*, 1966; Wicker and Brown, 1965) or variable-interval (VI) (Jarrard, 1963) schedules of food or water reinforcement in rats for several days. When rats (Brown, 1966; Brown *et al.*, 1960) or rhesus monkeys (Braun *et al.*, 1966; Yochmowitz and Brown, 1977) were irradiated throughout operant test sessions, responding decreased as a function of the cumulative dose delivered. A recent study demonstrated that moderate sublethal doses of ^{60}Co gamma radiation decreased responding under both FR and fixed-interval (FI) schedules of milk delivery in rats (Mele *et al.*, 1988). That study also demonstrated that performance under the FR schedule was more sensitive to gamma radiation than was performance under the FI schedule, in that FR response rates were decreased at a lower dose than the dose required to decrease FI response rates. A related study reported that a higher dose of gamma radiation was required to disrupt responding under an FR schedule of termination of foot shock than the dose that was sufficient to disrupt responding under an FR schedule of milk delivery (Mele *et al.*, 1990). Acute exposure to gamma radiation has recently been found to decrease response rates and increase error rates in a dose-dependent manner in rats performing a repeated-acquisition of response-chains task (Winsauer and Mele, 1993).

Disruptions in behavior induced by sublethal doses of ionizing radiation have been shown to be reversible, with a return to pre-irradiation levels of performance serving to define behavioral recovery after exposure (Kimeldorf and Hunt, 1965; Jarrard, 1963; Mele *et al.*, 1988, 1990). However, the possibility remains that residual damage may exist following certain levels of exposure. For example, in studies that used radiation-induced lethality as the endpoint, animals that had been exposed to sublethal doses of ionizing radiation succumbed following a second exposure if the individual sublethal doses were sufficiently high and occurred within the appropriate time interval (see review by Sacher, 1958). Thus, lethality induced by a re-irradiation challenge indicated an interaction between the two exposures, and suggested that recovery following the initial exposure was incomplete at the time of the second exposure. Re-irradiation challenge has also been used to demonstrate incomplete recovery in functional aspects of specific organ systems (Baum, 1967; Hubner *et al.*, 1981; Stewart and Oussoren, 1990; Terry *et al.*, 1989). In contrast, few studies have used re-irradiation challenge to evaluate residual damage following recovery from radiation-induced behavioral deficits. One study reported that the performance of rats responding under a continuous-reinforcement (or FR-1) schedule was more severely disrupted after the second of two exposures to moderate or high doses (approximately 4 or 8 Gy) of gamma radiation when the exposures occurred one week apart (Wicker and Brown, 1965). In contrast, when low to moderate doses of gamma radiation (0.5-4.5 Gy) were given repeatedly at 6-week intervals to rats responding under either FR or FI schedules, the effects on performance were similar after each of three exposures (Mele *et al.*, 1988).

The present study extended the evaluation of the effects of gamma radiation on schedule-controlled performance in rats. One goal was to define more precisely the dose-effect and time-course functions that relate changes in performance to acute exposures. To achieve this goal, the effects of a range of radiation doses (2.25-9.0 Gy) were examined over an extended period (6 weeks) postexposure. A second goal was to extend the evaluation of effects on performance of repeated exposures to gamma radiation. Here, the effects of two exposures to higher doses of gamma radiation (6.75 Gy and 9.0 Gy) than those used previously were examined. Performance was maintained under a multiple FI 2-min, FR 50 schedule of milk presentation. A multiple schedule consists of two or more component schedules presented successively during a session, each in the presence of a discriminative stimulus (Ferster and Skinner, 1957).

The use of a multiple schedule allowed for the extension of results obtained previously when FI 2-min and FR-50 schedules were used independently as simple (*i.e.*, single) schedules (Mele *et al.*, 1988).

MATERIALS AND METHODS

Animals

Experimentally naive male Sprague-Dawley rats (Charles River Breeders, Raleigh, North Carolina) were housed individually in plastic Micro-Isolator cages containing sterilized wood-chip bedding. Free access to commercial rodent chow and acidified water (pH = 2.5-3.0) were provided. Acidified water is commonly used to reduce the possibility of opportunistic bacterial infection in irradiated animals (McPherson, 1963). When the rats were approximately 100 days old, body weights were gradually reduced to and then maintained at 80% of free-feeding levels by providing a measured amount of chow (6-15 g for individual rats) 30-60 min after each daily session. On weekends, when operant testing was not conducted, additional chow was provided to maintain body weights at the appropriate level. At the time of the initial irradiation, group mean (± SE) body weights ranged from 373 (± 7) g to 384 (± 14) g. Individual body weights across all groups ranged from 345-438 g. Animal housing rooms were kept at 21 ± 1° C with 50 ± 10% relative humidity. A 12-hr light cycle was in effect with lights on from 0600-1800.

Apparatus

Ten identical operant conditioning chambers (Coulbourn Instruments, Inc., Lehigh Valley, Pennsylvania, model E10-10) were used. A response lever protruded into the chamber on the left side of the front wall 6.2 cm above the steel grid floor, three cue lights were located 3.4 cm above the lever, a house light and a Sonalert speaker were located in the upper middle portion of the front wall, and an opening in the front wall 1.1 cm above the floor allowed access to a dipper that presented 0.06 ml of sweetened condensed milk (a 1:1, v:v mixture of Borden Eagle Brand and tap water). Each chamber was enclosed in a sound- and light-attenuating cubicle that contained an exhaust fan for ventilation. All cubicles were located in a single room with masking noise present continuously. A PDP-11/73 computer (Digital Equipment Corp., Inc., Maynard, Maryland) running SKED-11 software (State Systems, Inc., Kalamazoo, Michigan) was located in a nearby room where it controlled experimental contingencies and recorded data. Cumulative recorders (Gerbrands Corp., Arlington, Massachusetts) were used to evaluate within session patterns of responding.

Behavioral Procedure

Rats were trained to respond under a multiple FI 2-min, FR 50 schedule of milk reinforcement (Ferster and Skinner, 1957). Under the FI schedule, the first lever-press that occurred after a 2-min interval resulted in the presentation of the milk-filled dipper for 4 sec; responses that occurred within the 2-min interval had no programmed consequences. Under the FR schedule, the dipper was presented after 50 responses had been made. The house light was turned on when the FI component was in effect, and the cue lights and Sonalert were turned on when the FR component was in effect. Performance under the FI 2-min schedule was established first, followed by training under the multiple FI FR schedule. A low value of each schedule was used initially (*i.e.*, FI 10 sec and FR 1). Schedule values were increased gradually until final values were in effect. Daily sessions began with an FI component, and FI and FR components alternated until each had occurred three times. There was a 150-sec limited hold on each FI and FR component. Components terminated with the first reinforcer delivered after 10 min or after the limited hold had timed out, whichever occurred first. The value of the limited hold was set to prevent or reduce the likelihood of terminating a component within a given FI or FR. Under these schedule parameters, a maximum of 15 total reinforcers could be obtained under the FI schedule during a session (*i.e.*, five reinforcers obtained within each of the three FI components). A 10-sec timeout occurred after the termination of each component at which time all stimuli were extinguished and responses had no programmed consequences. Daily sessions lasted approximately 1 hr, were conducted between 0800-1300, and occurred 5 days per week, Monday through Friday. Training under the final multiple FI FR schedule continued for at least eight weeks to stabilize baseline control performance (until there were no consistent trends in rates and patterns of responding from day to day over several weeks); animals were habituated to the irradiation procedures during this period.

Radiation Procedure

Rats were assigned to one of five treatment groups (n = 6-7 per group) so that baseline response rates under each schedule were similar across groups. To the extent possible, animals from different dose groups were balanced across operant chambers and time of day for testing. Initially, all rats were habituated to the irradiation procedure over at least eight occasions (one or two per week) prior to irradiation. Habituation sessions consisted of placing the rats into clear-plastic well-ventilated tubes that provided loose restraint. Tubes were stacked one above the other in a plastic stand. Restrained in this way, the rats were transported to and from the ^{60}Co facility at the Armed Forces Radiobiology Research Institute (AFRRI). The usual daily test session began shortly after the rats were removed from the restraining tubes. Total restraint time was 20-30 min, which included the time necessary for delivery of the highest radiation dose to be tested. Comparison between baseline sessions and the last four sessions during which the rats were restrained in exposure tubes and transported to and from the ^{60}Co facility showed that this method of restraint did not alter performance in any consistent manner.

On the day of irradiation, four groups of rats were administered bilateral whole-body midline tissue doses of 2.25, 4.5, 6.75, or 9.0 Gy of gamma-photon radiation at a nominal dose rate of 2.5 Gy/min from the AFRRI ^{60}Co source. All rats were put into the sealed exposure room for a duration equal to that required for delivery of the highest dose of radiation. Behavioral test sessions began approximately 10 min after irradiation. Eight weeks after initial irradiation, rats that had been given either the 6.75-Gy or 9.0-Gy dose were given a second irradiation at the same dose given initially. Irradiation days were designated as day 1 and always occurred on Mondays.

Prior to irradiation, the desired midline tissue dose rate (MTD) was established using an acrylic rat phantom and a tissue-equivalent ionization chamber with calibration traceable to the National Institute of Standards and Technology. Dosimetric measurements were made according to established protocols for determining absorbed dose from high-energy photon beams (American Association of Physicists in Medicine, 1983). The ratio used for estimation of the tissue-to-air dose rate (the MTD at the abdominal level) was 0.93.

Data Collection and Analysis

Individual performance measures calculated for each session for FR and FI responding included mean overall response rates, postreinforcement pause durations, and running response rates. The number of reinforcers obtained per session under the FI schedule was also examined because FI response rates and reinforcer rates can vary independently from each other. Overall response rates were calculated by dividing the total number of responses emitted under each schedule by the total time each schedule was in effect, excluding the time the dipper was raised. Postreinforcement pause durations were defined as the time elapsed from the end of a dipper presentation until the first response of the next FR or FI. Running response rates were response rates calculated with the postreinforcement pause durations omitted.

For FI performance, an index of curvature was calculated to provide a quantitative measure of the temporal distribution of responses within the interval (Fry *et al.*, 1960). Typical performance under FI schedules is characterized by relatively low response rates during earlier portions of the interval and relatively high response rates during later portions of the interval. To calculate the index of curvature, responses within the FI were counted in four successive 30-sec segments of the interval. In this case, the index can reach a maximum of +0.75, which indicates that all responses occurred in the last 30-sec segment; an index of 0.0 indicates that responses were equally distributed over the four segments.

Radiation-induced changes in performance measures were analyzed statistically over week 1 (days 1-5) after exposure; the exposure day was designated day 1. Pre-irradiation control data consisted of all nonsham-irradiation sessions (n = 6) that occurred during the two-week period that immediately preceded the first exposure (three nonsham sessions per week). Response rates and the index of curvature were analyzed with repeated-measures analysis of variance for overall main effects and interactions, F-tests for simple-main effects, and post hoc Dunnett's test for multiple comparisons. Separate analyses were performed on absolute response rates under each schedule. Radiation dose (five levels) was the between-subjects factor and day (six levels including pre-irradiation control and days 1-5 postexposure) was the within-subject factor. For direct comparison of effects of radiation on FI and

TABLE 1. Pre-irradiation Performance Under a Multiple FI 2-min, FR 50 Schedule of Reinforcement.

	Gamma Radiation Dose (Gy)				
	Sham (N = 7)	2.25 (N = 6)	4.5 (N = 7)	6.75 (N = 7)	9.0 (N = 6)
FR Responses Per Sec	3.29 (0.65)	3.50 (0.77)	3.04 (0.41)	3.03 (0.42)	3.60 (0.54)
FI Responses Per Sec	0.94 (0.24)	0.65 (0.10)	1.00 (0.25)	0.69 (0.16)	0.73 (0.15)
FI Index Of Curvature	0.39 (0.08)	0.31 (0.10)	0.34 (0.06)	0.39 (0.08)	0.38 (0.10)

Entries are group means with one SE in parentheses.

FR response rates, response rates after irradiation (five levels: days 1-5) were expressed as a percentage of pre-exposure control values in order to reduce the variability that can occur when averaging absolute response rates. Postreinforcement-pause durations were analyzed with the Friedman analysis of variance and the Wilcoxin matched-pairs signed-ranks test; nonparametric tests were used because of the substantial increase in variability in pause durations that sometimes occurred after exposure. The alpha level for all tests was set at $p < 0.05$.

RESULTS

Under baseline control conditions, overall FR response rates were substantially higher than overall FI response rates (Table 1). Consistent with this schedule-dependent difference in overall response rates, postreinforcement pause durations were shorter (Table 2) and running response rates were higher (Table 3) under the FR schedule than under the FI schedule. The FI index of curvature (Table 1) indicates that response rates were relatively low early in the interval and relatively high later in the interval.

Dose-dependent and time-dependent effects of gamma radiation on overall FI and FR response rates are presented in Fig. 1. Analysis of variance showed that the main effect of gamma-radiation dose on absolute response rates was not significant under either schedule, the main effect of day over days 1-5 after exposure was significant for each schedule, $F(5,140) = 17.71$ and 14.33 for FI and FR, respectively, p's < 0.0001, and the gamma-radiation dose x day interaction was significant for both the FI and FR schedule, $F(20,140) = 4.04$ and 7.41, respectively, p's < 0.0001. Response rates were not altered significantly under either schedule in any treatment group on the day of exposure (day 1), nor in the sham-exposed group and the group irradiated with 2.25 Gy at any time after exposure. After irradiation with 4.5 Gy, both FR (days 2 and 3) and FI (days 2-4) response rates decreased significantly (Dunnett's test, p's < 0.01) from pre-exposure levels. On day 5, response rates in each component had recovered to approximately 80% of pre-exposure levels. FI response rates (percentage of pre-irradiation control values) were reduced significantly more than FR response rates, $F(1,6) = 9.26$, $p < 0.025$. After irradiation with 6.75 Gy, significant

TABLE 2. Effects of Gamma Radiation on Postreinforcement Pause Durations Under a Multiple FI 2-min, FR 50 Schedule of Reinforcement.

	Gamma Radiation Dose (Gy)				
	Sham (N = 7)	2.25 (N = 6)	4.5 (N = 7)	6.75 (N = 7)	9.0 (N = 6)
FI Control	43.8 (6.4)	31.5 (8.3)	39.0 (7.9)	39.53 (10.6)	35.9 (7.4)
Day 1	47.2 (6.8)	31.3 (6.7)	43.1 (8.7)	40.4 (11.4)	37.4 (6.4)
Day 2	59.1 (12.4)	41.0 (11.3)	69.8* (14.9)	55.3* (9.7)	62.9* (10.9)
Day 3	50.5 (7.9)	35.8 (8.1)	59.0* (9.5)	50.6 (6.0)	57.5 (9.6)
Day 4	44.4 (7.3)	34.8 (9.4)	50.0* (7.2)	49.3 (7.6)	73.4* (11.0)
Day 5	46.5 (7.7)	34.0 (9.2)	45.5 (9.9)	45.5 (8.3)	118.0* (34.0)
FR Control	3.7 (0.7)	5.4 (1.5)	2.9 (0.4)	4.0 (1.1)	3.3 (0.5)
Day 1	3.9 (0.8)	8.4 (3.5)	2.9 (0.4)	5.4 (2.4)	3.2 (0.5)
Day 2	3.8 (0.9)	11.1 (4.9)	6.8* (2.1)	10.3* (4.7)	5.8* (1.4)
Day 3	4.1 (0.8)	5.5 (1.4)	7.7* (3.5)	7.7* (2.5)	8.4* (3.2)
Day 4	3.8 (0.8)	7.4 (2.7)	4.1 (0.6)	12.0* (4.4)	16.4* (5.8)
Day 5	3.5 (0.6)	4.8 (1.0)	4.8 (1.0)	8.6 (3.4)	187.7* (99.0)

Entries are group mean postreinforcement pause durations in seconds with one SE in parentheses. *$p < 0.05$, Wilcoxin matched-pairs signed-ranks test.

TABLE 3. Effects of Gamma Radiation on Running Response Rates Under a Multiple FI 2-min, FR 50 Schedule of Reinforcement.

	Gamma Radiation Dose (Gy)				
	Sham (N = 7)	2.25 (N = 6)	4.5 (N = 7)	6.75 (N = 7)	9.0 (N = 6)
FI Control	1.29	0.88	1.33	0.93	1.02
	(0.22)	(0.10)	(0.25)	(0.13)	(0.44)
Day 1	1.29	0.74	1.19	0.76	1.05
	(0.23)	(0.10)	(0.25)	(0.17)	(0.18)
Day 2	1.51	0.72	0.79*	0.68	0.69
	(0.26)	(0.09)	(0.13)	(0.12)	(0.14)
Day 3	1.55	0.70	0.81*	0.66	0.55*
	(0.27)	(0.10)	(0.21)	(0.13)	(0.10)
Day 4	1.49	0.78	1.03	0.74	0.45*
	(0.24)	(0.10)	(0.23)	(0.16)	(0.10)
Day 5	1.51	0.86	1.18	0.91	0.31*
	(0.26)	(0.10)	(0.23)	(0.13	(0.15)
FR Control	4.10	4.89	3.62	3.69	4.60
	(0.84)	(1.17)	(0.50)	(0.45)	(0.74)
Day 1	3.97	4.85	3.97	3.86	4.67
	(0.75)	(1.25)	(0.57)	(0.53)	(0.69)
Day 2	4.15	4.80	2.67	3.68	3.56
	(0.84)	(1.18)	(0.38)	(0.79)	(0.37)
Day 3	4.07	4.54	2.17*	3.38	3.18*
	(0.81)	(0.97)	(0.52)	(0.78)	(0.32)
Day 4	4.10	4.74	2.84	2.92	1.95*
	(0.77)	(1.11)	(0.39)	(0.61)	(0.35)
Day 5	4.24	4.68	3.21	4.27	0.59*
	(0.74)	(0.97)	(0.48)	(1.05)	(0.23)

Entries are group mean responses per second with one SE in parentheses. *p < 0.01 versus control, Dunnett's test. Results of ANOVAs are as follows. FR: gamma radiation dose x day interaction, $F(20,140) = 6.36$, $p < 0.0001$, and main effect of day, $F(5,140) = 9.72$, $p < 0.0001$. FI: gamma radiation dose x day interaction, $F(20,140) = 4.06$, $p < 0.0001$, and main effects for radiation dose, $F(4,28) = 3.29$, $p < 0.05$, and day, $F(5,140) = 4.94$, $p < 0.0005$.

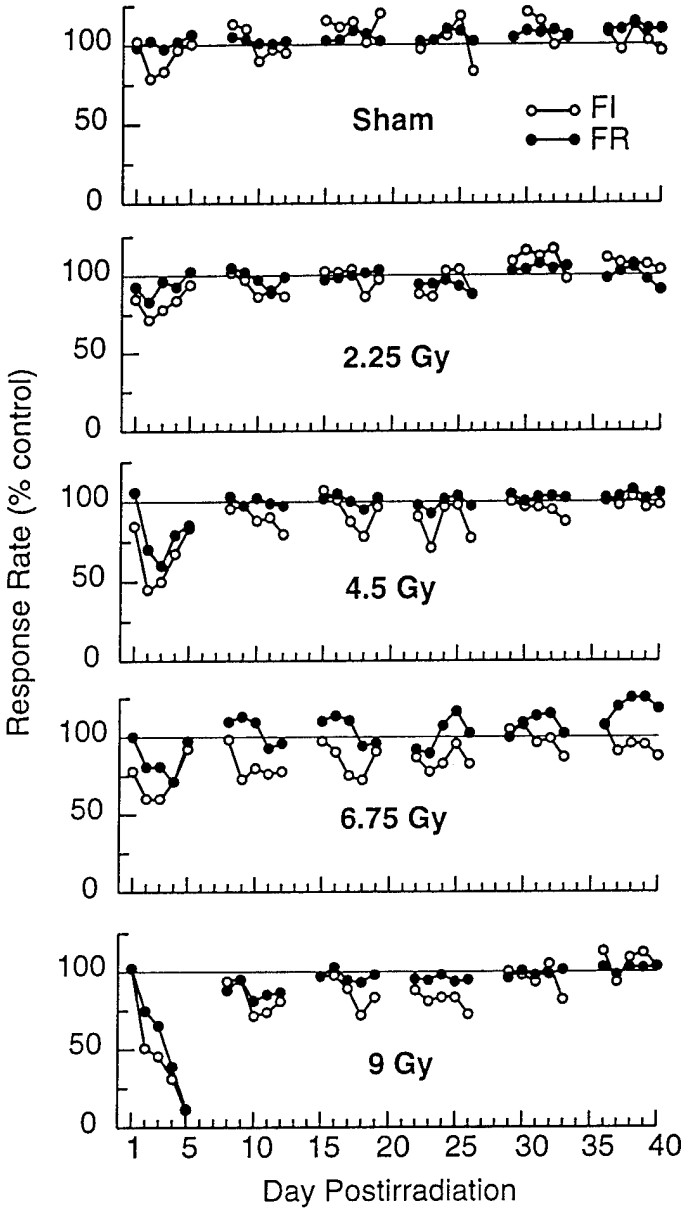

FIG. 1. Dose-dependent effects of gamma radiation on overall response rates maintained under a multiple FI 2-min, FR 50 schedule of milk presentation in rats. Separate groups of rats (n = 6-7 per group) were exposed to the indicated doses of ^{60}Co gamma radiation. The session on day 1 (Monday) began approximately 10 min after irradiation. Subsequent sessions occurred at 24-hr intervals, Monday through Friday. The horizontal line at 100% on the ordinate indicates the mean control response rate calculated from six sessions that occurred prior to irradiation. Each point represents the group mean response rate for a single session.

(Dunnett's test) decreases occurred in FI (day 2, $p < 0.01$ and day 3, $p < 0.05$) and FR (day 4, $p < 0.05$) response rates. Both FI and FR response rates recovered to greater than 90% of pre-irradiation levels on day 5. Although FI response rates (percent of control) decreased more than FR response rates, these differences did not achieve statistical significance. After irradiation with 9.0 Gy, there was a progressive decline in responding in each component over days such that both FI and FR response rates were reduced to approximately 10% of pre-exposure levels on day 5; significant (Dunnett's test) decreases in response rates occurred on day 2 ($p < 0.05$) and days 3-5 (p's < 0.01) under FR and days 2-5 (p's < 0.01) under FI. When reductions in response rates were expressed as percent of control, FI response rates were shown to decrease significantly more rapidly than FR response rates, as indicated by the significant main effect of schedule, $F(1,5) = 15.51$, $p = 0.01$, and the significant

schedule x day interaction, $F(4,20) = 3.79$, $p < 0.025$. Furthermore, at each of the three highest doses of gamma radiation, the changes in relative response rates over days were highly significant (p's ≤ 0.002 for main effects of day).

Response rates at the beginning of week 2 (day 8) postexposure were essentially at or close to control levels in the three most heavily exposed groups. Subsequently, however, FI response rates of each of these groups decreased during one or more sessions in week 2 and intermittently in weeks 3 and 4. The magnitudes of these reductions were typically less than those during week 1 and were not clearly dose related, though their frequency appeared to be greater at the two higher doses. In addition, small decreases in FR response rates were evident over much of week 2 after irradiation with 9.0 Gy. One rat in the 9.0-Gy treatment group died prior to testing on day 9; death occurred after this rat's response rates on day 8 had returned to better than 90% of pre-exposure levels. During weeks 5-6 postexposure, response rates were generally at pre-irradiation control levels in each treatment group.

Gamma radiation produced dose-related increases in both FI and FR postreinforcement pause durations during week 1 after exposure (Table 2). Peak increases under each schedule typically occurred on day 2 or 3 after irradiation with 4.5 or 6.75 Gy, whereas pause durations increased steadily over days 1-5 after the 9.0-Gy exposure. During week 2 after irradiation, pause durations decreased toward control values in these three groups to the extent that significant increases were no longer evident (not shown). At no time did either the sham exposure or the 2.25-Gy dose alter pause durations significantly.

Running response rates under each schedule were reduced for 2-3 days during week 1 following exposure to the 4.5-9.0 Gy doses (Table 3). The time courses of these reductions were similar to those observed for overall response rates (Fig. 1), although relative reductions in running response rates were somewhat less than those in overall response rates. The 4.5-Gy and 9.0-Gy doses reduced both FI and FR running response rates significantly (Table 3). In contrast, the reductions in running response rates induced by the 6.75-Gy dose failed to achieve statistical significance during any of the first five days postexposure, even though in the ANOVA the main effects of dose and day and the interaction were significant.

Cumulative records indicated that radiation-induced changes in response rates and pause durations were generally evident throughout entire sessions. For some rats, the magnitudes of these changes appeared to be similar during each of the three presentations of each component schedule, while for other rats, these changes became more pronounced as the session progressed.

The FI index of curvature was not altered significantly by any dose of gamma radiation. This indicates that the relative distribution of responses within the interval was unaffected despite the often marked suppression of response rates that occurred after irradiation. In contrast, there was a dose-related reduction in the number of FI reinforcers earned per session during week 1 after exposure. All rats in the sham and 2.25-Gy exposure groups earned the maximum of 15 FI reinforcers during each of these postexposure sessions (the only exception was one rat in the sham-exposure group that obtained 11 FI reinforcers on day 2). In both the 4.5-Gy and 6.75-Gy treatment groups, approximately one-half of the rats (three and four of seven respectively) earned 10-14 reinforcers under the FI schedule during one or more of these sessions. After the 9.0-Gy exposure, the number of FI reinforcers earned per session decreased during week 1 until day 5 when the group mean $\pm$ SE was 9.5 ± 1.5; only one of six rats earned 15 FI reinforcers during each of the first five sessions postirradiation. With rare exception, all rats in each treatment group earned the maximum of 15 FI reinforcers per session over weeks 2-6 after irradiation.

A second exposure to 6.75 Gy of gamma radiation eight weeks after the first exposure did not alter either FI or FR response rates significantly different from those observed after the first exposure (Fig. 2); the main effect of exposure number and the exposure number x day interaction were not significant for either schedule, while the main effect of day was significant for the FR schedule only, $F(4,24) = 4.22$, $p = 0.01$. One rat exhibited large increases in FI response rates during weeks 1 and 2 after the second exposure, an effect that was not observed after the initial exposure; these increases account for the large SEs shown in Fig. 2. However, further analysis of FI response rates with the data from this animal omitted also failed to reveal significant differences between the two exposures on any given day.

In contrast to the behavioral results, re-irradiation with 6.75 Gy had a marked effect on survival in that three of seven rats died between days 20-32 after the second exposure. For several days prior to death, there was typically a progressive deterioration in performance, a failure to consume the entire daily ration of chow,

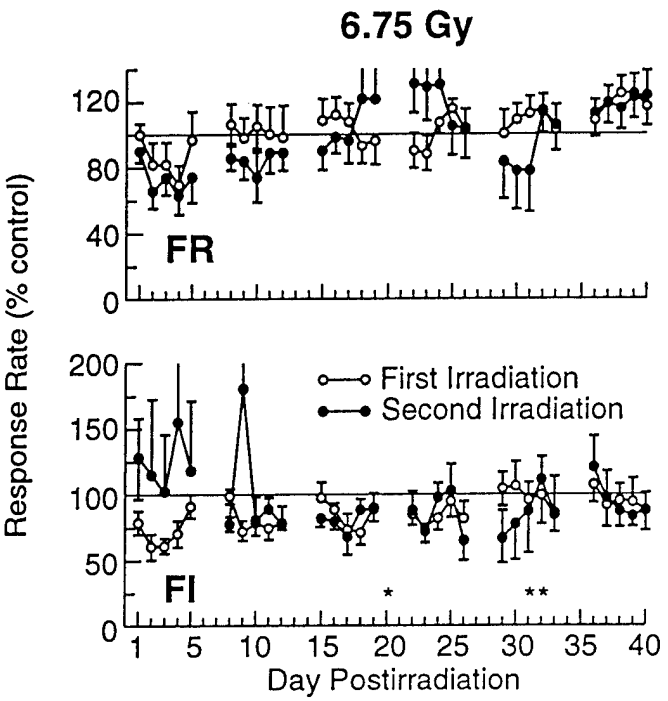

FIG. 2. Effects of two exposures to 6.75 Gy of ^{60}Co gamma radiation on overall response rates maintained under a multiple FI 2-min, FR 50 schedule of milk presentation in seven rats. An 8-week interval separated the two exposures. The session on day 1 (Monday) began approximately 10 min after irradiation. Subsequent sessions occurred at 24-hr intervals. The horizontal line at 100% on the ordinate indicates the mean control response rate calculated from six sessions that occurred prior to each exposure. Each point represents the group mean response rate for a single session. Vertical lines about the means indicate + 1 SE. Asterisks along the abscissa indicate deaths that occurred after the second exposure.

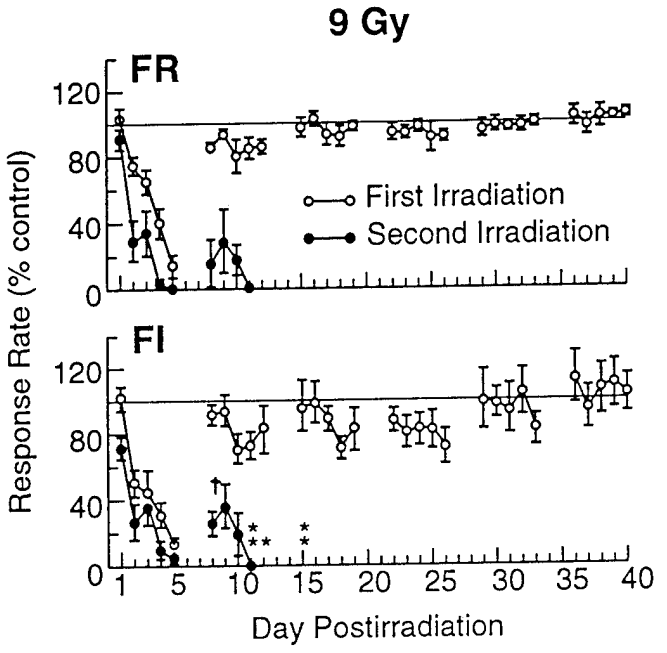

FIG. 3. Effects of two exposures to 9.0 Gy of ^{60}Co gamma radiation on overall response rates maintained under a multiple FI 2-min, FR 50 schedule of milk presentation. Six rats were irradiated initially, and the five surviving rats received a second exposure eight weeks later. The session on day 1 (Monday) began approximately 10 min after irradiation. Subsequent sessions occurred at 24-hr intervals. The horizontal line at 100% on the ordinate indicates the mean control response rate calculated from six sessions that occurred prior to each exposure. Each point represents the group mean response rate for a single session. Vertical lines about the means indicate ± 1 SE. The cross and the asterisks along the abscissa indicate deaths that occurred after the first and second exposures, respectively.

and a drop in body weight. Also at this time, these rats were hypothermic, as assessed by gross handling, and had noticeably pale eyes, indicating radiation-induced anemia.

The five rats that survived the initial 9.0-Gy irradiation received a second 9.0-Gy exposure eight weeks after the first. Compared to the initial irradiation, the second exposure produced a more rapid decline in both FR and FI response rates over week 1 postexposure (Fig. 3). For the five rats undergoing both 9.0-Gy irradiations, there was a significant effect of exposure number for FR response rates, $F(1,4) = 26.74$, $p < 0.01$, and a significant effect of day for both FR and FI response rates, $F(4,16) = 49.27$ and 39.89, respectively, both p's < 0.0001.

There was also a pronounced difference between the two 9.0-Gy exposures in terms of the degree of recovery during week 2. Whereas both FR and FI response rates recovered substantially during week 2 after the initial exposure, response rates recovered to a much lesser degree after the second exposure before dropping precipitously to essentially zero by day 11. All rats in this group died between days 11-15 after the second 9.0-Gy exposure.

All rats consumed their entire daily ration of chow on each day after exposure to 2.25, 4.5, or 6.75 (both exposures except just prior to death as noted previously) Gy of gamma radiation. After the initial 9.0-Gy exposure, five of six rats left a small portion of their daily ration of chow (range of 1-4 g) unconsumed on day 5. After the second 9.0-Gy exposure, the anorexia on day 5 was typically more pronounced in four of five rats (range of 8-14 g of food unconsumed). Body weights also were reduced on day 5 after each 9.0-Gy exposure; on average, body weights decreased 6.7 ± 2.3 g and 17.8 ± 1.9 g after the first and second 9.0-Gy irradiations, respectively. Recovery of pre-irradiation body weights was evident in the majority of rats during week 2 after the first exposure. However, after the second irradiation, changes in food consumption and body weights during

week 2 varied markedly among individual rats. At the time of death, some rats appeared to be recovering from the acute effects of radiation while others were deteriorating.

For the rats that died after the two 6.75-Gy or 9.0-Gy exposures, the doses received and the time course of deaths indicated radiation-induced hematopoietic dysfunction with resultant infection and/or bleeding as the probable cause of death. Pathology examinations of animals that died confirmed the existence of hematopoietic damage, including severe and diffuse depletion of lymphoid and spleen tissues and mild-to-marked hemosiderosis. The 6.75-Gy irradiations produced mild-to-moderate multifocal hemorrhage, while the 9.0-Gy irradiations produced widespread acute hemorrhage that was especially severe in the gastrointestinal tract, lungs, thoracic cavity, pericardium, pancreas, and testes.

DISCUSSION

The present results confirm and extend those of a previous study from this laboratory showing that ^{60}Co gamma radiation dose-dependently disrupted performance under an FR schedule of reinforcement in rats (Mele *et al.*, 1988). That study found that 0.5 and 1.5 Gy of gamma radiation did not alter either response rates or postreinforcement pause durations under a simple FR-50 schedule of milk presentation. Similarly, it was observed here that 2.25 Gy produced small, nonsignificant reductions in FR response rates and increases in FR postreinforcement pause durations when FR performance was examined as a component of a multiple schedule. In contrast, a dose of 4.5 Gy decreased FR response rates and increased FR pause durations under the simple and multiple schedules to a similar degree. Taken together, the findings of these two studies suggest that for acute whole-body exposures, the threshold dose of gamma radiation that disrupts FR-50 performance lies between 2.25 and 4.5 Gy.

In our earlier study (Mele *et al.*, 1988), we also reported that 6.5 Gy of gamma radiation disrupted FR performance. That finding, however, must be interpreted with some caution because 6.5 Gy was tested only in rats that had been exposed previously to lower doses of gamma radiation. The present study, therefore, sought to extend the evaluation of the effects of gamma radiation on FR performance to include doses greater than 4.5 Gy. Exposure to 4.5 and 6.75 Gy produced reversible disruptions in FR responding that were comparable in magnitude and time course. In contrast, exposure to 9.0 Gy produced a progressive decline in FR responding to levels that were markedly below those found with lower doses.

Dose-dependent decreases in response rates and increases in postreinforcement pause durations in the FI component of the multiple FI FR schedule were also found in the present study. In contrast, the characteristic temporal distribution of responses that occurred under the FI schedule, as quantified by the index of curvature, was not altered significantly by any dose of radiation. These findings confirm and extend those of a previous study that used a simple (*i.e.*, single) FI 2-min schedule of milk presentation (Mele *et al.*, 1988). The findings of these two studies differed, however, in the doses of gamma radiation that decreased FI response rates. In the present study, FI response rates were reduced significantly by doses of 4.5-9.0 Gy. The earlier report, in contrast, found that 6.5 Gy, but not 4.5 Gy, decreased FI response rates. Thus, there was an apparent shift to the left in the dose-response curve for gamma radiation-induced decreases in FI response rates in the present study compared to the curve reported earlier.

One factor that could account for the differential sensitivity of FI performance to gamma irradiation found in these two studies was the use of a multiple FI FR schedule versus a simple FI schedule. Differential sensitivities of behaviors under simple versus multiple schedules have been reported for a number of agents (Ator, 1982; Barrett and Stanley, 1980; Laties *et al.*, 1981; Waller, 1961). It may be that an interaction between the FI and FR components of the multiple schedule increased the sensitivity of FI responding to gamma radiation.

An interaction between the components of the multiple schedule used here was evident during training when FI response rates of most rats increased after the FR component was introduced; FI response rates increased and stabilized at a level that was 2-3 times higher than under the simple FI schedule used in our previous study (Mele *et al.*, 1988). This is not surprising, however, since with multiple schedules, increases in response rates in interval-schedule components induced by ratio-schedule components have been reported (Hemmes and Eckerman, 1972; Waller, 1961). Because baseline response rate is one factor that may influence, to varying degrees, the effects of a number of agents on operant responding (Dews and Wenger, 1977; Sanger and Blackman, 1976), it may be that gamma radiation

decreased higher pre-irradiation FI response rates to a greater degree than lower rates (*i.e.*, a rate-dependent effect). However, there was no correlation (r = -0.01) between pre-irradiation baseline response rates and maximal decreases in response rates during week 1 after exposure to 4.5 Gy, even though individual baseline response rates within this group of rats varied by a factor of 10 (0.19-1.98 responses per second) (cf. Urbain *et al.*, 1978; Heffner *et al.*, 1974). In addition, although radiation decreased overall response rates, there were no significant changes in the index of curvature. These results, which indicate that the varying response rates that occurred during different segments of the FI were altered uniformly after irradiation, are not consistent with a rate-dependent relationship. At present, there are few data to suggest that baseline response rate is a primary determinant of the effect of gamma radiation on schedule-controlled performance.

Previously, we reported that gamma radiation disrupted performance under simple FI and FR schedules in a schedule-dependent manner; that is, FR performance was disrupted by a lower dose of radiation (4.5 Gy) than the dose (6.5 Gy) that disrupted FI performance (Mele *et al.*, 1988). Schedule-dependent effects also occurred under the multiple schedule in the present study, although the characteristics of this schedule dependency differed from the characteristics found for simple schedules. Under the multiple schedule, both FI and FR performances were disrupted significantly during week 1 after exposure to gamma radiation doses of 4.5-9.0 Gy, and FI performance was frequently disrupted more than FR performance. Subsequently, a subtle but consistent difference was that FI response rates took several weeks longer to stabilize at control levels than the time required for FR rates to stabilize. Taken together, these results suggest that schedule-dependent effects of gamma radiation vary with the context (*i.e.*, simple or multiple schedules) in which the individual schedules occur (cf. Ator, 1982; Laties, *et al.*, 1981; Waller, 1961).

The specific factors that may have contributed to the schedule-dependent effects of gamma radiation within the context of a multiple schedule are unclear. A classic rate-dependent relationship can be ruled out since FR response rates were 2-3 times greater than FI response rates (see above also). In contrast, the potential contribution of differences in baseline reinforcement densities generated by the FI and FR schedules is unknown. Other possibilities relate to the suggestion that differential effects of certain drugs on multiple FI FR performance may be due to a greater "coherence" of FR than FI responding, the relative independence between response rates and reinforcement rates under FI schedules (Dews and DeWeese, 1977), or to the fact that FI response rates are typically more variable (across successive intervals) than FR response rates (across successive ratios) which could render FI rates more susceptible to radiation-induced suppression. Whatever factors determined the schedule-dependent effects found here, the finding that both FI and FR postreinforcement pause durations were increased and running response rates were decreased indicates radiation affected the structure of behavior similarly under both schedules.

It is important to recognize that other factors also may have influenced to varying degrees the specific results obtained here; these factors include the parameter values of the FI and FR schedules (Barrett and Stanley, 1980; McMillan, 1969) and the duration or frequency of change of the multiple schedule components (Ator, 1982). In contrast, it is unlikely that radiation affected control exerted by the light and tone stimuli used to designate components under the multiple schedule, since discrimination thresholds have been reported to be unaltered (visual) or slightly lowered (auditory) by photon radiation (Kimeldorf and Hunt, 1965, pp 131-165).

An earlier study reported that approximately 2-8 Gy of ^{60}Co gamma radiation decreased response rates under a continuous reinforcement (or FR-1) schedule of water presentation in rats (Wicker and Brown, 1965). That study, however, did not report which specific doses reduced response rates significantly relative to pre-irradiation control values, nor did it report how disruptions in response rates changed over days after exposure. Several other studies reported that x rays (250 kVp) decreased response rates under FR (Brown, 1966; Brown *et al.*, 1960; Brown *et al.*, 1966) and VI (Jarrard, 1963) schedules of reinforcement. Although these findings are, in general, consistent with the results reported here, direct comparisons between these earlier studies and the studies from this laboratory are difficult to make because of numerous differences in irradiation and behavioral parameters. These differences include type of ionizing radiation and dose rate, acute presession versus protracted within-session exposures, amount and specific areas of the body irradiated, and reinforcement schedule and type of reinforcer.

The present study found substantial, if not complete, recovery of pre-irradiation rates and patterns of

responding in all irradiated groups of rats by the end of the first week or the beginning of the second week after exposure. Recovery in the 9.0-Gy exposure group was particularly striking, and raises the question as to whether the intervening weekend (days 6-7 postexposure) without operant testing was a factor in determining the rate of recovery. Although data directly addressing this point are lacking, other findings seem to suggest that time off from testing is not a major factor that influences the expression of at least some behavioral decrements after irradiation. Specifically, one study found that 6.0 Gy of x rays (250 kVp) decreased locomotor activity progressively over days 1-8 postexposure regardless of whether rats were or were not tested on days 5 and 6 (Haley *et al.*, 1958).

Although reduction in food intake is one of the more sensitive indicators of exposure to ionizing radiation (Anno *et al.*, 1989; Jarrard, 1963; Smith and Tyree, 1954), it is notable that there was no indication of anorexia in the present study, as measured by consumption of the daily ration of chow, except for one day in the group given the highest radiation dose. The general absence of an observable anorectic effect was likely due to the reduced body weights at which the rats were maintained and/or the restricted amount of chow that was given each day (Mele and Winsauer, 1995). It has also been reported that the amount of chow consumed during the first hour after food presentation was reduced in irradiated rats maintained on a restricted feeding schedule, but that typically all chow was consumed over the subsequent 23-hr period (Mele and Winsauer, 1995). Conceivably, such an apparent alteration in the temporal pattern of eating could have decreased the effective deprivation level of the animals in the present study at the time of operant testing, which then could have reduced responding. In another study, however, in the instances when radiation decreased both operant responding and food intake in rats, these two effects could be at least partially dissociated (Mele *et al.*, 1988). It is also worth mentioning that partial food satiation (Sidman and Stebbins, 1954) and gamma radiation (Mele *et al.*, 1988; present study) have been reported to alter FR performance somewhat differently; both treatments increased postreinforcement pause durations whereas radiation also decreased running response rates. The results of those earlier studies indicate effects of ionizing radiation other than or in addition to anorexia must also be considered when evaluating radiation-induced changes in appetitive operant behavior. Because sublethal doses of ionizing radiation have been reported to decrease several types of motor activity in rats (Kimeldorf and Hunt, 1965, pp 185-200), disruptions in motor output also may be involved in the effects reported here. It is likely that radiation-induced changes in operant performance derive from a combination of effects on motivational and motor systems at least. This would be consistent with results showing that, in addition to anorexia, some of the more sensitive behavioral indices of radiation exposure in humans are lethargy, weakness, and fatigue (Anno *et al.*, 1989).

A recent study from this laboratory reported that 10 Gy of gamma radiation decreased FR response rates over week 1 postexposure to a degree similar to that observed here with 9.0 Gy (McDonough *et al.*, 1992). That study, however, found that response rates after the 10-Gy irradiation remained severely reduced after week 1, and all irradiated rats died shortly thereafter. In contrast, the present study found that 9.0 Gy was lethal to only one of six rats, and that complete recovery of pre-irradiation performance levels occurred in all survivors. Even the one rat that died after the 9.0-Gy exposure showed substantial behavioral recovery prior to death. These observations demonstrate that severe, nearly complete cessation of operant performance following irradiation is not merely an indication that the animal is about to die. Furthermore, the finding that classical radioprotectant drugs were relatively more effective in attenuating radiation-induced lethality compared to radiation-induced disruption in operant performance provides additional evidence that these two effects of radiation exposure can be at least partially dissociated (McDonough *et al.*, 1992).

Despite recovery of pre-irradiation performance values after the initial exposure, prolonged effects were revealed following re-irradiation with either 6.75 Gy or 9.0 Gy. The most striking effect was that re-irradiation was lethal to rats given these doses a second time, with the incidence of lethality being directly related to dose and the duration of survival being inversely related to dose. Even though two exposures to 6.75 Gy produced cumulative effects resulting in lethality, there was no cumulative (*i.e.*, more pronounced) effect in terms of behavioral disruption. Similarly, three exposures to 4.5 Gy of gamma radiation at 6-week intervals produced replicable, noncumulative effects on FR and FI performance (Mele *et al.*, 1988). In that study, however, all animals survived the three 4.5-Gy exposures. In contrast, the present study showed that re-irradiation with 9.0 Gy increased both the incidence of lethality

and the magnitude of the behavioral deficit. Thus, the effects of repeated exposures to gamma radiation that are separated by long (6-8 week) interirradiation intervals vary as a function of the dose administered and the specific biological endpoint (schedule-controlled performance versus lethality) examined.

The clear temporal separation between performance disruptions and deaths after the second 6.75-Gy irradiation suggests that there were different mechanisms underlying these effects. Although the temporal separation between these effects after the second 9.0-Gy exposure was less distinct, the partial recovery of performance that preceded death also suggests separate mechanisms at this higher exposure level.

Numerous studies have investigated recovery following radiation exposure by determining how radiation LD_{50}s change as a function of prior irradiation with sublethal doses (see review by Sacher, 1958). For example, studies using rats or mice found that if an initial exposure was sufficiently low (*i.e.*, less than one-half of the acute LD_{50}), then recovery from the effects of that exposure (measured over periods ranging from several hours to 29 days) was said to be complete, in that animals receiving a second exposure had LD_{50}s similar to those of animals not previously irradiated (Kohn and Kallman, 1957; Mole, 1956; Vogel *et al.*, 1957). However, if an initial exposure exceeded approximately one-half of the acute LD_{50}, then incomplete recovery and residual damage were inferred by the finding that LD_{50}s of a second irradiation were lowered in animals that had been irradiated previously. In a study that examined a long (*i.e.*, 60-day) inter-irradiation interval similar to that used here, a decreased LD_{50} in rats was found following the second of two exposures to approximately 6.5 Gy of 250-kVp x rays (Hursh *et al.*, 1954). Subsequent studies determined that hematopoietic tissue was an important site of residual damage following repeated sublethal exposures (Baum, 1967; Baum and Alpen, 1959; Hubner *et al.*, 1981; Miller *et al.*, 1958; Siegers *et al.*, 1981). In the present study, the effects on survival and hematopoietic tissue of the two exposures to 6.75 Gy and 9.0 Gy are consistent with these earlier findings, given that the LD_{50} for ^{60}Co gamma rays in Sprague-Dawley rats has been reported to be 9.5 Gy (Bogo, 1988).

The data presented further define the dose-effect and time-course functions that relate changes in behavior to exposure to gamma radiation. The identification of schedule-dependent and context effects indicates that behavioral factors are important aspects of the functional consequences of radiation exposure. The results also show that residual damage following higher levels of exposure can be separated for measures of behavior and survival. These findings emphasize the need for continuing the identification and examination of prolonged behavioral consequences of acute and repeated exposure to ionizing radiation.

ACKNOWLEDGEMENTS

This work was supported by the Armed Forces Radiobiology Research Institute (AFRRI), Defense Nuclear Agency. Research was conducted according to the principles enunciated in the "Guide for the Care and Use of Laboratory Animals" prepared by the Institute of Laboratory Animal Resources, National Research Council, NIH Publication 86-23. AFRRI is fully accredited by the American Association for Accreditation of Laboratory Animal Care. We thank Dr. Steven Stiefel for performing the pathology examinations, and Ms. Carol G. Franz and Mr. John R. Harrison for their expert technical assistance during the conduct of this investigation.

REFERENCES

American Association of Physicists in Medicine, Task Group 21, Radiation Therapy Committee. A protocol for the determination of absorbed dose from high energy photon and electron beams. *Med Phys* 1983; 10:741

Anno GH, Baum SJ, Withers HR, Young RW. Symptomatology of acute radiation effects in humans after exposure to doses of 0.5-30 Gy. *Health Phys* 1989; 56:821-838

Ator N. Modulation of the behavioral effects of carbon monoxide by reinforcement contingencies. *Neurobehav Toxicol Teratol* 1982; 4:51-61

Barrett JE, Stanley JA. Effects of ethanol on multiple fixed-interval fixed-ratio schedule performances: Dynamic interactions at different fixed-ratio values. *J Exp Anal Behav* 1980; 34:185-198

Baum SJ. A measure of nonreparable injury to hematopoietic stem cells in rats exposed repeatedly to x-rays. *Radiat Res* 1967; 32:651-657

Baum SJ, Alpen EL. Residual injury induced in the erythropoietic system of the rat by periodic exposures to x-irradiation. *Radiat Res* 1959; 11:844-860

Bogo V. Behavioral radioprotection. *Pharmacol Ther* 1988; 39:73-78

Braun RG, Farrer DN, Zappini W, Crook GH. Performance of rhesus monkeys during continuous low-level gamma radiation: An exploratory study. *Technical Report ARL-TR-66-18,* 6571st Aeromedical Research Laboratory, Holloman AFB, NM 88330, 1966

Brown WL. Response rate during x-irradiation and recovery following irradiation. *J Genet Psychol* 1966; 108:117-120

Brown WL, Blodgett HC, Henderson D, Ritter RM, Pizzuto JS. Some effects on operant conditioning of ionizing radiation to the whole head. *J Genet Psychol* 1966; 108:255-261

Brown WL, Overall JE, Logie LC, Wicker JE. Lever-pressing behavior of albino rats during prolonged exposures to x-radiation. *Radiat Res* 1960; 13:617-631

Dews PB, DeWeese J. Schedules of reinforcement. In: *Handbook of Psychopharmacology.* Iverson LL, Iverson SD, Snyder SH, eds., Vol 7, New York: Plenum Press, 1977, pp 107-150

Dews PB, Wenger GR. Rate-dependency and the behavioral effects of amphetamine. In: *Advances in Behavioral Pharmacology.* Thompson T, Dews PB, eds., Vol 1, New York: Academic Press, 1977, pp 167-227

Ferster CB, Skinner BF. *Schedules of Reinforcement,* New York, Appleton-Century Crofts, 1957

Fry W, Kelleher RT, Cook L. A mathematical index of performance on fixed-interval schedules of reinforcement. *J Exp Anal Behav* 1960; 3:193-199

Haley TJ, Flesher AM, Komesu N, McCulloh EF, McCormick WG. Effect of x-ray irradiation on muscle fatigue in rats. *Am J Physiol* 1958; 193:355-359

Heffner TG, Drawbaugh RB, Zigmond MJ. Amphetamine and operant behavior in rats. *J Comp Physiol Psychol* 1974; 86:1031-1043

Hemmes NS, Eckerman DA. Positive interaction (induction) in multiple variable-interval, differential-reinforcement-of-high-rate schedules. *J Exp Anal Behav* 1972; 17:51-57

Hubner GE, van Wangenheim KH, Feinendegen LE. An assay for the measurement of residual damage of murine hematopoietic stem cells. *Exp Hematol* 1981; 9:111-117

Hursh JB, Van Slyke F, Casarett G. Use of a test dose to estimate life shortening produced in rats by a single dose of x-irradiation. *USAEC Report UR-318,* Univ Rochester, 1954

International Commission on Radiation Units and Measurements (ICRU). Report No. 33: *Radiation Quantities and Measurements.* Washington, DC, April 1980

Jarrard LE. Effects of x-irradiation on operant behavior in the rat. *J Comp Physiol Psychol* 1963; 56:608-611

Kimeldorf DJ, Hunt EL. *Ionizing Radiation: Neural Function and Behavior.* New York, Academic Press, 1965

Kohn HI, Kallman RF. Acute lethality studies with the rat: The LD50, death rate, and recovery rate. *Radiat Res* 1957; 7:85-97

Laties VG, Wood RW, Rees DC. Stimulus control and the effects of d-amphetamine in the rat. *Psychopharmacology* 1981; 75:277-282

McDonough JH, Mele PC, Franz CG. Comparison of behavioral and radioprotective effects of WR-2721 and WR-3689. *Pharmacol Biochem Behav* 1992; 42:233-243

McMillan DE. Effects of d-amphetamine on performance under several parameters of multiple fixed-ratio, fixed-interval schedules. *J Pharmacol Exp Ther* 1969; 167:26-33

McPherson CW. Reduction of pseudomonas aeruginosa and coliform bacteria in mouse drinking water following treatment with hydrochloric acid or chlorine. *Lab Animal Care* 1963; 13:737-744

Mele PC, Franz CG, Harrison JR. Effects of sublethal doses of ionizing radiation on schedule-controlled performance in rats. *Pharmacol Biochem Behav* 1988; 30:1007-1014

Mele PC, Franz CG, Harrison JR. Effects of ionizing radiation on fixed-ratio escape performance in rats. *Neurotoxicol Teratol* 1990; 12:367-373

Mele PC, Winsauer PJ. Behavioral assessment of antiemetic drugs in rats. In: *Radiation and the Gastrointestinal Tract.* Dubois A, King GL, Livengood DR, eds., Boca Raton, Florida, CRC Press, 1995, pp 251-265

Miller LS, Fletcher GH, Gerstner HB. Radiobiologic observations on cancer patients treated with whole-body x-irradiation. *Radiat Res* 1958; 8:150-165

Mole RH. Quantitative observations on recovery from whole-body irradiation in mice. I. Recovery after single large doses of radiation. *Brit J Radiol* 1956; 29:563-569

Sacher GA. Reparable and irreparable injury: A survey of the position in experiment and theory. In: *Radiation Biology and Medicine.* Claus WD, ed., Reading, Massachusetts, Addison-Wesley, 1958, pp 283-313

Sanger DJ, Blackman DE. Rate-dependent effects of drugs: A review of the literature. *Pharmacol Biochem Behav* 1976; 4:73-83

Sidman M, Stebbins WC. Satiation effects under fixed-ratio schedules of reinforcement. *J Comp Physiol Psychol* 1954; 47:114-116

Siegers MP, Van Wangenheim KH, Hubner GE, Feinendegen LE. Residual damage and discontinuity of recovery in the hematopoietic system of mice following gamma-irradiation. *Exp Hematol* 1981; 9:346-354

Smith DE, Tyree EA. Influence of x-irradiation upon body weight and food consumption of the rat. *Am J Physiol* 1954; 177:251-260

Stewart FA, Oussoren Y. Re-irradiation of mouse kidneys: A comparison of re-treatment tolerance after single and fractionated partial tolerance doses. *In J Radiat Biol* 1990; 58:531-544

Terry NHA, Tucker SL, Travis EL. Time course of loss of residual radiation damage in murine skin assessed by retreatment. *Int J Radiat Biol* 1989; 55:271-283

Urbain C, Poling A, Millam J, Thompson T. *d*-Amphetamine and fixed-interval performance: Effects of operant history. *J Exp Anal Behav* 1978; 29:385-392

Vogel HH, Clark JW, Jordan DL. The rate of recovery from gamma radiation injury as a function of the amount of injury. *Fed Proc* 1957; 16:132

Waller MB. Effects of chronically administered chlorpromazine on multiple-schedule performance. *J Exp Anal Behav* 1961; 4:351-359

Wicker JE, Brown WL. The effect of gamma radiation upon operant water-reinforcement behavior. *J Genet Psychol* 1965; 106:295-299

Winsauer PJ, Mele PC. Effects of sublethal doses of ionizing radiation on repeated acquisition in rats. *Pharmacol Biochem Behav* 1993; 44:809-814

Yochmowitz MG, Brown GC. Performance in a 12-hour, 300-rad profile. *Aviat Space Environ Med* 1977; 48:241-247

MS #2092

Int. J. Cancer: **63,** 124–129 (1995)

Publication of the International Union Against Cancer
Publication de l'Union Internationale Contre le Cancer

INCREASED SUSCEPTIBILITY OF *ras*-TRANSFORMED CELLS TO PHENYLACETATE IS ASSOCIATED WITH INHIBITION OF p21^{ras} ISOPRENYLATION AND PHENOTYPIC REVERSION

Sonsoles SHACK[1], Li-Chuan CHEN[1], Alexandra C. MILLER[2], Romano DANESI[1,3] and Dvorit SAMID[1,4]

[1]*Clinical Pharmacology Branch, National Cancer Institute, and* [2]*Radiation Biochemistry Department, Armed Forces of Radiation Research Institute, Bethesda, MD 20814, USA.*

Alterations in the expression of *ras* oncogenes are characteristic of a wide variety of human neoplasms. Accumulating evidence has linked elevated *ras* expression with disease progression and with failure of tumors to respond to conventional therapies, including radiotherapy and certain chemotherapies. These observations led us to investigate the response of *ras*-transformed cells to the differentiation-inducer phenylacetate (PA). Using gene transfer models, we show that PA caused cytostasis in *ras*-transformed mesenchymal cells, associated with increased expression of 2′,5′-oligoadenylate synthetase, an enzyme implicated in negative growth control. PA also induced phenotypic reversion characterized by loss of anchorage-independent growth, reduced invasiveness and increased expression of collagen α type I, a marker of cell differentiation. The anti-tumor activity of PA was observed in cases involving either Ha- or Ki-*ras* and was independent of the mode of oncogene activation. Interestingly, in contrast to their relative resistance to radiation and doxorubicin, *ras*-transformed cells were significantly more sensitive to PA than their parental cells. The profound changes in tumor cell and molecular biology were associated with reduced isoprenylation of the *ras*-encoded p21. Our results indicate that PA can suppress the growth of *ras*-transformed cells, resistant otherwise to free-radical based therapies, through interference with p21^{ras} isoprenylation, critical to signal transduction and maintenance of the malignant phenotype.

The *ras* gene family encodes for closely related 21-kDa proteins that bind guanine nucleotides, exhibit intrinsic GTPase activity and are thought to play a central role in signal transduction and growth control (Barbacid, 1987; Khosravi-Far and Der, 1994). p21^{ras} is first made in the cytosol as a pro-protein and matures following a series of post-translational modifications, including farnesylation, proteolytic cleavage of carboxyl terminal and its methylation and palmitoylation (Hancock *et al.,* 1989).

Activation of *ras* often leads to breakdown of normal growth control. Indeed, alterations in the expression of the *ras* oncogene family are characteristic of a wide spectrum of human neoplasms and are often associated with disease progression and poor prognosis (Khosravi-Far and Der, 1994). In some cases, *ras* activation occurs during early stages of neoplastic transformation, when it might be required for the development and maintenance of the malignant phenotype. Increased production of the membrane-associated protein p21^{ras} may also be responsible in part for the failure of cancer radiotherapy (Samid *et al.,* 1991; Miller *et al.,* 1993*a*) and chemotherapy—*e.g.,* cisplatin and doxorubicin (Miller and Samid, 1995). To overcome these problems, differentiation therapy seeking to reverse the phenotype of cancer cells may provide an alternative to treatment of tumors in cases where conventional therapies were not effective. Our recent attention has focused on phenylacetate (PA) and related aromatic fatty acids, such as phenylbutyrate (PB), as a novel class of differentiation-inducers (Samid *et al.,* 1992, 1993, 1994; Liu *et al.,* 1994).

PA is a metabolite of phenylalanine (PAla) with demonstrable anti-tumor activity in tissue culture (Samid *et al.,* 1992, 1993, 1994; Liu *et al.,* 1994), in animal models (Samid *et al.,* 1994; Ram *et al.,* 1994) and in humans (Thibault *et al.,* 1994, 1995). Pre-clinical studies indicate that PA causes selective tumor cytostasis and differentiation in various hematopoietic (Samid *et al.,* 1992) and solid (Samid *et al.,* 1992, 1993, 1994; Liu *et al.,* 1994) tumors at doses (mM range) achievable in humans with no significant toxicity (Brusilow *et al.,* 1984; Thibault *et al.,* 1994, 1995). Phenotypic changes induced by PA in tumor cells are characterized by alterations in gene expression, reduction in proliferative capacity, loss of invasiveness and inability to form tumors in recipient mice (Samid *et al.,* 1992, 1993, 1994). Initial phase I clinical trials have shown that PA treatment resulted in clinical improvement in patients with advanced glioma multiforme or hormone-refractory prostatic cancer, who failed to respond to conventional therapies (Thibault *et al.,* 1994, 1995). It was, therefore, of interest to examine the relationship between *ras* expression and tumor responsiveness to PA.

MATERIAL AND METHODS

Cell cultures and reagents

Studies included the following murine cell lines: NIH 3T3 fibroblasts and subclones transformed by LTR-activated c-Ha-*ras* (designated V7T), EJ*ras* (RS504), v-Ki-*ras* (DT) or the bacterial *neo* gene (3T3-*neo*). The human cellular model included a cell line established from a patient with osteosarcoma (HOS, with undetectable *ras* expression) and subclones transformed by EJ*ras* (AD5), v-Ki-*ras* (KRIB) or *neo* (HOS-*neo*). All of these cell lines were previously described (Samid *et al.,* 1991; Miller *et al.,* 1993*a*). Cultures were propagated in Dulbecco's modified Eagle medium supplemented with 2 mM glutamine, 10% heat inactivated FCS (GIBCO, Grand Island, NY), 100 U/ml penicillin and 100 μg/ml streptomycin (Sigma, St. Louis, MO). The sodium salt of PA was provided by Elan Pharmaceutical Research (Gainesville, GA). Doxorubicin (DOX) and PAla were purchased from Sigma. Phenylacetylglutamine (PAG) was synthesized as previously described (Liu *et al.,* 1994).

Quantitation of cell growth and viability

Growth rates of cells exposed to PA were determined by cell enumeration with a hemocytometer following detachment with trypsin-EDTA and by an enzymatic assay using 3-[4,5-dimethylthiazol-2-yl]-2,5-diphenyl tertrazolium bromide (MTT; Mosmann, 1983). These 2 assays produced essentially the same results. Growth rates were also determined by thymidine

[3]Present address: University of Virginia, Division of Hematology/Oncology, Building MR-4, Box 1131, Charlottesville, VA 22908.

[4]To whom correspondence and reprint requests should be addressed: National Cancer Institute, Building 10, Room 12C103, Bethesda, MO 20892, USA. Fax: (301) 402-1997.

Received: March 31, 1995 and in revised form May 25, 1995.

incorporation. Cells were labeled with 1 μCi/ml[^{3}H]-deoxythymidine (Dupont, NEN, Boston, MA), and TCA precipitable radioactivity was determined by liquid scintillation counter. Cell viability was assessed by Trypan blue exclusion. A colony-formation assay was used to determine cell survival following treatment with DOX. Briefly, exponentially growing cells were plated onto 100-mm culture dishes in triplicate at densities of 100 to 10,000 cells, and the drug was added after a 24-hr attachment period. Ten days later, cells were fixed with methanol and stained with 1% crystal violet and colonies composed of more than 50 cells were counted as survivors.

Cell irradiation

Exponentially growing cells in 100-mm dishes were treated as a monolayer in complete media under aerobic conditions and given a total dose of 2–10 Gy (2.0 Gy/min) from a Theratron-80 Cobalt-60 source (Atomic Energy of Canada, Ottawa) as previously described (Miller *et al.,* 1993*a*). Following irradiation, cells were detached by trypsin/EDTA and plated at different cell densities onto 60-mm diameter Petri dishes, and 10 days later the number of surviving colonies was determined as described above.

Colony formation in semi-solid agar

For analysis of anchorage-independent growth, cells were harvested with trypsin-EDTA and resuspended at 1.0×10^4 cells per ml in growth medium containing 0.36% agar (Difco, Detroit, MI). Two milliliters of cell suspension were added to 60-mm plates (Costar, Cambridge, MA), which were precoated with 4 ml of solid agar (0.9%). Tested drugs were added at various concentrations, and colonies composed of 30 or more cells were counted after 3 weeks.

Growth on Matrigel

Cells were first treated with drugs in plastic tissue culture dishes for 4–6 days and then replated (5×10^4 cells per well) onto 16-mm dishes (Costar) coated with 250 μl of Matrigel, a reconstituted basement membrane (Collaborative Research, Bedford, MA), at the concentration of 10 mg/ml. Assessment of invasiveness was performed as previously described (Samid *et al.,* 1993). Drugs were also removed from some treated dishes to determine the reversibility of PA's effect. Invasive cells show a characteristic net-like formation within 12 hr of seeding, and invasion into the Matrigel was evident after 6–9 days.

Northern blot analysis and DNA probes

Cytoplasmic RNA was extracted from exponentially growing cells and separated by electrophoresis in 1% agarose-formaldehyde gels by standard procedure (Maniatis *et al.,* 1982). Separated RNA was blotted onto nytran filters and hybridized with radiolabeled DNA probes as previously described (Samid *et al.,* 1991). The *ras* probe, a 2.9-kb Sac I fragment of the human c-Ha-*ras* gene was obtained from Oncor (Gaithersburg, MD). The β-actin probe (Oncor) was used as control to ensure equal loading of the samples. Probes were labeled with ^{32}P-dCTP (NEN, Wilmington, DE) using a random-primed DNA labeling kit (Ready-To-Go, Pharmacia LKB, Piscataway, NJ). Membranes were hybridized with probes according to the Quikhyb protocol provided by Stratagene (La Jolla, CA) at 68°C for 1 hr and washed twice for 15 min each at room temperature with 2 × standard saline-citrate (SSC)/0.1 × SDS and once at 60°C for 30 min with 0.1 × SSC/0.1 × SSD. Autoradiography was performed using Kodak XAR5 films at −70°C with intensifying screens.

Metabolic labeling of proteins and p21 immunoprecipitation

For labeling experiments, cells were seeded at a density of 3×10^6 per T75-cm^2 flask (Costar) and drugs (PA and *d*-limonene, 5 mM each) were added the next day. After 3 days of continuous treatment, cells were labeled for 3 or 24 hr at 37°C in methionine-free Dulbecco's medium (GIBCO) with 100 μCi/ml ^{32}S-L-methionine (ICN, Costa Mesa, CA). In addition, cells were pre-treated with lovastatin for 24 hr before harvest to inhibit endogenous synthesis of mevalonate and enhance labeling signal. To obtain whole cell extracts, labeled cells were lysed with 1 ml of lysis buffer (0.05 M Tris-HCl, pH 8.0 with 1% Triton X-100, 5 mM $MgCl_2$, and 0.1 M NaCl) and lysates were immunoprecipitated with monoclonal antibody (MAb) to p21 (antibody Y12-239; Oncogene Science, Manhasset, NY) for 4 hr at room temperature as previously described (Miller *et al.,* 1993*a*). After washing with lysis buffer, immunoprecipitated proteins were separated by SDS-PAGE on 12.5% gels. Dried gels were exposed to Kodak X-Omat film with intensifying screens.

Analysis of p21^{ras} isoprenylation

V7T cells were seeded in 100-mm culture dishes with the above-mentioned medium and supplements until 75% confluent. Cultures were replenished with fresh medium containing PA at 0, 6 or 12 mM and the treatment lasted for 24 hr. In addition, 30 μM of lovastatin was added to inhibit endogenous production of mevalonic acid, thus preventing the dilution of radiolabel (R,S)-[5-^{3}H]mevalonolactone (100 μCi/ml, 50–60 Ci/mmol; American Radiolabeled Chemicals, St Louis, MO). Each dish received radioactive mevalonolactone in 500 μl of medium after 8 hr of drug treatment and the treatment continued overnight. Cells were harvested with 1.5 mM EDTA and centrifuged and the cell pellet was disrupted in lysis buffer, containing 1% (v/v) Nonidet-P40, 50 mM Tris (pH 7.6), 2 mM EDTA, 100 mM NaCl and protease inhibitors (20 μg/ml PMSF and 5 μg/ml each of pepstatin, antipain and aprotinin) for 30 min at 4°C. Samples were centrifuged at 25,000*g* for 30 min and the supernatant was used for further analyses. Protein concentrations were determined by the BCA protein assay reagent kit (Pierce, Rockford, IL) with BSA as standard. Protein concentration was adjusted to 3 mg/ml and each milliliter of samples was mixed with 20 μl of anti-v-Ha-*ras* (Y13-259, Oncogene Science) at 4°C for 6 hr. Immune complexes were precipitated overnight on a rotating platform by addition of 40 μl of protein A/G-Sepharose beads (Oncogene Science) in lysis buffer. Immunoprecipitates were pelleted by centrifugation at 25,000*g* for 15 min and washed 4 times with 1 ml each of ice-cold lysis buffer. Pellets were dissolved in 20 μl of sample buffer (50 mM Tris, pH 6.8, containing 100 mM dithiothreitol, 10% glycerol and 0.025% bromophenol blue) and heated at 95°C for 5 min and subjected to electrophoresis on a 12.5% SDS-PAGE gel. Gels were equilibrated for 30 min with fluorography enhancer, dried under vacuum at 80°C for 2 hr and finally exposed to a Kodak XOMAT-AR film at −70°C. Gels were also stained with silver stain to ensure equal loading of samples.

RESULTS

Increased susceptibility of ras*-transformed cells to growth arrest induced by PA*

To examine the effect of PA on *ras*-transformed cells, V7T cells which contain the c-Ha-*ras* protooncogene activated by a LTR promoter, were initially used for the investigation. The results show that PA caused cytostasis, as indicated by the reduced growth rates and ^{3}H-thymidine incorporation in V7T and parental cells after 4 days of treatment (Fig. 1*a*). Interestingly, V7T, as well as other *ras*-transformed NIH3T3 subclones, were significantly more susceptible than the parental cells to the growth-inhibiting effect of PA at various concentrations. Estimated IC_{50} values for V7T and parental cell lines confirmed the increased sensitivity to PA (Table I). In contrast, the *ras*-transformants were significantly less sensitive to killing by DOX and radiation than the parental and *neo*-transfected cells, as indicated by the LD_{50} and D_o values, respectively (Table I).

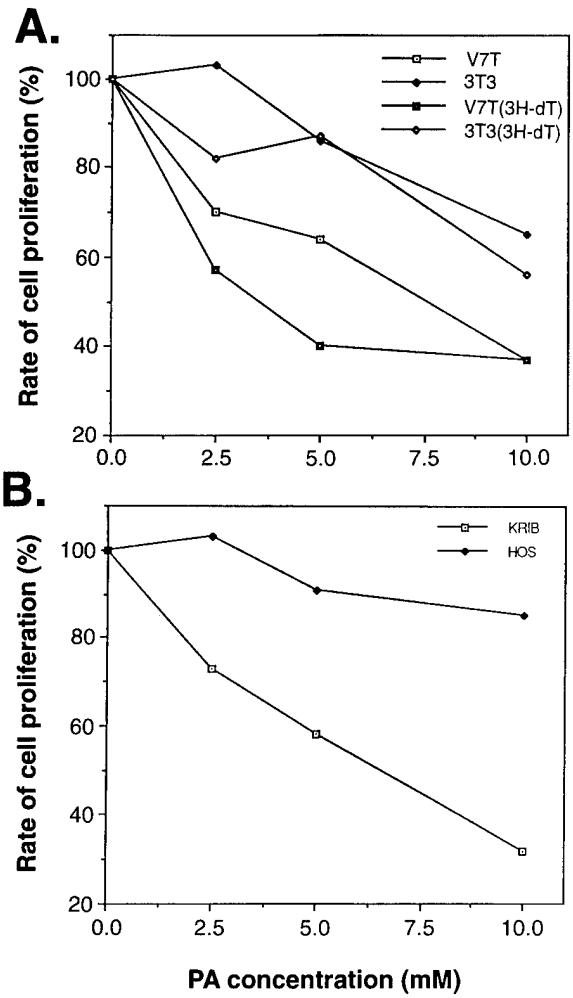

FIGURE 1 – Selective cytostasis induced by phenylacetate (PA). *(a)* Murine NIH3T3 and its related subclones, V7T, transformed by c-Ha-*ras* driven by LTR; changes in cell proliferation rate were determined after 4 days of treatment by cell enumeration and thymidine incorporation (^{3}H-dT). *(b)* Human osteosarcoma (HOS) and its subclone transformed by v-Ki-*ras* (KRIB). Growth rates were determined by cell enumeration. Results from MTT assay were essentially the same (data not shown).

TABLE I – SENSITIVITY OF *ras*-TRANSFORMED CELL LINES TO PHENYLACETATE (PA), DOXORUBICIN (DOX) AND RADIATION

Cells	Transfected gene	IC_{50} of PA (mM)[1]	LD_{50} of DOX (nM)[2]	D_0 of radiation (Grays)[3]
3T3		14.0 ± 0.2	74	1.26 ± 0.12
3T3-neo	*neo*	13.5 ± 0.5	80	1.29 ± 0.10
V7T	c-Ha-*ras*[4]	5.6 ± 0.4	420	1.76 ± 0.08
DT	v-ki-*ras*	5.9		
HOS		14.3 ± 0.3	100	0.83 ± 0.11
HOS-neo	*neo*	15.0 ± 0.5	106	0.80 ± 0.07
AD5	EJ*ras*	6.2 ± 0.5	310	1.46 ± 0.05
KRIB	v-Ki-*ras*	6.8 ± 0.2	330	1.44 ± 0.10

[1]IC_{50}: dose causing 50% inhibition of cell proliferation.–[2]LD_{50}: dose causing 50% cell killing.–[3]D_0: dose required to decrease cell population by 37%. Data are the means ± SE of at least 2 experiments with 3 dishes per treatment.–[4]Activated by LTR promoter.

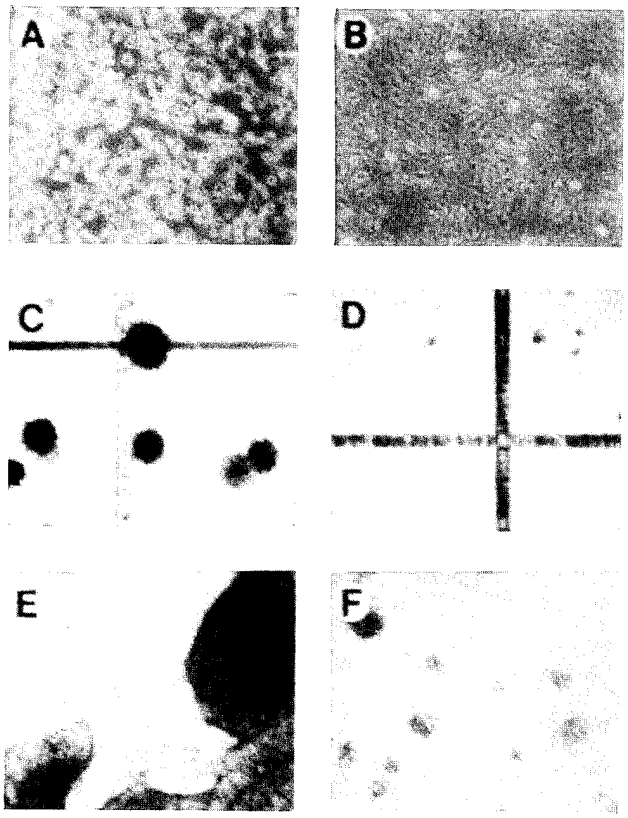

FIGURE 2 – Evidence of phenotypic reversion of *ras*-transformed V7T cells by phenylacetate (PA). *(a,b)* Regained contact inhibition. Untreated control cultures were composed of refractile and spindly cells, which piled up to form multilayers *(a)*. In contrast, cells treated with PA (5 mM) for 7 days displayed a "flat" morphology and formed monolayer, indicative of regained contact inhibition of growth *(b)*. *(c,d)* Reduced anchorage-independent growth. Untreated V7T cells formed large colonies in soft agar with rough borders, characteristic of highly motile cells *(c)*, while PA-treated cells failed to form colonies, indicative of anchorage-dependence *(d)*. *(e,f)* Decreased invasiveness of by PA-treated cells. V7T cells grown on reconstituted basement membrane (Matrigel) formed netlike structure, which degraded the membrane barrier and eventually formed monolayer on the plastic surface beneath *(e)*. In contrast, PA-treated V7T cells failed to form "nets" and developed isolated, small colonies incapable of Matrigel degradation *(f)*.

To further examine the sensitivity of *ras*-transformed cells to PA, we determined the response of AD5, KRIB and human cells as well as their parental and mock-transfected cell lines to PA, DOX and radiation (Table I). The results confirmed that HOS cells transformed by either member of the *ras* oncogene family were more sensitive to PA than the parental or mock-transfected cells. Inversely, these *ras*-transformed cells were less sensitive to DOX and more resistant to radiation than the parental and *neo*-transfected cells, as previously described (Samid *et al.*, 1991; Miller *et al.*, 1993*a*; Miller and Samid, 1994). Further studies, focusing on the effects of PA on tumor cell and molecular biology, employed V7T cells as the model.

Induction of phenotypic reversion by PA

Reduced proliferative capacity of V7T cells treated with PA was accompanied by morphological changes indicative of phenotypic reversion. Following 7 days of treatment with 5–10 mM of PA, V7T cells regained contact inhibition of growth, as illustrated in Figure 2 and confirmed by the reduced saturation

TABLE II – EFFECT OF PHENYLACETATE (PA), PHENYLACETYLGLUTAMINE (PAG) AND PHENYLALANINE (PAla) ON SATURATION DENSITY OF V7T CELLS

Treatment	Number of cells × 10^{-6}/cm^2
None	13.6 ± 0.5
PA 10 mM	2.9 ± 0.1[1]
PAG 10 mM	13.0 ± 0.4
PAla 10 mM	12.6 ± 0.6

Mean ± SD of 2 independent experiments of duplicate samples.– [1]Significant difference ($p < 0.05$) in means between the control and treated groups.

TABLE III – EFFECT OF PHENYLACETATE (PA) AND PHENYLACETYLGLUTAMINE (PAG) ON ANCHORAGE-INDEPENDENT GROWTH OF V7T CELLS IN SOFT AGAR

Treatment	Number of colonies	Characteristics of colonies
None	820	500 large colonies with irregular shape
PA 10 mM	220	40 large colonies and the rest small with smooth edge
PAG 10 mM	580	Similar to the untreated colonies

Number of colonies represents the average of 2 independent experiments of triplicate samples. Standard deviations were below 15% of the means. Only colonies with more than 50 cells were counted.

density summarized in Table II. In contrast to PA, neither its precursor, PAla (10 mM), nor the end-metabolite, PAG (10 mM), restored contact inhibition. In addition, PA-treated V7T cells had lost anchorage-independence (Fig. 2; Table III), characteristic of neoplastic cells. There were not only decreases in the number of colonies formed in soft agar but also changes in their sizes and morphology following treatment (Fig. 3). While untreated cells formed colonies with irregular borders, characteristic of high motility, the small colonies in the PA-treated group had smooth edges and were unable to proliferate further. Finally, the V7T cells treated with PA also lost their ability to invade a reconstituted basement membrane (Matrigel; Fig. 2*e, f*) and were unable to form net-like structures, resembling the behavior of normal fibroblasts (Samid *et al.,* 1994). The effect of PA on contact inhibition and invasiveness was reversible with 48 hr upon removal of the drug (data not shown).

Molecular markers of cytostasis and differentiation

The morphological alterations of V7T cells by PA were associated with changes in gene expression, including increases in mRNA levels coding for collagen α1, a marker of fibroblast differentiation, and for 2′,5′-oligoadenylate synthetase (2-5ASyn; Fig. 3*a*), a gene coding for an enzyme implicated in negative growth control (Rimoldi *et al.,* 1990). In a time-course study, PA at 5 mM caused significant increases in 2-5ASyn expression 24–72 hr after treatment (Fig. 3*b*). Reduction in Ha-*ras* expression was documented in one subclone isolated from PA-treated V7T cells; however, such a change was not observed in other subclones or in a mixed population of V7T cultures (Fig. 3*a*).

Inhibition of p21^{ras} prenylation

p21^{ras} plays an important role in growth control (Barbacid, 1987; Khosravi-Far and Der, 1994) and must undergo several post-translational modifications, including farnesylation, to become associated with the plasma membrane and be biologically active (Hancock *et al.,* 1989; Khosravi-Far and Der, 1994). Suppression of the growth of *ras*-transformed cells by PA could be due to inhibition of protein isoprenylation since PA blocks isoprenoid synthesis *via* inhibition of mevalonate pyrophosphate decarboxylase (Shama Bhat and Ramasarma, 1979;

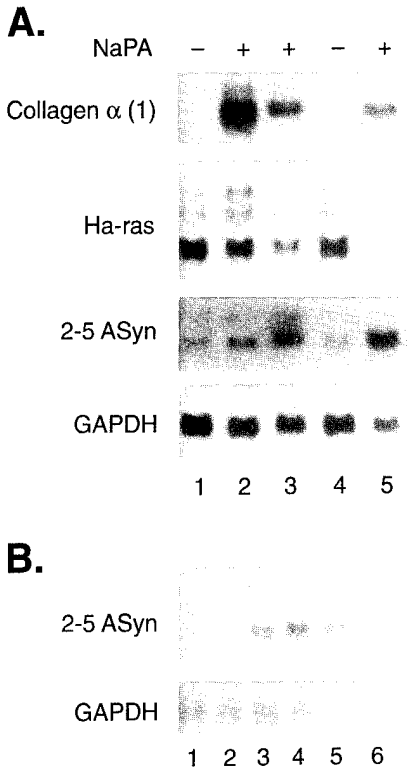

FIGURE 3 – Molecular correlates of cytostasis and differentiation. Northern blot analysis of cytoplasmic RNA (20 μg/lane) isolated from V7T cells treated with 5 mM of sodium phenylacetate (NaPA). *(a)* Increased expression of collagen α1, a marker of fibroblast differentiation, and 2′,5′-oligoadenylate synthetase (2-5 ASyn), coding for an enzyme implicated in negative growth control. Lane 1, untreated control cells; lane 2, V7T cells treated with PA for 4 days; lane 3, R1, a revertant subclone derived from PA-treated V7T, was exposed to NaPA continuously; lane 4, treatment of R1 was discontinued for 4 days to determine the reversibility of NaPA's effect; lane 5, R1 retreated with NaPA. Results indicate that down-regulation of Ha-*ras* and up-regulation of collagen α1 and 2-5ASyn are dependent on PA. *(b)* Time-dependent changes in the expression of 2-5ASyn following PA treatment: lane 1, V7T control; lanes 2–5, cells treated with NaPA (5 mM) for 12, 24, 48 and 72 hr, respectively; lane 6, cells treated with 10 mM of phenylacetylglutamine (PAG) for 72 hr.

Castillo *et al.,* 1991; Samid *et al.,* 1994). To test this hypothesis, we next examined the effect of PA on p21^{ras} post-translational processing. Using 2 experimental approaches, we show that PA inhibited p21^{ras} farnesylation in a dose-dependent fashion (Fig. 4*a, b*).

The first approach, utilizing metabolic labeling of cellular proteins with ^{35}S-methionine, revealed the shift from prenylated, membrane-bound p21 to increasing amounts of the free, cytosolic p21 after treatment with either PA or *d*-limonene, a known inhibitor of farnesyl pyrophosphate transferase (Fig. 4*a*). However, the synthesis of p21 *per se* was not affected by PA treatment (Fig. 4*a*). The second approach used the isoprenoid precursor ^{3}H-mevalonate to label prenylated proteins. The results confirm that PA inhibited p21^{ras} farnesylation in a dose-dependent manner (Fig. 4*b*).

DISCUSSION

Alterations in *ras* superfamily may contribute to neoplastic transformation and disease progression in a large variety of human malignancies (Khosravi-Far and Der, 1994). The *ras*

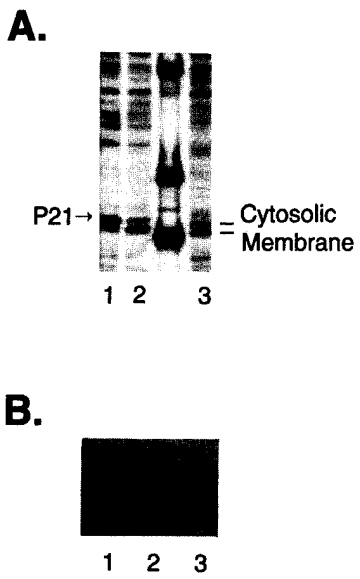

FIGURE 4 – Inhibition of $p21^{ras}$ prenylation by phenylacetate (PA). *(a)* Autoradiograph of proteins subjected to immunoprecipitation of $p21^{ras}$ by Y13-239 MAb, following metabolic labeling with ^{35}S-L-methionine. Lane 1, cells exposed to 5 mM of *d*-limonene for 72 hr (positive control); lane 2, untreated V7T; lane 3, cells treated with 5 mM of PA for 72 hr. Molecular markers are shown between lanes 2 and 3. Note the shift of $p21^{ras}$ from its prenylated membrane form to the cytosolic form following PA treatment. However, there is no change in total p21 protein produced. *(b)* $p21^{ras}$ immunoprecipitation following protein labeling with S-[2-^{14}C]mevalonate (16 μCi/ml), the precursor of farnesol. Lane 1, V7T control; lanes 2 and 3, cells treated for 24 hr with 6 and 12 mM of PA, respectively. Comparable amount of proteins was loaded in each lane, as indicated by staining with Coomassie brilliant blue (not shown).

genes may also be responsible for increased resistance of tumors to killing by radiation and free-radical-based chemotherapy (Samid *et al.,* 1991; Miller *et al., 1993a;* Miller and Samid, 1995). Therefore, *ras* biosynthesis and its post-translational modification necessary for membrane localization and biological activity have become important targets for therapeutic intervention. To this end, we have previously documented that depletion of intracellular glutathione content down-modulated *ras* expression at the post-transcriptional level and increased radiation sensitivity of *ras*-transformed cells (Miller *et al., 1993b*). Several compounds, including the tetrapeptide analogs L-731,735/L-731,734 (Kohl *et al.,* 1993) and benzodiazepine peptidomimetics (James *et al.,* 1993), have been shown to selectively inhibit $p21^{ras}$ farnesylation and transformation in cell cultures. Furthermore, a decline in $p21^{ras}$ prenylation by lovastatin was associated with increased sensitivity to killing by radiation or DOX (Miller *et al., 1993a;* Miller and Samid, 1995).

In the present study we show that PA, an inhibitor of protein prenylation, induced cytostasis and phenotypical reversion of *ras*-transformed cells refractory to conventional therapy. The aromatic fatty acid PA has been identified as a relatively non-toxic differentiation inducer and has entered clinical trials for the treatment of adults with cancer (Samid *et al.,* 1992; Thibault *et al.,* 1994, 1995). Inhibition of the mevalonate pathway and protein prenylation by PA appears to be among the mechanisms of action responsible for tumor growth arrest and maturation (Samid *et al.,* 1994). In the present studies we focused on the effect of PA on *ras* expression in *ras*-transformed cell lines. To explore more closely the relationship between *ras* and PA, we used gene transfer models to minimize the genetic variability among tested cells.

Studies involved murine and human cell lines neoplastically transformed by different *ras* DNA constructs, in which oncogene activation was due to either transcriptional activation (LTR-c-Ha-*ras*), mutation (EJ*ras*) or retroviral transduction (v-Ki-*ras*). The central finding was that, while the *ras*-transformants were relatively resistant to radiation and doxorubicin treatments, they were significantly more sensitive to growth inhibition by PA than the parental cells or those transduced with the bacterial *neo* gene. The increased susceptibility of *ras*-transformed cells has been recently confirmed in cultured cells derived from patients with adenocarcinomas of the pancreas, prostate, colon and lung (data not shown). In addition to cytostatis, PA induced biological and molecular changes consistent with cell differentiation. For example, following treatment with PA the *ras*-transformed V7T cells had regained contact inhibition of growth in culture, lost anchorage-independent growth in soft agar and reduced ability to invade a reconstituted basement membrane. Northern blot analysis showed increased expression of the fibroblast differentiation marker collagen α type I and of 2-5ASyn coding for an enzyme involved in negative growth control. The profound changes in cell and molecular biology were accompanied by reduced $p21^{ras}$ prenylation. This effect is consistent with previous findings showing that PA inhibits cholesterol synthesis and protein prenylation (Shama Bhat and Ramasarma, 1979; Castillo *et al.,* 1991; Samid *et al.,* 1994). Inhibition of $p21^{ras}$ farnesylation may thus contribute to the cytostasis and phenotypic reversion induced by PA as this post-translational modification is required for membrane localization of $p21^{ras}$ and its biological functions in mitogenesis and neoplastic transformation (Hancock *et al.,* 1989).

Lovastatin, another inhibitor of the mevalonate pathway (Alberts, 1988), was found to block the post-translational modification of $p21^{ras}$ at concentrations significantly greater than those needed to inhibit cholesterol synthesis and cell proliferation (DeClue *et al.,* 1991). Moreover, other oncogene-transformed cells (*e.g.,* v-*src* and v-*raf*) that do not require isoprenoids for biological functions of these transforming oncoproteins were equally sensitive to lovastatin compared to *ras*-transformed cells (DeClue *et al.,* 1991). This suggests that the anti-tumor activity of lovastatin may be independent of the *ras* pathway. By contrast, we found that comparable concentrations of PA were effective in inhibiting protein isoprenylation and in inducing cytostasis in *ras*-transformed cells, while *src*-transformed cells, though growth-inhibited by PA, did not undergo phenotypic reversion (data not shown). In addition, a rescue study with farnesyl pyrophosphate shows that this isoprenoid is able to partially reverse the cytostatic effect of PA (data not shown). Taken together, our findings suggest that blocking of the *ras* pathway may play a more important role in the anti-cancer activity of PA than that of lovastatin. Nevertheless, it cannot be ruled out that additional mechanisms may contribute to the anti-cancer activity of PA. Studies are in progress to determine whether other oncogene-transformed cells are responsive to PA treatment.

Lipid accumulation occurred in various tumor cells following treatment with PA (Samid *et al.,* 1992, 1993, 1994). In addition to inhibition of cholesterol synthesis, PA, in a way similar to other fatty acids, can conjugate with co-enzyme A, enter the pathway to chain elongation and interfere with lipid metabolism in general (Smith and Stern, 1983). PA has also been shown to stimulate the human peroxisomal proliferator-activated receptor (hPPAR; data not shown), a member of the nuclear steroid receptor superfamily (Issermann and Green, 1990; Keller *et al.,* 1993). PPAR is a ligand-activated transcriptional factor known to regulate fatty acid and cholesterol

metabolism in mammalian cells (Issermann and Green, 1990; Keller *et al.,* 1993). Modulation of lipid metabolism rather than direct cell-killing may have potential for chemotherapeutic treatment of patients who fail to respond to conventional therapies (Kuhajda *et al.,* 1994).

In summary, the differentiation agent PA inhibits $p21^{ras}$ post-translational processing, an effect associated with growth arrest and phenotypic reversion of *ras*-transformed cells. The increased susceptibility of *ras*-transformed cells documented here using gene transfer models may have clinical implications as over-expression of *ras* has been implicated in resistance to conventional therapies, including ionizing radiation and some cytotoxic chemotherapies. PA could thus provide an alternative treatment (primary or adjuvant) to suppress the growth of malignant cells, which otherwise escape response due to over-expression of *ras.*

ACKNOWLEDGEMENTS

We thank Dr. D. Rimoldi for her help with molecular analysis. This study was supported by funds from Elan Pharmaceutical Research Corporation through a Cooperative Research and Development Agreement (CACR-0139).

REFERENCES

ALBERTS, A.W., Discovery, biochemistry, and biology of lovastatin. *Amer. J. Cardiol.,* **62,** 10J–15J (1988).

BARBACID, M., *ras* genes. *Ann. Rev. Biochem.,* **56,** 779–927 (1987).

BRUSILOW, S.W., DANNEY, M., WABER, L.J., BATSHAW, M., BURTON, B., LEVITSKY, L., ROTH, K., MCKEETHREN, C. and WARD, J., Treatment of episodic hyperammonemia in children with inborn errors of urea synthesis. *N. Engl. J. Med.,* **310,** 1630–1634 (1984).

CASTILLO, M., MARTINEZ-CAYUELA, M., ZAFRA, M.F. and GARCIA-PEREGRIN, E., Effect of phenylalanine derivatives on the main regulatory enzymes of hepatic cholesterogenesis. *Mol. cell. Biochem.,* **105,** 21–25 (1991).

DECLUE, J.E., VASS, W.C., PAPAGEORGE, A.G., LOWY, D.R. and WILLUMSEN, B.M., Inhibition of cell growth by lovastatin is independent of *ras* function. *Cancer Res.,* **51,** 712–717 (1991).

HANCOCK, J.F., MAGEE, A.L., CHILDS, J.E. and MARSHALL, C.J., All Ras proteins are polyisoprenylated but only some are palmitoylated. *Cell,* **57,** 1167–1177 (1989).

ISSEMANN, I. and GREEN, S., Activation of a member of the steroid hormone receptor superfamily by peroxisome proliferators. *Nature (Lond.),* **347,** 645–650 (1990).

JAMES, G.L., GOLDSTEIN, J.L., BROWN, M.S., RAWSON, T.E., SOMERS, T.C., MCDOWELL, R.S., CROWLEY, C.W., LUCAS, B.K. and LEVINSON, A.D., Benzodiazepine peptidomimetics: potent inhibitors of *ras* farnesylation in animal cells. *Science,* **260,** 1937–1942 (1993).

KELLER, H., DREYER, C., MEDIN, J., MAHFOUDI, A., OZATO, K. and WAHLI, W., Fatty acids and retinoids control lipid metabolism through activation of peroxisome proliferator-activated receptor-retinoid × receptor heterodimers. *Proc. nat. Acad. Sci. (Wash.),* **90,** 2160–2164 (1993).

KHOSRAVI-FAR, R. and DER, C.J., The Ras signal transduction pathway. *Cancer Met. Rev.,* **13,** 67–89 (1994).

KOHL, N.E., MOSSER, S.D., DESOLMS, S.J., GIULIANI, E.A., POMPLIANO, D.L., GRAHAM, S.L., SMITH, R.L., SCOLNICK, E.M., OLIFF, A. and GIBBS, J.B., Selective inhibition of *ras*-dependent transformation by a farnesytransferase inhibitor. *Science,* **260,** 1934–1937 (1993).

KUHAJDA, F.P., JENNER, K., WOOD, F.D., HENNIGAR, R.A., JACOBS, L.B., DICK, J.D. and PASTERNACK, G.R., Fatty acid synthesis: a potential selective target for antineoplastic therapy. *Proc. nat. Acad. Sci. (Wash.),* **91,** 6379–6383 (1994).

LIU, L., SHACK, S., STETLER-STEVENSON, W.G., HUDGINS, W.R. and SAMID, D., Differentiation of cultured human melanoma cells induced by the aromatic fatty acids phenylacetate and phenylbutyrate. *J. Invest. Dermatol.,* **103,** 335–340 (1994).

MANIATAS, T., FRITSCH, E.F. and SAMBROOK, J., *Molecular cloning: a laboratory manual* (1st ed.), Cold Spring Harbor Laboratory Press, Cold Spring Harbor, NY (1982).

MILLER, A.C., CLARK, E.P., KARIKO, K. and SAMID, D., Increased radioresistance of EJ*ras*-transformed human osteosarcoma cells and its modulation by lovastatin, an inhibitor of $p21^{ras}$ isoprenylation. *Int. J. Cancer,* **53,** 302–307 (1993*a*).

MILLER, A.C., GAFNER, J., CLARK, E.P. and SAMID, D., Posttranscriptional down-regulation of *ras* oncogene expression by inhibitors of cellular glutathione. *Mol. cell. Biol.,* **13,** 4416–4422 (1993*b*).

MILLER, A.C. and SAMID, D., Tumor resistance to oxidative stress: association with *ras* oncogene expression and reversal by lovastatin, an inhibitor of $p21^{ras}$ isoprenylation. *Int. J. Cancer,* **60,** 249–254 (1995).

MOSMANN, T., Rapid colorimetric assay for cellular growth and survival: application to proliferation and cytotoxicity assays. *J. Immunol. Methods,* **65,** 55–63 (1983).

RAM, Z., SAMID, D., WALBRIDGE, S., OSHIRO, E.M., VIOLA, J.J., TAO-CHENG, J.-H., SHACK, S., THIBAULT, A., MYERS, C.E. and OLDFIELD, E.H., Growth inhibition, tumor maturation, and extended survival in experimental brain tumors in rats treated with phenylacetate. *Cancer Res.,* **54,** 2923–2927 (1994).

RIMOLDI, D., DIFFENBACH, C.W., FRIEDMAN, R.M. and SAMID, D., 2′,5′-Oligoadenylate synthetase gene expression in revertants of *ras*-transformed NIH3T3 fibroblasts. *Exp. Cell Res.,* **191,** 76–82 (1990).

SAMID, D., MILLER, A.C., GAFNER, J. and CLARK, C.P., Increased radiation resistance in transformed and non-transformed cells with elevated *ras* proto-oncogene expression. *Rad. Res.,* **126,** 244–250 (1991).

SAMID, D., RAM, Z., HUDGINS, W.R., SHACK, S., LIU, L., WALBRIDGE, S., OLDFIELD, E.H. and MYERS, C.E., Selective activity of phenylacetate against malignant gliomas: resemblance to fetal brain damage in phenylketonuria. *Cancer Res.,* **54,** 891–895 (1994).

SAMID, D., SHACK, S. and MYERS, C.E., Selective growth arrest and maturation of prostate cancer cells *in vitro* by non-toxic, pharmacological concentrations of phenylacetate. *J. clin. Invest.,* **91,** 2288–2295 (1993).

SAMID, D., YEH, A. and PRASANNA, P., Induction of erythroid differentiation and fetal hemoglobin production in human leukemic cell treated with phenylacetate. *Blood,* **80,** 1576–1581 (1992).

SHAMA BHAT, C. and RAMASARMA, T., Inhibition of rat liver mevalonate pyrophosphate decarboxylase and mevalonate phosphate kinase by phenyl and phenolic compounds. *Biochem. J.,* **181,** 143–151 (1979).

SMITH, S. and STERN, A., The effect of aromatic CoA esters on fatty acid synthetase: biosynthesis of ω-phenyl fatty acid. *Arch. Biochem. Biophys.,* **222,** 259–265 (1983).

THIBAULT, A., COOPER, M.R., FIGG, W.D., VENZON, D.J., SARTOR, A.O., TOMPKINS, A.C., WEINBERGER, M.S., HEADLEE, D.J., MCCALL, N.A., SAMID, D. and MYERS, C.E., A phase I and pharmacokinetic study of intravenous phenylacetate in patients with cancer. *Cancer Res.,* **54,** 1690–1694 (1994).

THIBAULT, A., SAMID, D., COOPER, M.R., FIGG, W.D., TOMPKINS, A.C., PATRONAS, N., HEADLEE, D.J., KOHLER, D.R., VENZON, D.J. and MYERS, C.E., Phase I study of phenylacetate administered twice daily to patients with cancer. *Cancer,* **75,** 2932–2938 (1995).

RADIATION RESEARCH 144, 301–309 (1995)

Neutron and Gamma-Radiation Sensitivity of Plasmid DNA of Varying Superhelical Density

C. E. Swenberg and J. M. Speicher[1]

Applied Cellular Radiobiology, Armed Forces Radiobiology Research Institute, 8901 Wisconsin Avenue, Bethesda, Maryland 20889-5603

Swenberg, C. E. and Speicher, J. M. Neutron and Gamma-Radiation Sensitivity of Plasmid DNA of Varying Superhelical Density. *Radiat. Res.* **144**, 301–309 (1995).

Several families of negatively supercoiled topoisomers of plasmid pIBI30 were prepared by a modification of the procedure of Singleton and Wells (*Anal. Biochem.* **122**, 253–257, 1982). The average superhelical density (σ) was determined by two-dimensional agarose gel electrophoresis and varied from –0.010 to –0.067, corresponding to a change in the number of supercoils from 3 to 19 and an effective volume change from 1.6×10^8 to 4×10^8 Å^3. Samples were exposed to either fission-neutron or ^{60}Co γ radiation and assayed for single-strand breaks by agarose gel electrophoresis. Form I DNA for all topoisomers decreased exponentially with increasing dose. The D_{37} values for both neutron and γ radiation increased monotonically with increasing $|\sigma|$. Using a branched plectonemic (interwound) form for DNA over the range of σ studied and standard (single-hit) target theory, a quantitative linear fit to $(D_{37})^{-1}$ as a function of the effective DNA radius, S(Å), was obtained. The model predicts that both the slope (a) and the intercept (b) of $(D_{37})^{-1}$ as a function of S(Å) are directly proportional to the length of DNA and the radiation fluence. Furthermore, the ratio b/a ($= r_0$) at $\sigma = 0$ depends only on the ionic strength of the medium and is independent of the radiation source parameters. Our results support the model and we calculate $r_0 = 13.4 \pm 1.4$ nm, a value consistent with other investigations. Our results are consistent with studies using ^{137}Cs (Milligan *et al.*, *Radiat. Res.* **132**, 69–73, 1992) but disagree with data obtained for X rays (Miller *et al.*, *Int. J. Radiat. Biol.* **59**, 941–949, 1991).

INTRODUCTION

DNA supercoiling, i.e. the coiling of the axis of the double helix, is ubiquitous in biological systems. Supercoiling can result either from DNA winding around proteins, e.g. the histones of eukaryotes, or from the imposition of other topological constraints, e.g. as occurs in covalently closed duplex DNA. Plasmid DNA constitutes a useful model system for investigating interactions between topologically constrained DNA and radiation fields and other environmental insults. *In vitro* studies involving supercoiled plasmid have revealed a number of unusual DNA structures (*1*, *2*) that have subsequently been identified *in vivo*. Plasmids have served as useful model systems for numerous radiation studies in addition to their role as vectors.

A given plasmid can assume a large number of distinct and easily identifiable, topologically inequivalent conformations verifiable by gel electrophoresis. These different conformational states can be classified by their linking number (Lk; ref. *3*). Lk, a topological invariant, is defined as the number of revolutions that one strand makes around the other if the molecule is constrained to lie in a plane. More useful, because it is independent of plasmid size, is the descriptor superhelical density (or specific linking difference, σ), which can be defined as $\Delta Lk/Lk_0$, where ΔLk, the mean linking difference, is equal to $(Lk - Lk_0)$, and Lk_0 is the equilibrium mean linking number of the plasmid after nicking and ligation under defined experimental conditions (*4*, *5*). We adopt an alternative identity for Lk_0—the number of base pairs (M) divided by 10.5 (the average value of the helical repeat under physiological ionic conditions). In almost all cases, native plasmid DNAs isolated from eukaryotic cells have σ values that are negative, a condition corresponding to more base pairs per turn than predicted by the Watson-Crick model.[2]

In this paper the dependence of single-strand breaks (SSBs) on DNA superhelical state is measured for values of σ varying from –0.010 to –0.067. Since an increase in $|\sigma|$ is proportional to DNA compactness, larger $|\sigma|$ correspond to smaller radiation target volumes. This range of superhelical

[1]To whom correspondence should be addressed.

[2]For experimental evidence of DNA existing *in vivo* in a positive superhelical state in the genome of the virus-like particle SSV-1, present in *Sulfolobus*, see M. Nudal, G. Mirambeau, P. Forterre, W. D. Reiter and M. Duguet, Positively supercoiled DNA in a virus-like particle of an archaebacterium. *Nature* **321**, 256–258 (1986).

0033-7587/95 $5.00

densities offered a simple means of testing target theory for the special case of DNA in small domains capable of assuming unusual conformational states. For the range of superhelical densities studied, we estimate a change in the effective DNA volume to be approximately equivalent to a factor of two. Recently published investigations of the dependence of D_{37} on σ (*6–8*) were confined to low-LET radiation and advanced conflicting conclusions. For our investigation, studies were extended to include high-LET radiation protocols employing fission neutrons.

This paper considers the analytical methodology with which a simplified model is developed to account quantitatively for the data employing the assumption that superhelical DNA adopts a branched, plectonemic form in solution. Some testable predictions of the model are presented.

MATERIALS AND METHODS

Protocol for preparation of supercoiled families (topoisomers) of pIBI30. Plasmid pIBI30 was isolated from *Escherichia coli* by alkaline lysis (*9*). Eukaryotic topoisomerase I (topo-I) was purchased from Bethesda Research Laboratory (BRL), Bethesda, MD, and was prepared for assay following the recommendations of the supplier. A protocol for relaxation of plasmid DNA was modified from the procedure of Singleton and Wells (*10*). In our method, 30–50 μg of plasmid was relaxed with 30 U of enzyme in the presence of 1.4, 2.0, 4.1, 5.9, 6.4, 9.7, 12, 16.4 or 22.6 μmol dm^{-3} ethidium bromide at 37°C for 4 h in a total volume of 150 μl per reaction tube. Native plasmid was subjected to the same manipulations by combining it in a reaction mixture containing all ingredients with the exception of topo-I and ethidium bromide. Since topoisomers were desired in quantity, and to maximize use of the enzyme, a typical preparation involved 12 reaction tubes (6 for each of 2 topoisomers). The individual tubes were combined in a single tube after incubation and prior to extraction.

Topoisomer reaction volumes were extracted once with buffer-saturated phenol (BRL catalog number 5513UA) and once with phenol:chloroform:isoamyl alcohol (proportions: 25:24:1), removing the aqueous phase to a fresh tube after each extraction. Extractions always employed equal volumes. The resulting volume was subjected to three extractions with water-saturated ethyl ether with careful removal of the organic layer to waste. After each extraction, a brief centrifugation (5,000 rpm for 1–5 min) aided in phase separation. Finally, resulting volumes were incubated for ≈10 min at 65°C with constant flow of N_2 gas to purge residual ether from the system.

Ethanol precipitation of topoisomer preparations was adapted from standard protocols. The DNA was dissolved in a small volume of 50 mmol dm^{-3} potassium phosphate buffer (pH 7.2) and stored at 4°C for a minimum of 24 h. If the lyophilization step of the topoisomer preparation involved multiple tubes, they were combined in a single tube using a vigorous wash-through method, which took advantage of the innate stability (resistance to shearing) of plasmid (supercoiled) DNA. Topoisomer preparations were brought to a final concentration of ≈200 μg/ml following a careful dilution protocol. DNA concentration was determined by scanning sample solutions at 260 nm on a diode array spectrophotometer (Hewlett Packard model 8450A, Palo Alto, CA). DNA purity was determined by monitoring the shape of the curve of a broad-spectrum scan (220–350 nm) of the DNA in solution and by monitoring the absorption ratio A_{260}:A_{280} of the DNA. DNA was certified as RNA-free and double-checked for absolute concentration by monitoring fluorescence of the topoisomers in the presence of Hoechst 33258 with a dedicated fluorometer (Hoefer Scientific Instruments, model TKO-100, San Francisco, CA). Two sets of purified supercoiled families of pIBI30 were prepared for use in our studies. One isomer set, designated *DEC 1991*, was prepared in late 1991 and used in experimental protocols in May and June of 1992. Its nicked-circular component comprised ≈26% of total DNA with a range of 23.7 to 30.3 for the six families of topoisomers. A second isomer set, designated *SEP 1992*, was prepared in the fall of 1992 and used in experimental protocols in October, November and December of 1992. Its nicked-circular component comprised ≈34.8% of total DNA with a range of 29.1 to 39.3 for the seven families of topoisomers.

Superhelical density (σ) analysis of supercoiled families. Supercoiled families of pIBI30 DNA were analyzed by two-dimensional (2D) agarose gel electrophoresis. The electrophoresis parameters were manipulated to yield maximum separation in both dimensions. Between dimensions, the gel was soaked in TBE buffer (89 mmol dm^{-3} Tris, 89 mmol dm^{-3} boric acid, 2.5 mmol dm^{-3} EDTA, pH 8.0) containing chloroquine of appropriate concentration. The gel (still on the Plexiglas plate) was prepared for electrophoresis in the second dimension by rotating it 90° from the original orientation before application of current.

We used the following specific parameters for 2D electrophoresis of pIBI30: (1) First dimension: Agarose gel composition (1.6%, 15 × 20 cm in TBE buffer); electrophoresis at constant voltage (100 V) at room temperature for 5 h in TBE buffer containing chloroquine at a concentration of 1 μmol dm^{-3}. (2) Gel soak: Five hours at room temperature in TBE buffer containing chloroquine at a concentration of 2 μmol dm^{-3}. (3) Second dimension: Electrophoresis at constant voltage (74 V) at 4°C for 13.5 h in TBE buffer containing chloroquine at a concentration of 2 μmol dm^{-3}.

Electrophoresis of a mixture containing all (nonirradiated) supercoiled families of pIBI30 resolved the full spectrum of topoisomers into discrete spots forming an image approximating a horseshoe (see Fig. 1D). Since we used chloroquine in both dimensions of electrophoresis, the fully relaxed topoisomer migrated the maximum distance in both directions. It was assigned an Lk of zero. All other spots had Lk less than zero, and each differed from its neighbor by an integral amount.

It is a simple matter to assign a ΔLk to the individual supercoiled families by running separate 2D gels for each family and comparing the pattern obtained with that obtained for the full spectrum of topoisomers. Nonirradiated supercoiled families were prepared just before analysis by dilution with potassium phosphate buffer (50 mmol dm^{-3}) and bromophenol blue/glycerol tracking-dye solution to a concentration of ≈0.2 μg DNA/5 μl; 5 μl was applied to the well. After electrophoresis, gels were photographed using positive/negative film (Polaroid 665 film, Cambridge, MA) with a Polaroid MP-4 camera. The photographic negatives were analyzed with a microdensitometer (Molecular Dynamics, model 300B, Sunnyvale, CA). Densitometric analysis yielded measurements of spot densities. Each family was characterized by ΔLk, defined as:

$$\Delta Lk = \Sigma Lk_i[x_i(\Sigma x_i)^{-1}], \quad (1)$$

where the sum extends over all individual spots associated with a given family (see Fig. 1), Lk_i is the linking number assigned to an individual spot i, and x_i denotes a measurement of density for the corresponding spot. Assuming a length of 2926 bp for pIBI30 and a helical pitch for DNA of 10.5 bp per turn, $\Delta Lk(2926/10.5)^{-1}$ converts ΔLk to σ, superhelical density.

Analysis of irradiated supercoiled families of pIBI30.[3] Supercoiled families (200 μg/ml) in 50 mmol dm^{-3} potassium phosphate buffer (pH 7.2) were exposed to fission neutrons (dose rate ≈5.1 Gy min^{-1}) and ^{60}Co γ irradiation (dose rate ≈10 Gy min^{-1}) at room temperature and ambient atmosphere in

[3]Dosimetry for fission-neutron and ^{60}Co γ irradiations was performed according to protocols documented carefully in several in-house publications. These publications, not generally available, include the following: DNA Report Nos. 5793F-1 and 5793F-2, AFRRI Technical Report TR83-2, AFRRI Contract Report CR85-1 and AFRRI Technical Note 73-3.

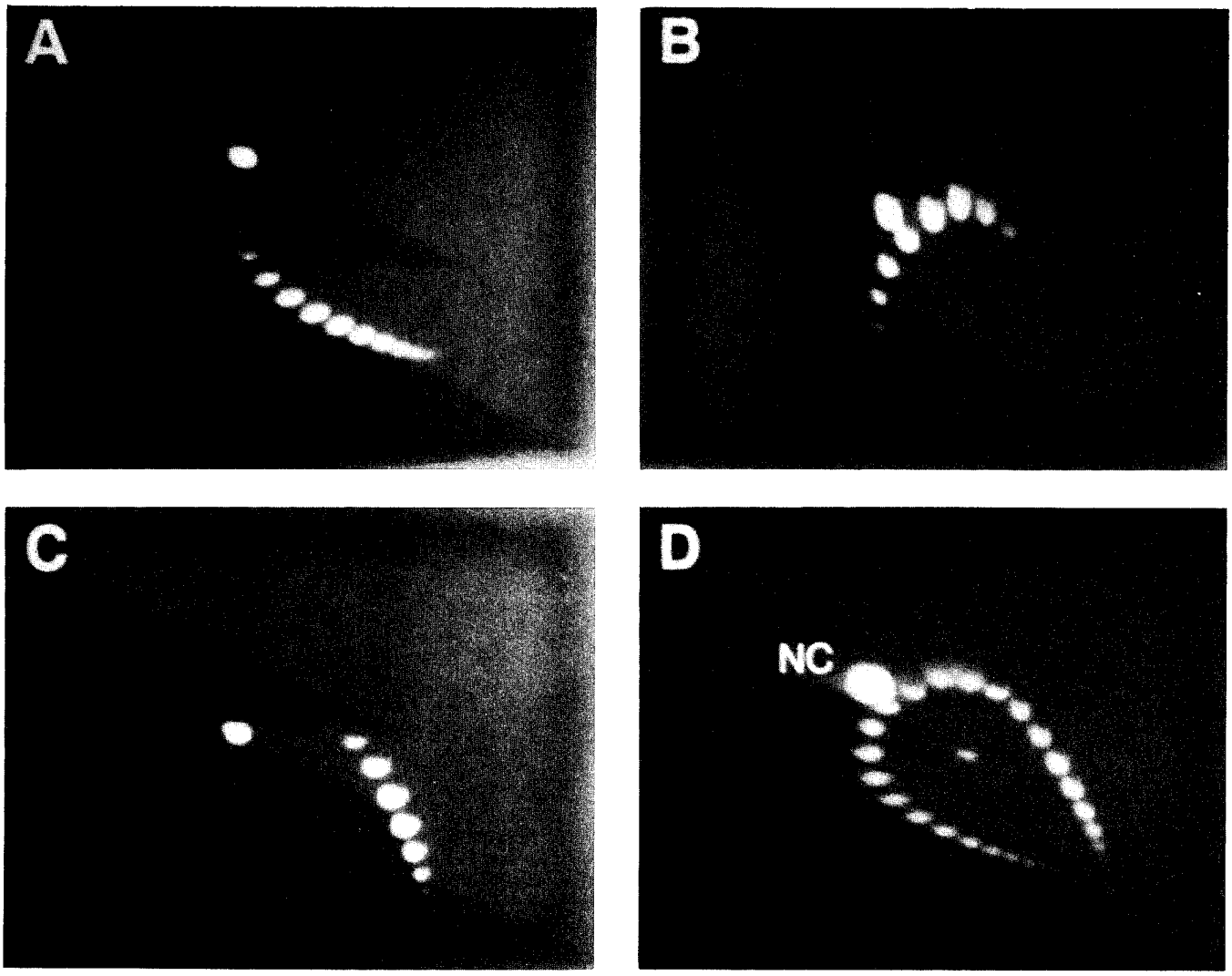

FIG. 1. Two-dimensional agarose gels of supercoiled families of pIBI30. Panel A: $\sigma = -0.0666$; panel B: $\sigma = -0.0401$; panel C: $\sigma = -0.0204$; panel D: mixture of all topoisomers. See text for electrophoresis parameters. NC designates nicked-circular DNA (Form II), the largest spot in all panels.

small volume conical, polypropylene tubes. The range of exposures was 0 to 50 Gy for fission-neutron irradiation and 0 to 15 Gy for ^{60}Co γ irradiation.

Gamma-irradiated samples were exposed to a bilateral radiation field produced by the AFRRI ^{60}Co facility. A calibrated tissue-equivalent ionization chamber (calibration traceable to the National Institute of Standards and Technology) was used for γ-irradiation dosimetry, following the AAPM TG21 protocol (*11*). The tissue-to-air-ratio was 0.98.

Prior to assay, irradiated topoisomers were stored at 4°C in tightly capped exposure tubes, which were further protected from desiccation by enclosure within sealed 50 ml conical centrifuge tubes. Although DNA was adversely affected by storage, the effect stabilized after approximately 14 days (as shown in Fig. 2). Samples generally were not assayed prior to the 20th day of storage, and then all samples for a specific experiment were assayed within 5 to 7 calendar days.

Radiation-induced SSBs as a function of dose were quantified by an agarose gel electrophoresis assay. This assay facilitates the determination of the D_{37}, i.e. the dose corresponding to an average of one hit [or SSB, caused by a disruption of the phosphodiester linkage of the sugar-phosphate (DNA) backbone] per plasmid as a function of σ. Irradiated samples were prepared just before analysis by dilution with potassium phosphate buffer (50 mmol dm^{-3}) and bromophenol blue/glycerol tracking-dye solution to a concentration of 0.075 μg/5 μl. Five microliters of this preparation was applied to each of several lanes such that the entire spectrum of experimental treatments (radiation doses) including control (no radiation) were represented at least twice on each of two lane-sets on a single gel. Also included on the gel were marker bands composed of native pIBI30 delineating the extremes of the linear response region, determined previously (data not shown). Agarose gels (1.6%, 15 × 20 cm, in TBE buffer) incorporating ethidium bromide (0.5 μg/ml) were run at constant voltage (75 V) for 2 h at room temperature. Electrophoresis resolved samples into three distinct bands, with the nicked-circular band widely separated from the rapidly migrating supercoiled band. After electrophoresis, gels were photographed with positive/negative film and the photographic negatives were analyzed with a microdensitometer. Densitometric analysis yielded measurements of band densities.

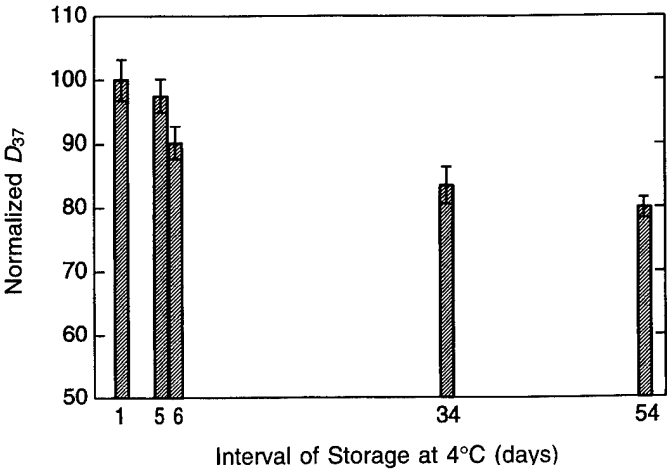

FIG. 2. The effect of sample storage at 4°C on D_{37} for a typical supercoiled family of pIBI30. D_{37} values were normalized to reflect unity = 1 day of storage.

RESULTS

A log/linear plot of the supercoiled (Form I) band densities (normalized to control) as a function of dose is illustrated in Fig. 3 for neutron- and γ-irradiated supercoiled families of pIBI30. The lines are the least-squares fit to the data according to the equation

$$\text{Form I}(D) = d\{\exp[-D(D_{37})^{-1}]\}, \quad (2)$$

where d is the intercept, D is dose and $(D_{37})^{-1}$ is an estimate of the sensitivity of the supercoiled family to SSBs.

Figure 4 shows plots of $(D_{37})^{-1}$ as a function of S(Å) (see definition below) and D_{37} as a function of σ for γ and neutron irradiation. Error bars indicate the standard error for two or three independent experiments. Where error bars are not evident, they are eclipsed by the symbol. The rescaled D_{37} values of Milligan *et al.* (*6*) are illustrated in this figure by open circles and were calculated (for Fig. 4C) using the relationship

$$D_{37\ \text{RESCALED}} = D_{37\ \text{ORIGINAL}}[\text{antilog}(\bar{m} - \bar{s})]^{-1},$$

where $\bar{m}$ and $\bar{s}$ denote the arithmetic mean of the log of the D_{37} values of Milligan and the authors of this report, respectively. Dashed lines in Fig. 4 are least-squares weighted fits to experimental data (see below).

ANALYSIS

In standard radiation target theory the effective size of the target and the number of hits required for inactivation are the important parameters (*12*). To determine the effective target size of a supercoiled DNA molecule in solution we assume that, in the underwound state, DNA adopts a plectonemic form with Y-branched vertices (*13*). Plectonemic forms for DNA with Y-branched vertices having two superhelical densities are shown in Fig. 5. Evidence obtained from the angular distribution of scattered light (*14–16*), direct visualization by cryo-electron microscopy (*3, 13, 17, 18*) and Monte Carlo simulations (*18–20*) supports the view that supercoiled DNA has a branched, underwound form in solution. The number and nature of the branching depend on the DNA base sequence (*21*) and size (*3, 15, 19*). Light-scattering data from PM2 bacteriophage (*15*) and electron micrograph studies on a 3.5 kb plasmid (*13*) suggest a value of two for the number of branch points.

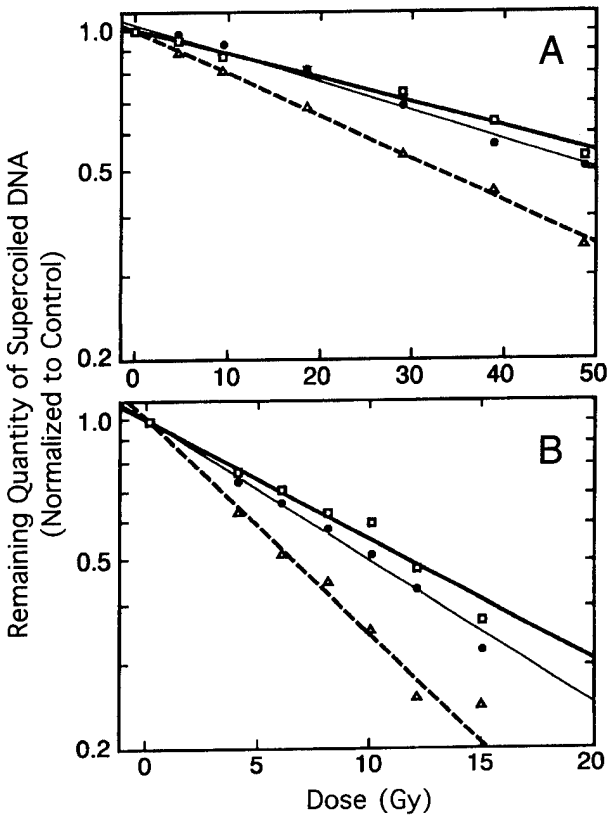

FIG. 3. Loss of supercoiled pIBI30 DNA (Form I) with increasing dose of fission neutrons (panel A) or ^{60}Co γ rays (panel B). Curves show the least-squares fit of the data (according to Eq. 2). For both panels, squares have σ = –0.0643, circles have σ = –0.0308, triangles have σ = –0.0148. Both panels show a log-linear plot of the data.

An understanding of the framework for the calculation of the effective target cross section for DNA in the radiation field requires elucidation of several important parameters as well as careful formula development. Superhelical pitch is designated by $2\pi p$. The length of the superhelix axis, ℓ, is defined as the sum of the lengths of the branched segments. The length of DNA is expressed as the value L,

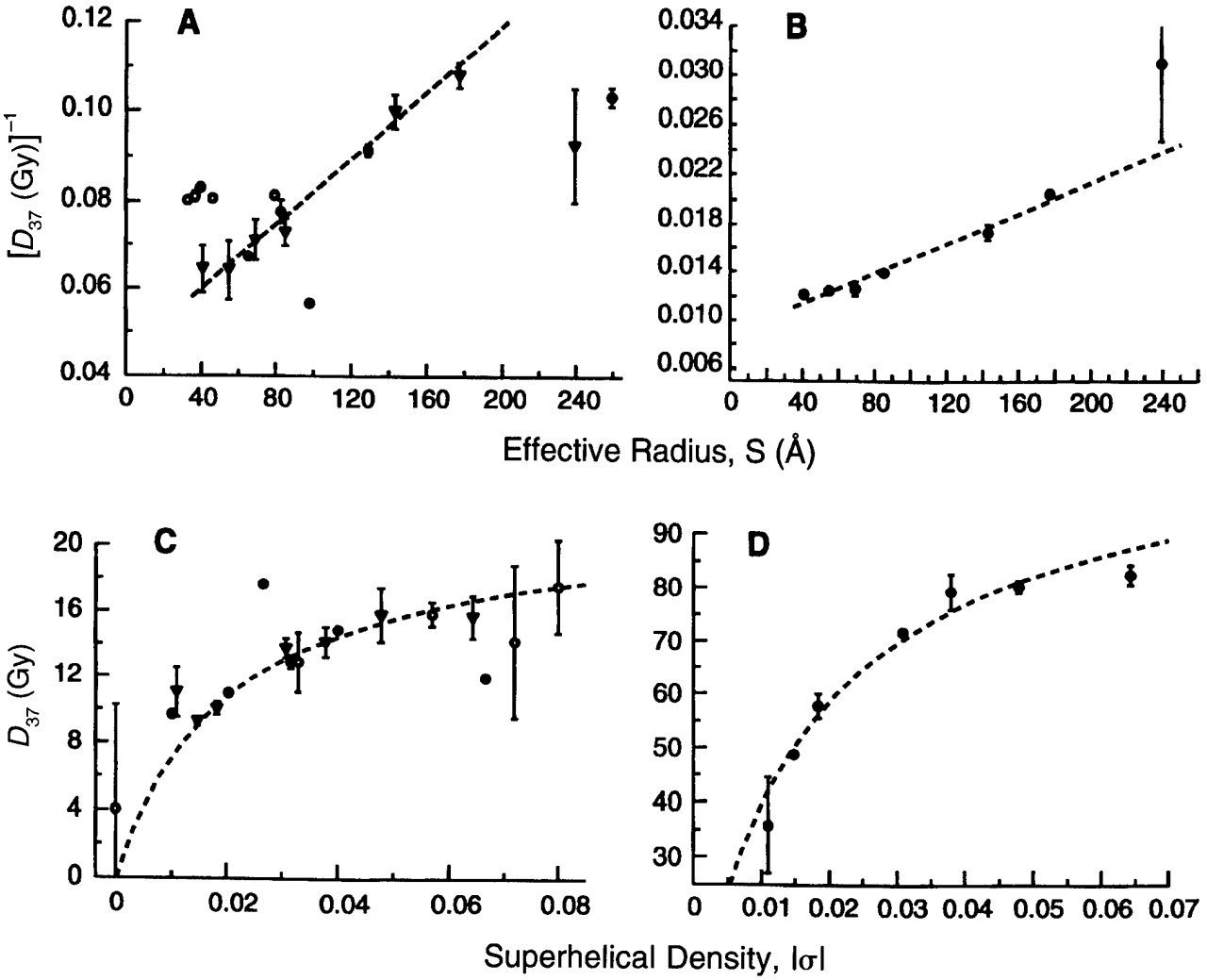

FIG. 4. Graphs of $(D_{37})^{-1}$ as a function of effective radius, S(Å) (panel A: γ radiation; panel B: fission neutrons) and (D_{37}) as a function of superhelical density, |σ| (panel C, γ radiation; panel D, fission neutrons). Solid circles denote mean of two or three experiments ± standard error (shown except where the symbol eclipses the error bars). Open circles represent the data of Milligan *et al.* (*6*) adjusted for the difference between the mean response of their data and that of the data reported here (see text). Dashed lines are theoretical fits.

which may be determined quite simply according to the formula: $L = 3.4(M - 1)$Å, where M represents base pairs. The distance between the DNA superhelix axis and the virtual cylinder axis is S in angstroms, or S(Å). The literature offers support for the assertion that ℓ is independent of σ (*13*) and that, to a good approximation, $\ell = 0.41L$ (*3*). Therefore, as shown in the work of Boles *et al.* (*13*), the geometrical relationship between L and the plectonemic DNA superhelix parameters can be expressed as

$$L = 2\pi n([S^2 + p^2]^{1/2}) + E\pi S, \qquad (3)$$

where $E = Y + 2$, Y is the number of branch points, n is the number of supercoils, and p is equal to $[(\ell - ES)/\pi n]$. Since the second term in Eq. (3) is quite small in comparison to the first, the value of Y to within a factor of 5 is unimportant. On the other hand, ℓ, being independent of σ (*13*), is a critical assumption. The investigations of Boles *et al.* (*13*) provide an estimate of n, namely: $n = -0.89\sigma Lk_0$, where $Lk_0 = M/10.5$.

The dependence of σ on the effective cylinder radius (S) may be derived from Eq. (3). This relationship, S(Å) = $g(\sigma)$, shown in Fig. 6, is determined by solving Eq. (3) for $Y = 2$, a measure of Y consistent with published values (*13*, *15*). It is also evident from Fig. 6 that, to an excellent approximation,

$$S(\text{Å}) = 2.62/|\sigma|, \qquad (4)$$

for |σ| greater than 0.01.

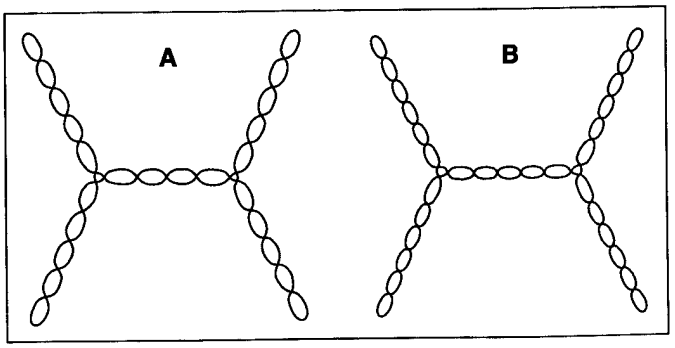

FIG. 5. Schematic of plectonemic DNA (4.6 kb) in solution with two branch points ($Y = 2$), $\ell = 6300$Å ($\ell/L = 0.4$). Panel A: $\sigma = -0.06$, $n = 23.4$, $r = 56$Å. Panel B: $\sigma = -0.079$, $n = 30.8$, $r = 43$Å. Redrawn from Cozzarelli *et al.* (*3*).

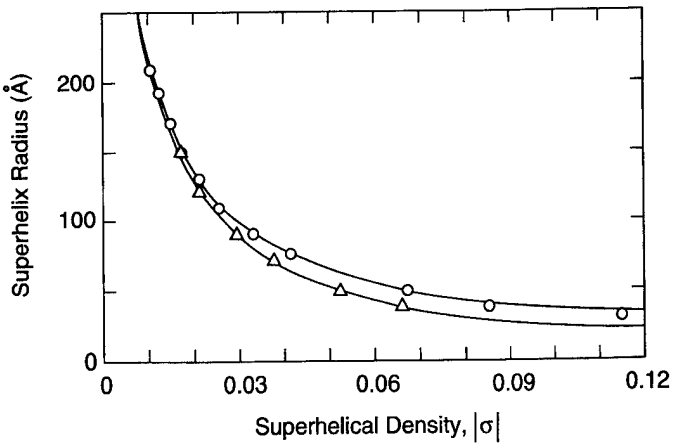

FIG. 6. The relationship between plectonemic superhelix radius, S(Å) and superhelical density (σ) for plasmid pIBI30. The curve fitted to the circles denotes the relationship derived from Eq. (3): $S(Å) = g(\sigma)$. The curve fitted to the triangles represents the approximation: $S(Å) = 2.62/\sigma$.

For any DNA molecule having an orientation α with respect to the incident radiation, the effective target area, $\delta A_e(\alpha)$, is the area projected onto a plane perpendicular to the beam direction. Geometrical considerations imply the relationship

$$\delta A_e(\alpha) = k_\alpha r = k_\alpha S + k_\alpha r_o, \quad (5)$$

where k_α depends on the particular molecule and is proportional to ℓ and L. r is the effective cylinder radius of the *virtual* cylinder delineating the molecule. Given the definition of S as the distance from the DNA superhelix axis to the cylinder axis, it follows that $r = S + r_o$, where r_o defines the *radiation* radius of the completely relaxed DNA molecule ($\sigma = 0$). We expect r_o to be a function of ionic strength since numerous studies have suggested that effective DNA radius varies with ionic environment (*20*, *22*, *23*). Summing for all configurations gives the total cross section for a radiation event impacting a DNA molecule (a hit),

$$\sigma_T = \Sigma_\alpha \delta A_e(\alpha). \quad (6)$$

For our model system where a single hit inactivates the molecule converting Form I to either nicked (Form II) or linear (Form III) DNA, the decrease in Form I DNA obeys the relationship

$$\text{Form I}(D) = \exp[-D(D_{37})^{-1}] = \exp(-\sigma_T F), \quad (7)$$

where F is fluence. We interpret our experimental D_{37} values using the formula

$$(D_{37})^{-1} = CLS + CLr_o = aS + b, \quad (8)$$

where C is a constant (for a given experiment collectively representing such parameters as dose rate, temperature, solvent ionic strength and radiation quality), a is the slope, and b is the intercept.

Employing the theoretical relationship $S(Å) = g(\sigma)$ (see Fig. 6), we have calculated an effective S(Å) for each family of topoisomers characterized by σ. Estimates of a and b may be derived from Fig. 4, which shows plots of $(D_{37})^{-1}$ as a function of S(Å) and D_{37} as a function of σ for γ and neutron irradiation. The dotted lines in the figure signify a biweighted line fit (parameter $c = 4.5$) for $(D_{37})^{-1}$ as a function of S(Å). This gives $a_\gamma = 3.7\ (\pm 0.2) \times 10^{-4}$ Å^{-1} Gy^{-1}, $b_\gamma = 4.5\ (\pm 0.2) \times 10^{-2}$ Gy^{-1}, $a_n = 6.2\ (\pm 0.4) \times 10^{-5}$ Å^{-1} Gy^{-1}, and $b_n = 8.9\ (\pm 0.5) \times 10^{-3}$ Gy^{-1}. Inferred values of b/a are 12.2 ± 1.3 nm for γ radiation and 14.4 ± 1.7 nm for fission neutrons.

Neither the data of Milligan and coworkers (*6*), shown in Fig. 4 as open circles, nor our data from γ-radiation experiments where $S > 200$ Å (corresponding to two points) were used in the biweighted fitting. Both the biweighted fits for our data for neutrons and γ radiation showed a significant regression coefficient ($P < 0.01$). In graphs of the D_{37} as a function of σ (Fig. 4C and D), the fitted curve shown uses the biweighted fit parameters a and b derived from the relationship of $(D_{37})^{-1}$ as a function of S(Å) and the definition $|\sigma| = 2.62/S(Å)$.

DISCUSSION

It is evident from Fig. 4 that single-hit target theory is valid for the range of superhelical densities studied when using $2\pi r\ell = 2\pi(r_o + S)\ell$ to calculate target cross section. The slight discrepancies at small $|\sigma|$ may be attributed to energy depositions occurring within the virtual cylinder as direct damage events exclusively. As the cylinder radius S increases, $|\sigma|$ decreases, and this assumption becomes more likely. There is no evidence for significant transitions in the secondary structure of pIBI30 such that DNA radiation sen-

TABLE I
Experimental Conditions Used in Several Investigations of the Radiation Sensitivity of Plasmid DNA

Investigators	Plasmid (bp)	Buffer (mmol dm^{-3})	pH	D_{37}[a]	Irradiation conditions: Temperature	[DNA] (μg/ml)	Dose rate (Gy min^{-1}): Gamma rays[b]	Neutrons
Swenberg and Speicher[c]	pIBI30 2926	50 KPO_4	7.2	16.9 11.6	Room temperature	200	10	5.1
Spotheim-Maurizot *et al.* (*27*)	pBR322 4362	50 KPO_4	7.3	26.2	0°C	200	2	0.3
Milligan *et al.* (*6*)	pUC18 2686	2 Tris 0.2 EDTA	8.0	61.3 48.8	Room temperature	50	6.18	
Miller *et al.* (*8*)	pIBI30 2926	10 Tris 1 EDTA	7.2	218.1 161.8	0°C	24	6	

[a] D_{37} is reported for native plasmid irradiated by γ or X rays. High and low values are reported where several determinations were made. Data were graciously provided by J. R. Milligan, who reported his data as D_0 values. Values reported for Miller *et al.* and for Spotheim-Maurizot *et al.* are estimates.

[b] Miller *et al.* used an X-ray source.

[c] This report.

sitivity is noticeably perturbed from the prediction of target theory. Presumably, in this plasmid, over the range of σ studied, either there is negligible formation of alternate structures (H- and Z-DNA and cruciforms), or, should they form, these structures do not alter radiation sensitivity significantly. However, we have observed changes in the DNA strand characteristics as indicated by S_1 nuclease assays for nicking and linearization of DNA. Topoisomers of pIBI30 having larger |σ| were linearized more readily by S_1 nuclease (data not shown), a clear indication of enhanced, localized single-strandedness.

It is well established that in double-stranded DNA the bases are shielded inside the double helix, and sugar moieties are relatively more exposed to hydroxyl radical attack. Thus •OH attack of deoxyribose (the precursor pathway to SSBs) may be more important in double-stranded DNA compared to single-stranded DNA (*24*). The agreement of our data with target theory and the enhancement in the ratio of single-stranded to double-stranded DNA as |σ| increases can be rationalized by assuming that either DNA denaturation sites (AT-rich regions) contribute only modestly to the total radiation sensitivity of the plasmid, or radical transfer occurs from bases to the ring structure of the sugar molecule. Generally, radical attack on bases results in point mutations, not strand breaks, unless radical transfer occurs. In single-stranded poly uridylic acid clear evidence exists for base radicals to transfer to the deoxyribose, initiating strand breaks (*25*). No evidence exists for such a pathway inside cells or for DNA in solution. Without further research, this puzzle will remain.

A rescaling of the data of Milligan and coworkers (*6*) makes it evident that their results concur with the results reported in this paper. Seemingly contradictory data published previously by us (*7*) were in error. (The error was traceable to an unreliable ΔLk for the native form of pIBI30.) The results of Miller *et al.* (*8*) are inconsistent with target theory and with data reported here. This discrepancy could be due to effects of the ionic environment employed in their investigation. Anderson and Bauer (*5*) have shown that very significant changes in superhelix density can occur in plasmid DNA by alterations in temperature and/or ionic conditions. It is even possible to alter the sign of σ by manipulating the ionic conditions.

Although our results confirm target theory, this need not be the case for other plasmids, or for plasmids subjected to conditions which were not investigated. In addition to temperature and ionic state, base composition is a major variable. For example, when |σ| increases, the presence of inverted repeats increases the likelihood of non-B DNA regions, e.g. Z-DNA tracks or cruciform structures. AT-rich DNA segments will enhance the occurrence of denatured sites with increases in |σ| or temperature. These structures are energetically unfavorable except in the case of closed-circular duplex DNA or for local regions of chromosomal DNA where structural alterations, driven by DNA supercoiled free energy ($\propto\sigma^2$), are favored. Furthermore, because of the difference in sugar conformation between positively and negatively supercoiled DNA and the increased flexibility of positively supercoiled DNA relative to negatively supercoiled DNA (*26*), we expect that the response of positively supercoiled DNA to ionizing radiation will differ from that of negatively supercoiled DNA. Table I (*27*) summarizes the conditions employed by several research laboratories investigating the radiation sensitivity of topoisomers of plasmid DNA.

Our hypothesis regarding the dependence of $(D_{37})^{-1}$ on S(Å) predicts that both the slope a and the intercept b are proportional to the length, L, of DNA, the radiation

parameters and solvent ionic strength (Eq. 8). However, the intercept to slope ratio, b/a, should be solely a function of solvent ionic strength. Although the calculated a_γ and b_γ (a measure of SSBs) are 5.5 ± 0.5 times larger than a_n and b_n, the ratios of b/a for the two radiation types are nearly equivalent [$r_o(\gamma) = 12.2 \pm 1.3$ nm and $r_o(n) = 14.4 \pm 1.7$ nm], lending support to the belief that r_o is solely a function of ionic strength. Since r_o is an order of magnitude larger than the geometric radius of DNA (~10 Å), the parameter r_o should be regarded as an effective *radiation* radius.

Similarly, when calculated (or measured) as a function of electrolyte concentration, DNA diameter is several times larger than the geometric diameter at low monovalent cation concentration (*28*). Dose-rate differences between the γ-irradiation protocol (10 Gy min^{-1}) and the neutron-irradiation protocol (5.1 Gy min^{-1}) may account for some (factor = 2) of the unexpectedly large difference (factor = 5.5 ± 0.5) between $a(\gamma/n)$ and $b(\gamma/n)$. A portion of the remaining incongruity (factor ≈3) may be attributable to qualitative radiation factors. The nonrandom, high-density distribution of radicals along the tracks of neutron-produced secondary particles greatly reduces the yield of reactive •OH radicals as this spatial pattern enhances recombination (*29*). A dense track of radicals is characteristic of neutron irradiation, as is a sparse and relatively random distribution of radicals for γ irradiation (*30, 31*). Spotheim-Maurizot *et al.* (*27*) have actually reported a disparity in SSB yield (factor = 2) in studies of neutron and γ irradiation of plasmids.

Our data demonstrate that induced SSBs can be accounted for quantitatively by simple target theory if it is assumed that supercoiled DNA adopts a branched plectonemic structure in dilute solution. Specifically, $(D_{37})^{-1}$ varied linearly with the DNA radius, S, as predicted by target theory. A premise that the ratio b/a is solely a function of ionic strength was confirmed by our inferred values of 12.2 ± 1.3 nm for γ irradiation and 14.4 ± 1.7 nm for fission-neutron irradiation of plasmid DNA of varying superhelical densities.

ACKNOWLEDGMENTS

We gratefully acknowledge statistical analysis by William Jackson, technical assistance by Colleen Loss and assistance with 2D electrophoresis techniques and access to original data provided by J. R. Milligan.

Received: February 23, 1994; accepted: July 11, 1995

REFERENCES

1. E. Palecek, Local supercoil-stabilized DNA structures. *Crit. Rev. Biochem. Mol. Biol.* **26**, 151–226 (1991).
2. R. D. Wells, Unusual DNA structures. *J. Biol. Chem.* **263**, 1095–1098 (1988).
3. N. R. Cozzarelli, T. C. Boles and J. H. White, Primer on the topology and geometry of DNA supercoiling. In *DNA Topology and Its Biological Effects* (N. R. Cozzarelli and J. C. Wang, Eds.), pp. 139–184. Cold Spring Harbor Laboratory Press, Cold Spring Harbor, NY, 1990.
4. J. C. Wang, Variation of the average rotation angle of the DNA helix and the superhelical turns of covalently closed cyclic lambda DNA. *J. Mol. Biol.* **43**, 25–39 (1969).
5. P. Anderson and W. Bauer, Supercoiling in closed circular DNA: Dependence upon ion type and concentration. *Biochemistry* **17**, 594–601 (1978).
6. J. R. Milligan, A. D. Arnold and J. F. Ward, The effect of superhelical density on single-strand break yield for gamma-irradiated plasmid DNA. *Radiat. Res.* **132**, 69–73 (1992).
7. C. E. Swenberg, J. M. Speicher and J. H. Miller, Does the topology of closed supercoiled DNA affect its radiation sensitivity? In *Biological Effects and Physics of Solar and Galactic Cosmic Radiation*, Part A (C. E. Swenberg, G. A. Horneck and E. G. Stassinopoulos, Eds.), pp. 37–47. Plenum Press, New York, 1993.
8. J. H. Miller, J. M. Nelson, M. Ye, C. E. Swenberg, J. M. Speicher and C. J. Benham, Negative supercoiling increases the sensitivity of plasmid DNA to single-strand break induction by X-rays. *Int. J. Radiat. Biol.* **59**, 941–949 (1991).
9. F. M. Ausubel, R. Brent, R. E. Kingston, D. D. Moore, J. G. Seidman, J. A. Smith and K. Struhl, In *Current Protocols in Molecular Biology*, pp. 1.7.1–1.7.11. Wiley Interscience, New York, 1988.
10. C. K. Singleton and R. D. Wells, The facile generation of covalently closed, circular DNAs with defined negative superhelical densities. *Anal. Biochem.* **122**, 253–257 (1982).
11. American Association of Physicists in Medicine, Task Group 21, Radiation Therapy Committee, A protocol for the determination of absorbed dose from high-energy photon and electron beams. *Med. Phys.* **10**, 741–771 (1983).
12. J. F. Fowler, Differences in survival curve shapes for formal multitarget and multi-hit models. *Phys. Med. Biol.* **9**, 177–188 (1964).
13. T. C. Boles, J. H. White and N. R. Cozzarelli, Structure of plectonemically supercoiled DNA. *J. Mol. Biol.* **213**, 931–951 (1990).
14. D. J. Jolly and A. M. Campbell, The three-dimensional structure of supercoiled deoxyribonucleic acid in solution. Evidence obtained from the angular distribution of scattered light. *Biochem. J.* **128**, 569–578 (1972).
15. A. M. Campbell, Conformational analysis of deoxyribonucleic acid from PM2 bacteriophage. The effect of size on supercoil shape. *Biochem. J.* **155**, 101–105 (1976).
16. A. M. Campbell, Conformational variation in superhelical deoxyribonucleic acid. *Biochem. J.* **171**, 281–283 (1978).
17. M. Adrian, B. ten-Heggeler-Bordier, W. Wahli, A. Z. Stasiak, A. Stasiak and J. Dubochet, Direct visualization of supercoiled DNA molecules in solution. *EMBO J.* **9**, 4551–4554 (1990).
18. J. Bednar, P. Furrer, A. Stasiak, J. Dubochet, E. H. Egelman and A. D. Bates, The twist, writhe and overall shape of supercoiled DNA change during counterion-induced transition from a loosely to a tightly interwound superhelix. Possible implications for DNA structure *in vivo*. *J. Mol. Biol.* **235**, 825–847 (1994).
19. A. V. Vologodskii, S. D. Levene, K. V. Klenin, M. Frank-Kamenetskii and N. R. Cozzarelli, Conformational and thermodynamic properties of supercoiled DNA. *J. Mol. Biol.* **227**, 1224–1243 (1992).
20. M. D. Frank-Kamenetskii, DNA supercoiling and unusual structures. In *DNA Topology and Its Biological Effects* (N. R. Cozzarelli and J. C. Wang, Eds.), pp. 185–215. Cold Spring Harbor Laboratory Press, Cold Spring Harbor, NY, 1990.
21. A. Campbell and R. Eason, Effects of DNA primary structure on tertiary structure. *FEBS Lett.* **55**, 212–215 (1975).
22. S. Y. Shaw and J. C. Wang, Knotting of a DNA chain during ring closure. *Science* **260**, 533–536 (1993).
23. B. S. Fujimoto, J. M. Miller, N. S. Ribeiro and J. M. Schurr, Effects of different cations on the hydrodynamic radius of DNA. *Biophys. J.* **67**, 304–308 (1994).

24. J. F. Ward, DNA damage and repair. In *Physical and Chemical Mechanisms in Molecular Radiation Biology* (W. A. Glass and M. N. Varma, Eds.), pp. 403–422. Plenum Press, New York, 1991.

25. D. Schulte-Frohlinde and E. Bothe, Identification of a major pathway of strand break formation in poly U induced by OH radicals in the presence of oxygen. *Z. Naturforsch. C.* **39**, 315–319 (1984).

26. P. R. Selvin, D. N. Cook, N. G. Pon, W. R. Bauer, M. P. Klein and J. E. Hearst, Torsional rigidity of positively and negatively supercoiled DNA. *Science* **255**, 82–85 (1992).

27. M. Spotheim-Maurizot, M. Charlier and R. Sabattier, DNA radiolysis by fast neutrons. *Int. J. Radiat. Biol.* **57**, 301–313 (1990).

28. V. V. Rybenkov, N. R. Cozzarelli and A. V. Vologodskii, Probability of DNA knotting and the effective diameter of the DNA double helix. *Proc. Natl. Acad. Sci. USA* **90**, 5307–5311 (1993).

29. A. Kuppermann, Diffusion kinetics in radiation chemistry: An assessment. In *Physical Mechanisms in Radiation Biology* (R. D. Cooper and R. W. Wood, Eds.), pp. 155–183. U.S. AEC Technical Information Center, Oak Ridge, TN, 1974.

30. A. Chatterjee and J. L. Magee, Theoretical investigation of the production of strand breaks in DNA by water radicals. *Radiat. Prot. Dosim.* **13**, 137–140 (1985).

31. D. T. Goodhead and H. Nikjoo, Track structure analysis of ultrasoft X-rays compared to high- and low-LET radiations. *Int. J. Radiat. Biol.* **55**, 513–529 (1989).

DISTRIBUTION LIST

DEPARTMENT OF DEFENSE

ARMED FORCES RADIOBIOLOGY RESEARCH INSTITUTE
ATTN: PUBLICATIONS BRANCH
ATTN: LIBRARY

ARMY/AIR FORCE JOINT MEDICAL LIBRARY
ATTN: DASG-AAFJML

ASSISTANT TO THE SECRETARY OF DEFENSE
ATTN: AE
ATTN: HA(IA)

DEFENSE NUCLEAR AGENCY
ATTN: TITL
ATTN: DDIR
ATTN: RAEM
ATTN: MID

DEFENSE TECHNICAL INFORMATION CENTER
ATTN: ACQUISITION
ATTN: ADMINISTRATOR

FIELD COMMAND DEFENSE NUCLEAR AGENCY
ATTN: FCIEO

INTERSERVICE NUCLEAR WEAPONS SCHOOL
ATTN: DIRECTOR

LAWRENCE LIVERMORE NATIONAL LABORATORY
ATTN: LIBRARY

UNDER SECRETARY OF DEFENSE (ACQUISITION)
ATTN: OUSD(A)/R&E

UNIFORMED SERVICES UNIVERSITY OF THE HEALTH SCIENCES
ATTN: LIBRARY

DEPARTMENT OF THE ARMY

HARRY DIAMOND LABORATORIES
ATTN: SLCSM-SE

OFFICE OF THE SURGEON GENERAL
ATTN: MEDDH-N

U.S. ARMY AEROMEDICAL RESEARCH LABORATORY
ATTN: SCIENCE SUPPORT CENTER

U.S. ARMY CHEMICAL RESEARCH, DEVELOPMENT, & ENGINEERING CENTER
ATTN: SMCCR-RST

U.S. ARMY INSTITUTE OF SURGICAL RESEARCH
ATTN: COMMANDER

U.S. ARMY MEDICAL DEPARTMENT CENTER AND SCHOOL
ATTN: MCCS-FCM

U.S. ARMY MEDICAL RESEARCH AND MATERIEL COMMAND
ATTN: COMMANDER

U.S. ARMY MEDICAL RESEARCH INSTITUTE OF CHEMICAL DEFENSE
ATTN: MCMR-UV-R

U.S. ARMY NUCLEAR AND CHEMICAL AGENCY
ATTN: MONA-NU

U.S. ARMY RESEARCH INSTITUTE OF ENVIRONMENTAL MEDICINE
ATTN: DIRECTOR OF RESEARCH

U.S. ARMY RESEARCH LABORATORY
ATTN: DIRECTOR

WALTER REED ARMY INSTITUTE OF RESEARCH
ATTN: DIVISION OF EXPERIMENTAL THERAPEUTICS

DEPARTMENT OF THE NAVY

BUREAU OF MEDICINE & SURGERY
ATTN: CHIEF

NAVAL AEROSPACE MEDICAL RESEARCH LABORATORY
ATTN: COMMANDING OFFICER

NAVAL MEDICAL RESEARCH AND DEVELOPMENT COMMAND
ATTN: CODE 42

NAVAL MEDICAL RESEARCH INSTITUTE
ATTN: LIBRARY

NAVAL RESEARCH LABORATORY
ATTN: LIBRARY

OFFICE OF NAVAL RESEARCH
ATTN: BIOLOGICAL & BIOMEDICAL S&T

DEPARTMENT OF THE AIR FORCE

BROOKS AIR FORCE BASE
ATTN: AL/OEBZ
ATTN: OEHL/RZ
ATTN: USAFSAM/RZB

OFFICE OF AEROSPACE STUDIES
ATTN: OAS/XRS

OFFICE OF THE SURGEON GENERAL
ATTN: HQ AFMOA/SGPT
ATTN: HQ USAF/SGES

U.S. AIR FORCE ACADEMY
ATTN: HQ USAFA/DFBL

U.S. AIR FORCE OFFICE OF SCIENTIFIC RESEARCH
ATTN: DIRECTOR OF CHEMISTRY & LIFE SCIENCES

OTHER FEDERAL GOVERNMENT

ARGONNE NATIONAL LABORATORY
ATTN: ACQUISITIONS

BROOKHAVEN NATIONAL LABORATORY
ATTN: RESEARCH LIBRARY, REPORTS SECTION

CENTER FOR DEVICES AND RADIOLOGICAL HEALTH
ATTN: DIRECTOR

GOVERNMENT PRINTING OFFICE
ATTN: DEPOSITORY ADMINISTRATION BRANCH
ATTN: CONSIGNED BRANCH

LIBRARY OF CONGRESS
ATTN: UNIT X

LOS ALAMOS NATIONAL LABORATORY
ATTN: REPORT LIBRARY

NATIONAL AERONAUTICS AND SPACE ADMINISTRATION
ATTN: RADLAB

NATIONAL AERONAUTICS AND SPACE ADMINISTRATION
GODDARD SPACE FLIGHT CENTER
ATTN: LIBRARY

NATIONAL CANCER INSTITUTE
ATTN: RADIATION RESEARCH PROGRAM

NATIONAL DEFENSE UNIVERSITY
ATTN: LIBRARY

NATIONAL INSTITUTE OF STANDARDS AND TECHNOLOGY
ATTN: IONIZING RADIATION DIVISION

U.S. DEPARTMENT OF ENERGY
ATTN: LIBRARY

U.S. FOOD AND DRUG ADMINISTRATION
ATTN: WINCHESTER ENGINEERING AND ANALYTICAL CENTER

U.S. NUCLEAR REGULATORY COMMISSION
ATTN: LIBRARY

RESEARCH AND OTHER ORGANIZATIONS

AUSTRALIAN DEFENCE FORCE
ATTN: SURGEON GENERAL

AUTRE, INC.
ATTN: PRESIDENT

BRITISH LIBRARY
ATTN: ACQUISITIONS UNIT

CENTRE DE RECHERCHES DU SERVICE DE SANTE DES ARMEES
ATTN: DIRECTOR

FEDERAL ARMED FORCES DEFENSE SCIENCE AGENCY FOR NBC PROTECTION
ATTN: LIBRARY

INHALATION TOXICOLOGY RESEARCH INSTITUTE
ATTN: LIBRARY

INSTITUTE OF RADIOBIOLOGY, ARMED FORCES MEDICAL ACADEMY
ATTN: DIRECTOR

KAMAN SCIENCES CORPORATION
ATTN: DASIAC

OAK RIDGE ASSOCIATED UNIVERSITIES
ATTN: MEDICAL LIBRARY

RESEARCH CENTER FOR SPACECRAFT RADIATION SAFETY
ATTN: DIRECTOR

RUTGERS UNIVERSITY
ATTN: LIBRARY OF SCIENCE AND MEDICINE

UNIVERSITY OF CALIFORNIA
ATTN: DIRECTOR, INSTITUTE OF TOXICOLOGY & ENVIRONMENTAL HEALTH
ATTN: LIBRARY, LAWRENCE BERKELEY LABORATORY

UNIVERSITY OF CINCINNATI
ATTN: UNIVERSITY HOSPITAL, RADIOISOTOPE LABORATORY

XAVIER UNIVERSITY OF LOUISIANA
ATTN: COLLEGE OF PHARMACY